ADDIS ABABA UNIVERSITY

ADDIS ABABA INSTITUTE OF TECHNOLOGY

SCHOOL OF CIVIL AND ENVIRONMENTAL ENGINEERING

Performance of Energy Pile Foundation In Layered Soil : The Case of United Bank Headquarter Building

---

By: Samuel Getiye

Advisor: Henok Fikre (Dr.-Ing)

A Thesis Submitted to the School of Graduate Studies in Partial Fulfillment of the Requirements for the Degree of Master of Science in Geotechnical Engineering

February,2020

Addis Ababa, Ethiopia

The undersigned have examined the thesis entitled '**Performance of Energy Pile Foundation in Layered Soils: The case of United Bank Headquarter Building**' presented by **SAMUEL GETIYE**, a candidate for the degree of **Master of Science (Geotechnical Engineering)** and hereby certify that it is worthy of acceptance.

Advisor	Signature	Date
Internal Examiner	Signature	Date
External Examiner	Signature	Date
Chair person	Signature	Date

UNDERTAKING

I, the undersigned, certify that research work titled "**Performance of Energy Pile Foundation in Layered Soils: The case of United Bank Headquarter Building**" is my own work. The work has not been presented elsewhere for assessment. Where material has been used from other sources, it has been properly acknowledged / referred.

***Signature*: ________________**

Undertaker's Full Name: Samuel Getiye

Place of Undertaking: Addis Ababa, Ethiopia.

Date: February 2020

ABSTRACT

Currently the issues of sustainable energy demands become critical due to the rapid growth of population and economy. The construction boom in the country has caused the rising of tall buildings for luxury hotels, shopping malls, apartment blocks, etc., particularly in Addis Ababa. The commercial and residential sectors already consume about 60% of the total generated electricity of the country. These trends have undoubtedly influenced the growth of energy demands of the country. Practical researches are indicating that energy demand problems can be mitigated to some extent by using energy pile foundations. Energy foundations are geostructures with a dual purpose: provides structural stability and enable the supported buildings to have a heating and cooling system through exchange of heat with the ground. To this end, the opportunities of meeting some of the country's energy demand by introducing energy pile foundation in commercial and residential buildings of Ethiopia were investigated by taking the new United Bank Headquarter Building as a case study. In order to evaluate the performance of energy pile under thermo-mechanical loading condition and the expected amount of energy yield, a preliminary design, simulation and economic analysis were conducted for the existing foundation building using Matlab Programming and Abaqus software. The results of the study revealed that during thermo-mechanical loading, the total axial stress in the pile shows significant increases due to thermal loading that causes axial expansion in the energy pile. In addition, the relative movement of the pile with respect to the surrounding soil mobilizes downward shaft resistance at the upper part and upward shaft resistance at NP. On the other hand, regarding the expected amount of energy extracted, the results of the preliminary study indicated that a significant amount of energy, 719,283.60kWh/year, can be generated. This amount could covers 93.62% of the estimated heating and cooling energy demand of the building. In addition, based on the current electricity tariff of Ethiopia, up to 38,122.03 USD can be saved annually with such energy geo-structure system. From this preliminary study outcomes, it can be concluded that energy pile foundation shall be used an alternative means of energy source by taking the essential design consideration of the additional axial stress due thermal loading.

ACKNOWLEDGMENTS

First, I would like to say thanks to *my family,* for their unlimited support and backing when I needed someone to rely upon, especially my wife.

Second in line, it is my great pleasure to forward my deepest gratitude to my *research advisors Dr.-Ing Henok Fikre* and *External advisor Prof.John McCartney (from University of California, San Diego)* for their guidance, suggestions and comments throughout my work.

Beside my advisors, I would like to thank *officials at ETG consulting (Eng. Zekarias & Eng. Derese), MH consulting (Eng. Epherem), MGM consulting and Ethiopian geological survey; Resident engineers of United Bank (Eng. Fasil)* and *Nib International Bank (Eng. Esayas)* and *all fellow of Geotechnical Engineering students* for their assistance and encouragement.

Finally yet importantly, I would like to thank the *Ethiopian Roads Authority (ERA)* for funding my graduate study of *Geotechnical Engineering* stream at the *Addis Ababa University.*

TABLE OF CONTENTS

LIST OF TABLES

LIST OF FIGURE

LIST OF SYMBOLS

b: Bottom of an element pile

D: Diameter of Pile

FE: Finite Element

i: Element number within the pile.

K_f: Stiffness of reinforced concrete foundation spring

K_s : Stiffness of side shear spring

K_{base} : Stiffness base spring

L_i: Length of each element of pile

M: Mechanical loading

MT: Thermomechanical loading

NP: Null point

P: Mechanical Load

ρ :Axial displacement of a pile.

Q: Axial forces of a pile

s: Side of an element pile

T: Thermal loading

t: Top of an element pile

LIST OF ABBREVIATION

EPs: Energy Piles

FEM: Finite Element Method

GSHP: Ground Source Heat Pump

HVAC: Heat, Ventilation and Air Conditioning

ME: Mechanical Engineer

NP: Null point or Neutral Point

CHAPTER 1: INTRODUCTION

1.1. Background

Currently, following the problem of climate change and sustainable energy demands, the idea of energy foundation has become popular. Energy foundations are geostructures with a dual purpose that provide structural stability and able to exchange heat with the ground, allowing the supported buildings and or infrastructure to be heated or cooled. Those structures use subsurface geothermal heat energy to heat or cool the building rather than deep geothermal technologies that utilize extremely high temperature (~ 5,000°C) at the earth's core for producing electricity (Olgun & McCartney, 2014).

Near subsurface geothermal energy is a naturally abundant energy resource due to a large fraction of the incident solar energy is absorbed by the ground. This renewable energy source can be used widely for heating and/or cooling of buildings and traffic areas by utilizing geostructures elements. The idea behind energy geostructures or energy foundations is to take advantage of the thermal storage capacity of the ground as an energy storage system by using the foundation of a building (e.g. piles or retaining walls) (Laloui et.al 2006; Olgun & McCartney, 2014).

Researches revealed that extracting heat energy via energy foundations is an innovative method and it is environmentally friendly because it uses clean and renewable energy. Due to this, during the past decades there were many energy pile systems installed all over the world, particularly in Austria, Germany, Switzerland and United Kingdom as well as in Japan and China (Brandl 2006; Laloui and Di Donna, 2011; Amatya et al. 2012; McCartney and Murphy 2012;). While energy foundations are gaining popularity throughout the world, there are still pending questions on their thermo-mechanical.

Researches are in progress to develop proper characterization, analysis and design of energy related geo-structures like energy piles. For simulating the thermo-mechanical behavior of energy piles, several numerical models have been developed by researchers. These models can be categorized in two main groups: load-transfer models (Knellwolf, 2011; Plaseied, 2012;

Suryatriyastuti, 2013; McCartney & Chen, 2016) and full-numerical models (Laloui et.al 2006; Ouyang 2011; Wang et.al 2015; Chakraborty, 2017).

The full-numerical approaches include the use of finite element or finite difference methods of calculation, which can be used to model any type of thermo active geostructures. However, finite-element methods are complex to perform for energy pile design due to the large number of parameters potentially needed that may require advanced testing. Alternatively, there is a simpler analytical method referred to as thermo-mechanical load transfer analysis also used. In the load-transfer analysis, t-z curve relationships that have already been developed for axial pile loads in the literature are used and adapted for thermal loads.

Many important factors that need to be considered in the design of energy piles, the impact of temperature on the induced stress-strain in the foundation is one of the critical factor, which may affect building performance. Research efforts on this regard highlight the impact of temperature during heating and cooling of the foundation may lead to expansion and contraction of the foundation and soil (Bourne-Webb et.al 2009; McCartney & Chen, 2016). Therefore, it is important to conduct further research to understand the mechanism of energy pile in terms of thermal response and thermo-mechanical behavior in different soil profiles.

1.2. Motivation

Geotechnical engineering has developed over the last century in association with a number of empirical, analytical and observational approaches. Geotechnical engineers applied those approaches in the design, analysis and construction of geo-structures to make stability for the supported structures. However, nowadays due to energy demands, climate change, rapid increase in population and depletion of natural resources, the role of geotechnical engineers has extended to geotechnical solutions for the environment and related issues of sustainability.

Recently, the research trends and the scope of the geotechnical engineering profession have extended in response to earth problems. This phenomenon made researchers to pay attention on the field of environmental geotechnics. Current research outcomes indicate that there are some critical areas where geotechnical engineers must play important roles to mitigate the problem of global change, energy demand and population growth in order to achieve a sustainable development.

Geotechnical engineering researches in our country has been attentive on characterizing the properties of soil; developing analytical methods for the design & analysis of shallow foundation and correlation of the properties of the soil to develop empirical equation. Even if the outcome of those researches has great contribution for the field of geotechnical engineering, the author strongly believes that the research trends in our country should also focus on the purpose of finding novel solutions to new problems related to environmental issues and energy demands.

1.3. Problem Statement

Following the rapid growth of population and economy, the city of Addis Ababa is expanding; as a result, commercial and residential buildings have been constructed. These trends have undoubtedly influenced the growth of energy demands of the country. The government has emphasized the importance of sustainable energy development in different policies. In this regard, the practice of other countries exercise should be considered to alleviate the problem of energy demands in the field of geotechnical engineering.

Geotechnical engineering has a role in the alternative energy sectors like near subsurface thermal energy. Research findings show that deep foundations can be used as energy storage while transmitting the load of the supported structures to the ground (Brandl 2006). Recent research efforts has indicated that in some extent the energy demands of the building can be covered by using energy geo-structure elements for heating and cooling requirement.

Since the idea of energy foundation is new for our country, creating an understanding about the behaviour and the mechanism of energy pile through research effort will be helpful for engineers who design geotechnical structures. Moreover, in order to apply such innovative technology for our country by adopting with local ground condition and standard code, conducting such type of researches is essential.

1.4. Objectives of the Research

The main objective of the research is to evaluate the performance of energy piles in layered soil profiles found in Addis Ababa**.** In doing so, the research aims to achieve the following particular objectives:

- Finite Element modeling of energy pile using Abaqus Software;
- Load transfer modeling of energy pile using matlab programming code;
- Evaluating of the performance of energy pile under thermo-mechanical loading;
- Evaluating of the expected amount of energy that can be extracted with energy piles;
- Conducting Economic analysis

1.5. Significance of the Research

For the government, the study shall contribute and offer new means of developing alternative renewable energy sources to achieving the Green Growth Strategy of attaining zero net carbon emission by 2025. Along with this, the results of the study are also expected to change the understanding and perspectives of architects and engineers towards considering foundation of buildings as a means of generating sustainable energy resources.

As the idea of energy pile foundation is new-fangled for our country, this study may give a new research idea and a base reference for the students. Furthermore, it could be scale up the research trends of the country by motivating the researchers to finding novel solutions for new problems related to environmental issues and energy demands.

1.6. Scope of the study

The study focus on investigate the behaviour of energy pile in layered soil. This involves detail soil investigation up to 50m depth and thermal soil conductivity test, which is not available in our country. Such a large-scale study will be cash-intensive and unfeasible due to the time constraint and resources. These possess a challenge to obtain some of the required primary input data at required locations and depths. Instead, available geotechnical investigation reports were compiled. The paper is also limited to single energy pile behaviour rather than group of energy piles.

1.7. Organization of Thesis

The thesis is organized in five chapters. The first chapter is a brief description of background of the study, its objective and scope. The second chapter reviews literature on energy pile definition, concepts, behaviour and design methods. The third chapter describes the methods and materials for numerical study. In the fourth chapter, analysis of the results and discussion are made. The last chapter summaries the thesis and present its findings as well as recommendations for future work are made.

CHAPTER 2: LITERATURE REVIEW

2.1. Review of Energy Piles

The utilization of ground thermal energy for heating and cooling of buildings has been started before some years back; people used horizontal and vertical heat absorber plastic pipes to extract subsurface thermal energy for space heating by integrated with ground source heat pump. Such ground systems are essential to reduce energy costs and improve the environmental performance of the buildings. Later, in the 1980s, deep foundations were first used for heat extraction by placing heat absorber pipes in concrete elements. At first from base slabs, then driven precast piles and later bored piles (1984) and diaphragm walls (1996) were successfully utilized for heating and cooling purposes and those types of ground structures are referred Energy Foundation (Brandl., 2006).

Energy piles are one of the most common types of energy foundation that incorporate heat exchanger pipes to heat and cool the supported structure. The use of energy piles have been increasingly grown across the world due to the dual role as bearing elements and their environmental benefits (Rammal, 2017). Nevertheless, energy piles have been implemented in Europe and other counties over the past couple of decades; there are still many pending questions on their thermo-mechanical behavior. Therefore, many universities and research centers have been focused both experimental and numerical work to enhance the understanding of the behaviour of energy piles under significant temperature changes. In this chapter, a brief background on energy piles, along with the open research questions regarding their thermo-mechanical behaviour are presented.

2.1.1. Definition and Concept

In different literature, the names given for piles that are designed for dual purpose for structural support and for efficient heating/cooling of buildings are different. Some literature used the name “heat exchanger pile”, for describing the piles that exchange heat between the ground and building for heating and cooling purpose while transferring the load of the supported structure to the ground (Laloui et.al 2006; Knellwolf, 2011).

In other literature, the name “thermo-active piles’’ used for define the piles that are thermally active during operation of the system to transfer heat from the ground while transferring the superstructure loads to the ground (Brandl., 2006; GSHP-Association, 2012; Olgun & McCartney, 2014). The name “Energy Piles” is mostly used in many literatures to define the Piles that are designed for mainly structural reasons, however it also acts as heat exchangers element through extracting the ground thermal energy for heating and cooling of the building (Amatya et.al 2012; Bourne-Webb, 2013; Di Donna et.al 2013; McCartney & Chen, 2016)).

In this paper, the name Energy piles is used to define piles that are designed to access and exploit the relative constant temperature of the ground for heating and cooling of buildings while transferring loads from the supper structure to the ground. In figure 2-1, the piles integrate closed loop high-density polyethylene plastic pipes of 20 to 25 mm diameter and 2 to 2.3 mm wall thickness attached to the reinforcement cage inside the pile concrete. A heat carrier fluid that connected to a heat pump system installed within the building is circulated to transfer heat to or from the subsurface (Brandl., 2006; Olgun , 2013).

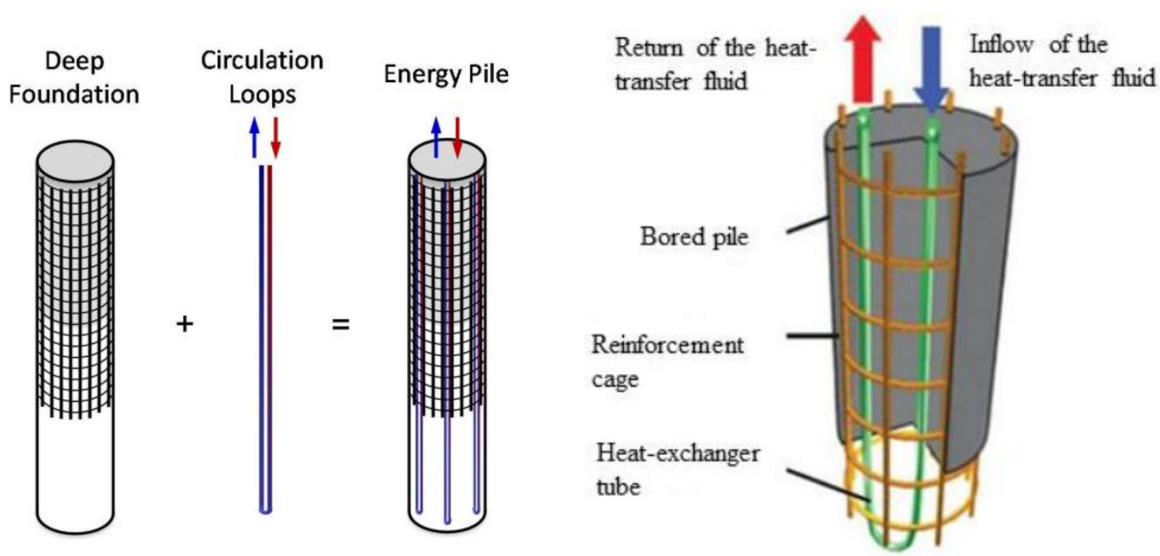

Figure 2-1: Energy Pile Configurations (After Olgun, 2013)

Brandl (2006) has discussed in detail the feasibility of incorporating a ground heat exchanger system within building foundations (piles) is a novel approach to improve the energy efficiency of building and provide necessary geotechnical support while using the same construction materials. As he said "*This method has broad appeal because concrete is an ideal medium as a heat absorber in the ground owing to its good thermal conductivity and thermal storage capacity. These new piles could be called "energy piles" or "thermo-piles" and can be described as dual-purpose structure elements since they utilize the required ground-concrete contact element that is constructed for structural reasons as a heat exchanger unit*".

As we know, concrete has a good thermal conductivity and thermal storage capacity, which makes it an ideal medium as an energy absorber (heat exchanger) (Saggu, 2015). To use these properties for energy pile, high-density polyethylene plastic pipes of 20 or 25 mm diameter, with 2.0 or 2.3 mm wall thickness respectively, have to be installed within the concrete. They are placed to form several individual closed coil or loops, which circulate a heat carrier fluid (heat transfer medium) of either water, water with antifreeze-glycol. (Details are presented in Brandl (2006))

Studies have shown that, the idea behind the use of energy piles from the fact that, at depths below 6-10 m from the ground surface, the temperature of the ground remains relatively constant throughout the year. In other words, ground temperatures are not affected by the ambient temperature changes (Olgun & McCartney, 2014). Thus, during winter, when the temperature of the ground is warmer than the ambient temperature, the heat energy can be extracted from the ground to heat a building. Similarly, during summer, the heat energy can be withdrawn from the ground with the use of a ground-source heat pump to cool a building as Sutman (2016) explained.

In most regions of Europe ,the seasonal ground temperatures remain relatively constant below a depth of 10–15 m. Values between 10^0C and 15^0C predominate to a depth of about 50 m (Fig. 2.2). Brandl (2006) point out that, such temperatures permit economical heating and cooling by thermo-active ground structures, and they represent ideal conditions for heat pumps. In the tropics the constant ground temperature at a depth of more than 10–15 m below the surface varies between T 20–25^{0}C, locally even 28^{0}C), which still allows cooling and heating of buildings.

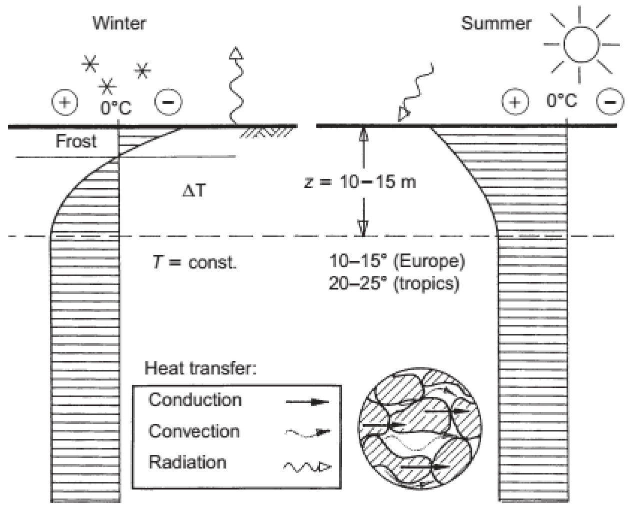

Figure 2-2: Ground temperature profile in Europe & Tropics (after Brandl 2006).

2.1.2. Benefits and limitations of energy piles

Energy piles represent a sustainable geo-energy solution with significant environmental and economic advantages and are becoming more significant with large advances in the development and design of these systems over time. Researches highlights that, energy piles have been found to provide substantial long-term cost savings in relation to conventional systems and with an investment-return period of 5–10 years depending on ground strata, subsurface properties, and alternative energy prices (Brandl , 1998; Adam & Markiewicz, 2009).

Ebnother (2008) and Olgun(2013) point out that the efficiency of these systems is inherently higher than that of air-source heat pumps because the ground maintains a relatively stable source of temperature throughout the year. In addition, Brandl (2006) summarized the following benefits of energy foundation:

- Environmentally friendly (non-polluting, sustainable energy)
- Less vulnerable to variation in energy source than hydropower (droughts), wind, and solar

- Less sensitive to energy price fluctuations
- Installation in foundation permits heat exchange system to be within building footprint, making more efficient use of material and space.

In spite of the fact that energy piles have numerous advantages, there are noticeable limitations, which are not ignored in the design and application of energy piles. In terms of design, Olgun & McCartney (2014) stated that the major of limitation that exists in the application of energy piles, there no refined design method that consider complex soil structure interaction of thermo-mechanical behaviour of energy piles. Specifically, most thermo-mechanical soil models proposed by researchers, do not account for the various soil and rock conditions and complicated geological strata. Due to this, thermo-mechanical design of energy piles relied on empirical and conservative relationships. Hence, applying a high factor of safety may possibly causes non-economic solutions and difficult in wider application of energy piles.

The other limitation that some engineers have concerned about this technology is, the serviceability issues for energy piles, and in the case failure, it is difficult to access heat exchangers embedded in the concrete. This is an important challenge that can be considered in the development of detail design, and requires collaboration with the geothermal designer, geotechnical engineer and structural engineer (Olgun & McCartney, 2014).

2.1.3. The Current Status and Application of Energy Piles around the World

Different researches revealed that extracting heat energy via energy foundations or other thermo-active ground structures is an innovative method and significantly more cost-effective than conventional systems, and it is environmentally friendly because it uses clean, renewable energy. Austria, Switzerland and Germany can be regarded as the pioneering countries that have investigated this technology for decades.

In Austria, as Monique (2010) describes, nearly 300 buildings are fitted with energy piles or energy diaphragm walls. Two notable examples reported by Brandl, (2006) and Adam and Markiewicz, (2009) are the Lainzer tunnel and Uniqa Tower in the center of Vienna. The section of the Lainzer tunnel, which operates by comprising 59 energy piles with 1.2 m in diameter and 17.1 m in length in its sidewalls. Of the numerous bored piles installed, every third pile is converted into an energy pile to extract geothermal energy for heating and cooling of railway stations and other administrative buildings. It is reported by the author that thermally induced stresses along the piles were much less than the ones caused by the earth pressure. In addition, it is stated that the heat exchange operation create a more uniform temperature profile along the piles.

The Swiss Federal Institute of Technology in Lausanne and Dock Midfield Airport are another application of energy piles projects, with length of 30 m and diameters ranging between 0.9-1.5 m have been used for heating and cooling of the building. Of the 440 foundation piles at Dock Midfield airport, 300 were energy piles for heating and cooling purposes. Performance assessment concluded that 85% of the annual heating and cooling demands was supplied energy piles (Laloui et.al, 2006). It is stated by the authors that the additional cost of implementing energy piles has already been compensated in eight years, with the energy savings.

Energy piles were used in some commercial buildings located in Frankfurt, Germany; 200 m high Frankfurt Main tower (Katzenbach, 2009). This building is founded on a 30 m x 50 m base supported by 213 piles, 112 of which are energy piles of 30 m in length, which produce 500kw for heating and cooling demands. Another application of energy piles in Germany is Berlin’s International Solar Center, which employs 200 energy piles to meet 20% of heating and 100% of cooling demands. The country has been quite receptive towards this new technology by offering incentives in an effort to promote alternative energy source to be economically viable, both heating and cooling of the building (Ebnother, 2008).

One of the first energy pile project in the United Kingdom is Keble’s six-storey new buildings, which started in 2001 at Oxford University. As Brandl(2006) reported, the structural foundation consist of 61 drilled shaft energy piles which fully cover the monthly costs for heating and cooling demands of the building. Both standard foundation piles and secant piles for retaining walls were outfitted with absorber pipes. Studies have shown that the system has been running without problems since its inception.

Stockton College is an example of one of a structure that utilizes large geothermal energy pile systems in United States of America. When built in the early 1990s, it was considered as the largest single seasonal underground thermal energy facility in the world, which utilized a large amount of heat exchanger wells and a water source heat pump unit to serve the heating and cooling of the College campus. The implementation of this system resulted in a reduction of 25% in electricity and 70% in natural gas consumption (Epstein, 1998).

Furthermore, this technology and fitting techniques have been exported to several countries like Netherlands, Belgium, France, Poland, Sweden, Norway, Canada and Iran and several others countries (Bourne-Webb, 2013; Brandl., 2006; Knellwolf, 2011; Laloui et.al, 2006; McCartney & Chen, 2016).

2.2. Design Issues

Many important factors that need to be considered in the design of energy pile systems have been identified in the past studies. As with conventional pile design, Brandl H.(2006) & Katzenbach (2009) sugested that an extensive geotechnical site investigation should be conducted to acquire detail information including (but not limited to) the following parameters;

- Geological strata (e.g. shallow profile as well as identification and depth of the foundation rock.)
- Geotechnical soil properties (e.g. water content, density, void ratio, hydraulic properties, strength parameters, etc.)
- Geothermal soil properties (e.g. thermal conductivity, specific heat capacity , in situ ground temperatures, the existence of thermal gradients, etc.)
- Hydrogeological properties (e.g. depth to groundwater, fluctuations of water levels, flow direction and velocities, etc.)
- Mineralogical and geochemical soil properties.

In addition to the site investigation, several construction issues need to be carefully considered in design of energy pile. The geometric layout of the reinforcement cage and heat exchangers in an energy foundation are critical for its constructability and performance. According to Olgun & McCartney (2014), the smallest diameter of an energy pile is typically 0.6 m. Since the reinforcement cage is typically undersized (75% smaller), diameters less than 0.6 m make it difficult to attach the heat exchanger tubing to the reinforcement cage.

2.3. General Thermomechanical Behaviour of Energy Pile

The effect of temperature on the behavior of the energy piles have a rather complex mechanism compared to a conventional pile under only a structural load. Efforts have been made by researchers on the behaviour and the framework of energy piles including the related soil structure interaction. Bourne-Webb (2009) presented a clear qualitative framework for describing the expected response of energy pile, to provide a basis for assessing and comparing field and numerical study's findings.

2.3.1. Thermal Load response

When a pile at working load is heated or cooled, a complex behaviour is imposed upon the pile that varies with different ground conditions and different degrees of end restraint. In the following, a simplified approach that outlined by Amatya (2012) & Bourne-Webb (2009, 2013) is used to describe the basic behaviour of energy piles with temperature change.

When a pile without a head load is heated, and assume it is a freestanding column, it will expand/contract in proportion to the coefficient of thermal expansion of concrete, $\alpha_c (\mu\varepsilon/^0 C)$ and the net change in temperature of the pile ($\triangle$T) to yield free axial thermal strain without any restraint:

$$\varepsilon_{T-Free} = \alpha_c \Delta T \qquad \text{Eq. 2-1}$$

Free strain will be expansive as a result of heating. The thermal strain will lead to a change in pile geometry.

$$\Delta L = L_0 \varepsilon_{T-Free} \qquad \text{Eq. 2-2}$$

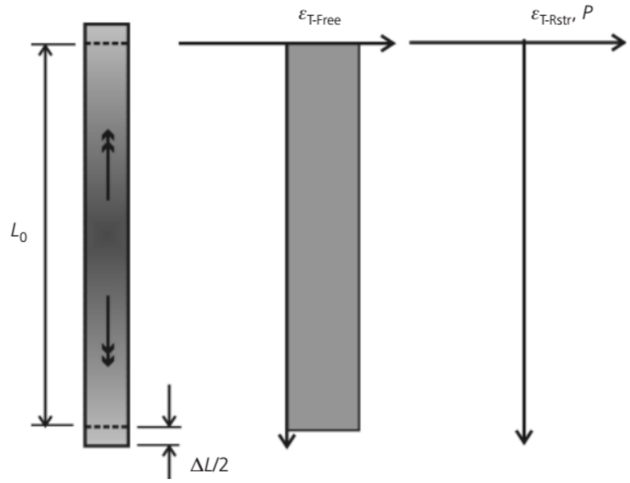

Figure 2-3: Thermal response of free bodies: heating (after Bourne-Webb, 2009)

In actual situation, a pile will not act as a free body, but will be restrained by the superstructure and associated loading at the pile head, and also by the presence the surrounding ground, through shear on the pile– soil interface and the base reaction. Thus, the measured strain change due to temperature change (ε_{T-Obs}) will be less than that given by Eq.2-1

$$\varepsilon_{T-Obs} \leq \varepsilon_{T-Free} \qquad \text{Eq.2-3}$$

The restrained axial strain $\varepsilon_{T-\mathrm{R}str}$ can be estimated

$$\varepsilon_{T-\mathrm{R}str} = \varepsilon_{T-Free} - \varepsilon_{T-Obs} \qquad \text{Eq.2-4}$$

The restrained strain creates thermal stress in the pile, and it should be considered in the design. For a given strain increment due to a temperature change, a thermally induced axial load can be estimated using the equation:

$$\begin{aligned} P_T &= -EA\varepsilon_{T-\mathrm{R}str} \\ &= -EA(\alpha_c \Delta T - \varepsilon_{T-Obs}) \end{aligned} \qquad \text{Eq.2-5}$$

Where, E is the pile Young’s modulus and *A* is the cross-sectional area of pile material. The negative sign in Eq.2-5 implies that the restrained strain due to pile– soil interaction provides a counterforce to restrict the pile deformation. Heating will yield a uniform compressional load.

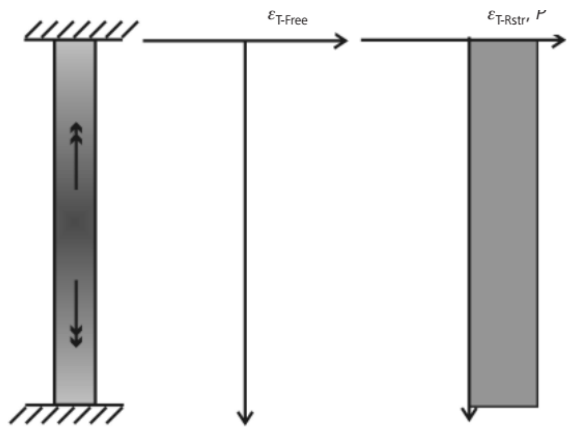

Figure 2-4 : Thermal response of restrained bodies: heating (after Bourne-Webb, 2009)

However, this type of perfect restraint does not exist in realty, the pile will be able to expand/contract slightly, and this will mobilize opposing reactions that will tend to reduce the induced axial load. In this regard, Bourne-Webb (2009) also clearly presented the effect of the surrounding soil on the response of the pile without mechanical loading. According to his description, as soil strength and stiffness increase, the restraint mobilized at the pile–soil interface will in turn increase as shown in Figure 2-5.

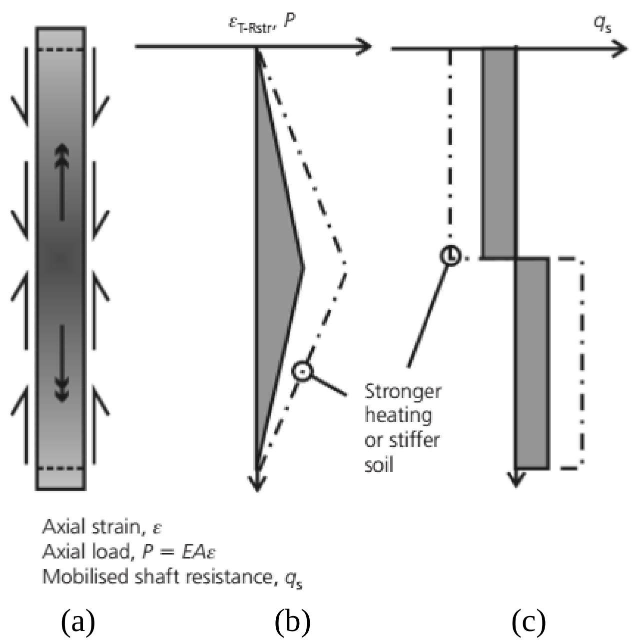

Figure 2-5: Effect of soil restraint during thermal loading(a) Heating (b) Axial Strain (c) Mobilized shaft resistance (after Bourne-Webb, 2009)

2.3.2. Combined Mechanical and Thermal Load Response

According to Amatya (2012), when a load-bearing pile serves as a heat changer, the total mobilized strain ε_{Total} at any depth can be estimated as:

$$\varepsilon_{Total} = \varepsilon_M + \varepsilon_{T-Obs} \qquad \text{Eq.2-6}$$

Where ε_M is the mechanical strain that imposed in the pile due to loading at the pile head, and ε_{T-Obs} is the strain due to thermal loading. The mechanical strain $\in_M$ is directly developed due to a mechanical load (P_M):

$$P_M = EA\varepsilon_M \qquad \text{Eq.2-7}$$

A combination of these two equations (Eq (2-5) and (2-7)) gives the total axial load, P_{Total}

$$P_{Total} = P_M + P_T \qquad \text{Eq.2-8}$$

The combined effects of mechanical and thermal loads were schematically described by Bourne-Webb (2013) as presented in figure 2-6:

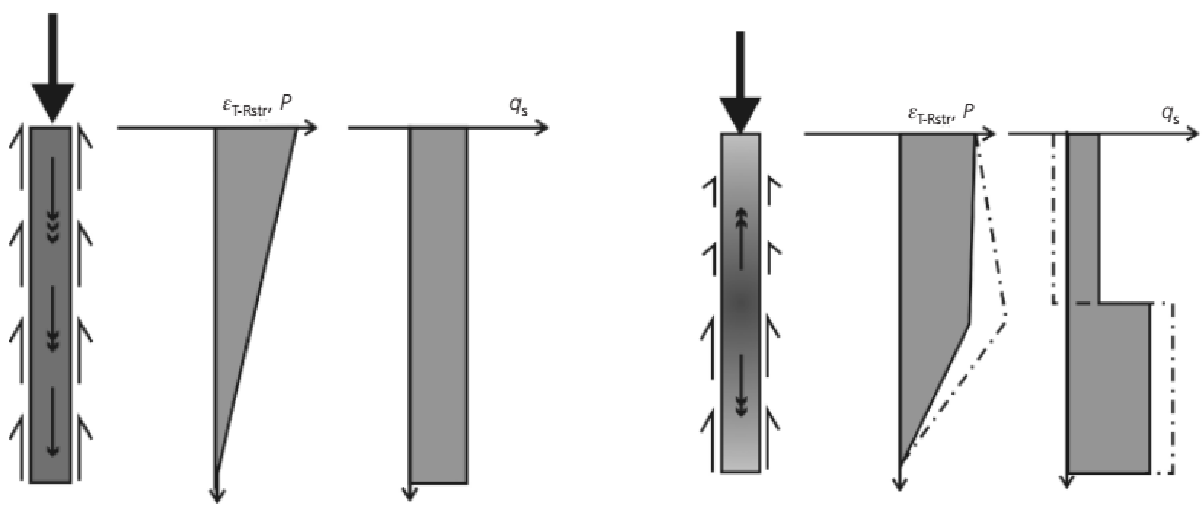

(a) (b)

Figure 2-6: Combined effect of thermo-mechanical loading ;(a) Mechanical Load Only (b) Thermo-mechanical Load; (after Bourne-Webb 2009)

The first part of the figure (Fig.2-6 (a)) shows the shaft resistance and axial load along the energy piles subjected to only mechanical load. As a result of the mechanical loading, uniform shaft resistance is mobilized along the length of the pile. However, the axial load along the pile decreases with depth due to shaft resistance. The second part of the figure (Fig.2-6 (b)) demonstrates the combined effects of thermal and mechanical loads. Dash-dotted lines represent the effect of stronger heating/resistance. It should be noted that for the case of larger shaft resistance or higher temperature increase, these effects would be more pronounced. Bourne-Webb (2009) thought that, if the applied mechanical load is very low, the effect of temperature increase could even overcome the positive shaft resistance of the mechanical load and result in negative shaft resistance at the upper portion.

Furthermore, multiple soil layers with varying shear strengths, different levels of end-restraining conditions at the head, tip of the pile, and varying temperature changes along the length of the pile, are some of the factors, which take this simplified framework to a level that is more complex mechanism (More details are presented in Amatya (2012),Bourne-Webb (2009,2013)).

2.4. Experimental Studies on Energy Piles

The two most known thermo-mechanical field tests on energy piles have been performed by Laloui (2006) and Bourne-Webb (2009). Laloui (2006) performed a series of thermal and mechanical loading tests on a full-scale foundation in Switzerland. In this field-test, one of the piles under a new four-story building at École Polytechnique Fédérale de Lausanne (EPFL) was used as an energy pile. The foundation tested by Laloui (2006) was a 25.8m-long drilled shaft having a diameter of 0.88 m was equipped with a single U-shaped polyethylene tube configuration. The temperature changes applied on the test pile were 21°C for the initial test, without structural load, and around 15°C (values usually encountered in heat exchanger piles) for the successive tests under structural load. The maximum thermally induced axial compressive load along the test pile was 2100 kN during the first test and 2700 kN during the fifth test. In Laloui’s field test study, due to thermal expansion of the test pile during the first test, negative shaft resistance (downward shaft resistance) at the upper portion of the pile and positive shaft resistance (upward) at the lower portion of the pile were observed.

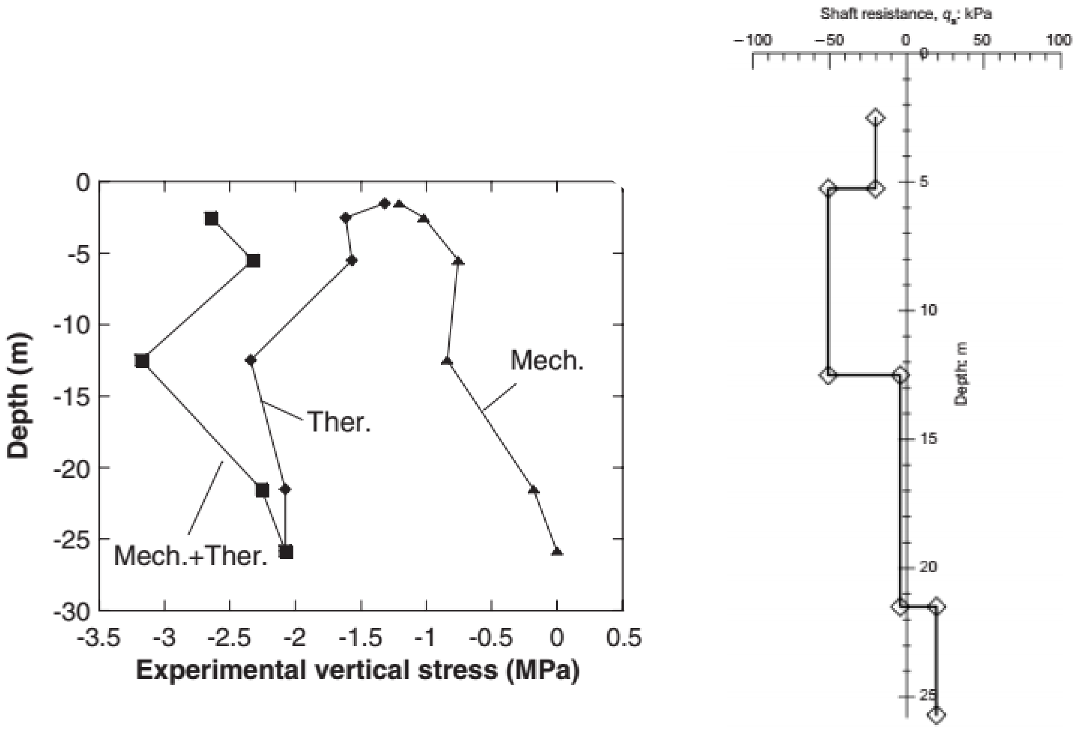

(a) (b)

Figure 2-7: (a) Experimental thermo-mechanical vertical stresses ,Test 1, △T =15°C (b) Experimental Thermal Mobilized shaft resistance, Test 1, △T =21°C.

In England at Lambeth College, the other important series of thermal and mechanical loading tests on a full-scale foundation was performed by Bourne-Webb (2009). In this field test, 23 m long, 0.6m diameter pile was loaded to a nominal working load of 1200 kN, and then cycles of cooling (input temperature at heat pump -6^{0}C) and heating (input temperature +56^{0}C) was applied. Likewise, Lausanne test result, the axial load increases in the upper part of the pile and then reduces with depth over the remaining length. In addition, negative shaft resistance at the upper portion and positive shaft resistance at the lower portion of the pile were observed.

2.5. Numerical Studies on Energy Piles

There are numerous factors that affect the thermal load response of energy pile. Such as, pile geometry and properties, soil conditions, extent of the temperature changes and the effect of the load from supper structures (Laloui et.al ,2006; Bourne-Webb, Amatya et.al, 2009; Olgun & McCartney, 2014).It is difficult to evaluate all these factors through experimental studies. Hence, efforts on advancement of numerical models for simulating the behavior of energy piles are crucial. Furthermore, for the design and wider application of the energy piles, numerical models play the most important role.

A number of studies have been published by various researchers for simulating the thermo-mechanical behavior of energy piles. As mention earlier, these models can be classified in two main groups: load-transfer models (Knellwolf, 2011; Plaseied, 2012; Suryatriyastuti, 2013; McCartney & Chen, 2016) and numerical models (Laloui et.al, 2006; Ouyang, 2011; Wang, 2015; Chakraborty, 2017). In the load-transfer models, t-z curve relationships that have already been developed for axial pile loads in the literature are used and adapted for thermal loads. On the other hand, full-numerical approaches include the use of finite element or finite difference methods of calculation, which can be used to model any type of thermo-active geostructures.

2.5.1. Load-Transfer Model

When a pile is subjected to an axial compressive load, the soil around the pile shaft generated upward frictional forces to resist the applied load. After the entire shaft resistance is mobilized, the underneath the toe of the pile reacts against the compressive load through a base resistance. The amount of the shaft resistance and toe resistance mobilized during an axial loading is proportional to the displacement along the soil-pile interface and at the pile toe, respectively. Load-transfer curves define the relationship between the displacement and unit resistance at the shaft and toe of the pile, namely t_s-z, t_b-z curves, respectively.

In various studies, the load-transfer approaches that are already developed for the axial loading of conventional piles are modified to model thermo-mechanical load transfer analysis of energy piles. In most of the studies using the load-transfer approach for energy piles, it is assumed that the soil behavior and hence the t_s-z, t_b-z curves are not affected by the temperature changes. Thus, the existing theory for conventional piles is utilized to relate the thermal displacement of the energy piles at the shaft and at the base (Knellwolf, 2011; Pasten, 2014; McCartney & Chen, 2016).

Knellwolf (2011) performed one of the first studies to modify the conventional load transfer approach from Coyle and Reese (1966) to consider thermo-mechanical load transfer analysis, where the pile is divided into rigid elements that are connected to each other and to the surrounding soil by the springs. The model is capable of simulating mechanical, thermal and thermo-mechanical behavior of the energy piles. In other words, the model allows the application of mechanical loading which is followed by thermal loading. However, the model is not capable of simulating the behavior of an energy pile during multiple temperature cycles.

In the approach of Burlon et al. (2013), a load-transfer method was also adapted for modeling the thermal response of energy piles by assuming that the temperature change only affects the pile behavior. The restraining effect of a structural load was simulated by the inclusion of a spring on top of the pile. Although the model was not verified by experimental results, the outcomes of the parametric study were collected into a design chart showing the thermally induced axial stresses and pile head movements with respect to various temperature changes and pile head fixity. In this approach, the mechanical and thermal loads are not coupled and their sequence does not have an influence on the overall pile behavior.

Another study where load-transfer approaches is utilized by Plaseied (2012), where the mobilized side shears and end bearing resistance springs were represented by hyperbolic curves (Fig.2-8). Plaseied (2012) also considered the role of radial expansion of the foundation elements, but did not perform a through parametric evaluation of this parameter. The algorithm in the model also fails to capture the exact location of the null point, and requires the user to choose the null-point, which leads to potentially inaccurate results.

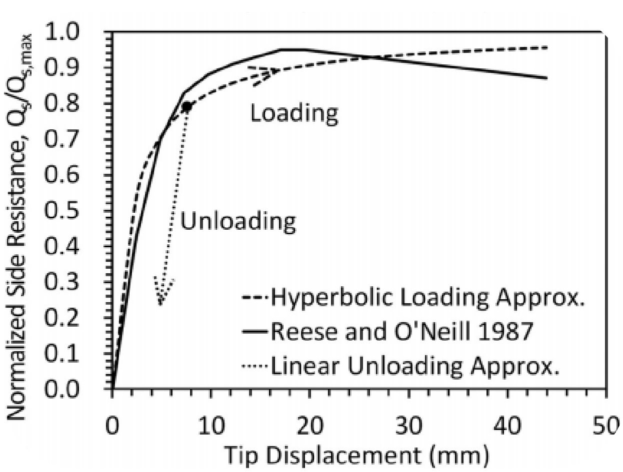

(a)

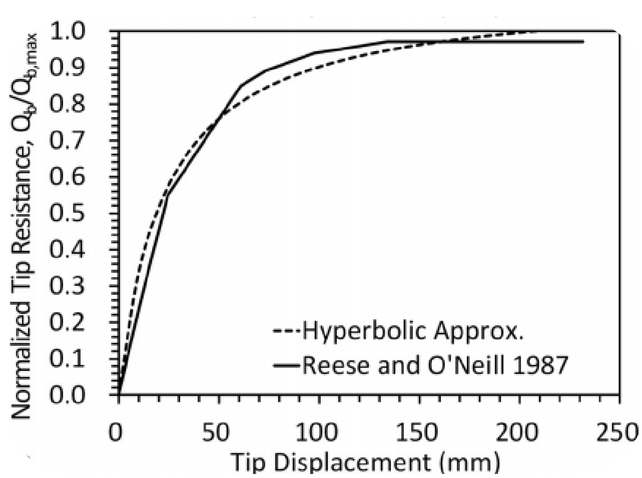

(b)

Figure 2-8: Typical nonlinear spring inputs and hyperbolic approximation for the load transfer analysis: (a) Normalized side shear resistance (b) Normalized tip resistance

Pasten & Santamarina (2014) modified the one-dimensional pile-soil load transfer method of Coyle and Reese (1966) to investigate the effect of cyclic thermal loading on energy piles. In the model, both the shaft friction and tip resistance were assumed linear elastic-perfectly plastic. The temperature change was assumed constant along the pile length, and the effect of temperature change on the pile-soil interaction was neglected. Although the model was not validated with experimental results, the model outputs show that as the structural load on top of the pile is increased, thermally induced settlements are also increasing and finally reaching an asymptotic value. Considering the nature of the load-transfer curve, increase in thermally induced settlements with increasing structural load would be expected.

Thermo-mechanical load transfer analysis has been validated on the basis of in-situ measurements of the loads and deformations experienced by heat exchanger test piles (Knellwolf 2011; Plaseied 2012), but the choice of parameters for this method need to be studied in order to put this method to practical use. One of the recent effort has been made by McCartney & Chen, 2016) ,where a parametric evaluation was performed to understand the effects of different parameters on the stress-strain response energy pile . The model modified by McCartney & Chen, (2016)was fitted to the experimental results from four different studies to calibrate the different model parameters.But,this effort is restricted to only homogenous cohesionless soil.

2.5.2. Numerical Model

Laloui et al. (2006) applied the finite element method to model the response of an energy pile. In this fully coupled thermo-hydro-mechanical finite element model, pore water pressure generation, solid displacements and heat flow were taken into consideration. A thermo-elastoplastic model was used for the simulation of the soil. A constant temperature change throughout the length of the pile was imposed in the model, and the values of temperature change were determined using the field test results. In this model, fully coupled equations govern the evolution of pore water pressure, solid displacement and heat flow under mechanical, hydraulic and thermal loading.

Mathematical formulation: Momentum conservation

$$\nabla\sigma + \rho_{sat} g = 0 \qquad \text{Eq.2-9}$$

where **σ** is the total (Cauchy) stress tensor with tensile stresses taken as positive, ρ_{sat} the total average mass density, $\rho_{sat} = n\rho_f + (1-n)\rho_s$,with ρ_f, ρ_s the mass density of the solid and the fluid phases, respectively; *n* is the porosity, **g** is the gravity vector.

The behaviour of the solid matrix is assumed to be governed by Terzaghi's concept of effective stress expressed by

$$\sigma = \sigma' - p\delta \qquad \text{Eq.2-10}$$

where δ is the Kroenecker's symbol, *p* the pore water pressure and σ' the effective stress tensor

related to the elastic strain ε^e by

$$\sigma' = D : \varepsilon^e \qquad \text{Eq.2-11}$$

where D is the elastic constitutive tensor depending on the Young's modulus, E; and Poisson's ratio, ν : Thus the momentum conservation equation takes the form

$$\nabla(D:\varepsilon^e) - grad\ \mathrm{p} + \rho_{sat} g = 0 \qquad \text{Eq.2-12}$$

Mass conservation

The continuity equation states:

$$\frac{\partial_t p}{Q} - \frac{\partial_t T}{Q'} + \nabla\partial_t u_{rf} + \nabla\partial_t u_s = 0 \qquad \text{Eq.2-13}$$

with T being the temperature, u_{rf} the relative fluid velocity with respect to solid and u_s us the solid displacement. Assuming linear compressibility and thermal expansion of phases, Q and Q' are given by

$$Q = \frac{1}{[n\beta_f + (1-n)\beta_s]}; \quad Q' = \frac{1}{[n\beta'_f + (1-n)\beta'_s]} \qquad \text{Eq.2-14}$$

where β_α is the compressibility of the phase α (α =s for solid or f for fluid) at constant temperature T; $\beta_\alpha^{'}$ is the coefficient of thermal (volumetric) expansion of the corresponding phase at constant pore water pressure. The temperature is assumed to remain the same in both phases. Darcy's law is used to describe the relative fluid velocity

$$\partial u_{rf} = -K^* grad(p + \rho_f gx) \qquad \text{Eq.2-15}$$

with K^* being the kinematic permeability tensor and **x** the position vector of the material point.

Energy conservation

With c; c_f and Λ being the total equivalent specific heat, the specific fluid heat, and the coefficient of the equivalent-medium thermal conductivity, respectively, and assuming Fourier's linear law, energy conservation is given by

$$\begin{aligned} &\rho c \partial_t T + \rho_f c_f \partial_f u_{rf} grad\ T + \rho c T \nabla \partial_t u_s + \rho_f c_f T \nabla \partial_t u_{rf} \\ &-\left[\frac{\beta'_f}{\beta_f} \nabla(n \partial_t u_s + \partial_t u_{rf}) + (1-n) \partial_T \sigma' : d_t \varepsilon_s \right] T - \nabla[\Lambda grad\ T] = 0 \end{aligned} \qquad \text{Eq.2-16}$$

In the case of heat exchanger piles, the heat convection as well as the porosity variation effects on the heat transfer may be neglected. The energy equation takes the following simple form:

$$\rho c \partial_t T - \nabla[\Lambda grad\ T] = 0 \qquad \text{Eq.2-17}$$

As may be seen, the fundamental laws governing static equilibrium (Equation (2-12)), fluid flow (Equation (2-13)) and heat flow (Equation (2-17)) are coupled throughout the dependent variables of solid displacement vector, pore water pressure and temperature in the medium. The energy equation (Equation (2-17)) can be solved independently from the other two because only the temperature appears as variable.

Constitutive behaviour of the solid matrix: Drucker–Prager thermo-elastoplastic model. The behaviour of clays and other fine-grained soils (usual host media for deep geostructures) is strongly affected by temperature variations and exhibits thermo-plastic behaviour . To describe such complex behaviour, several advanced thermo-mechanical models are available. In this work, a simple version of thermo-elastoplastic model is used for the simulation of the behaviour of both the concrete pile and the surrounding soil.

In incremental form, the total strain, $\dot{\varepsilon}$; is divided into two parts:

$$\dot{\varepsilon} = \dot{\varepsilon}^{Te} + \dot{\varepsilon}^{p} \qquad \text{Eq.2-18}$$

where $\dot{\varepsilon}^{Te}$, is the linear thermo-elastic strain rate and $\dot{\varepsilon}^{p}$ the plastic strain rate.

Thermo-elastic part: The thermo-elastic strain rate is expressed as

$$\dot{\varepsilon}_v^{Te} = \frac{\dot{p}'}{K} + \beta_s'\dot{T} \qquad \text{Eq.2-19}$$

$$\dot{\varepsilon}_d^{e} = \frac{\dot{q}}{G} \qquad \text{Eq.2-20}$$

where $\dot{\varepsilon}_v^{Te}$ is the volumetric strain rate and $\dot{\varepsilon}_d^{e}$ the deviatoric strain rate; $\dot{q}$ is the deviatoric stress rate and $\dot{p}'$ the rate of the mean effective pressure. K and G are bulk and shear elastic moduli, respectively. $\dot{T}$ is the temperature increment and β' the thermal expansion coefficient of the solid skeleton.

Plastic part: The plastic strain rate is given by

$$\dot{\varepsilon}^{p} = \lambda.\psi \qquad \text{Eq.2-21}$$

with λ being the plastic multiplier and ψ the direction of the strain increment derived from the plastic potential. An associated model with the Drucker–Prager yield limit is adopted here

$$f = \frac{2\sin\phi}{\sqrt{3}(3-\sin\phi)}\sigma_I + \sigma_{II}^{d} - \frac{6c\sin\phi}{\sqrt{3}(3-\sin\phi)} \qquad \text{Eq.2-22}$$

where σ_I *and* σ_{II}^{d} are the first invariant of the effective stress tensor and the second invariant of the deviator of the effective stress tensor, respectively. ϕ is the internal friction angle and c the cohesion. No strain hardening or thermal softening is considered.

Numerical integration

Equations (2-12) (equilibrium), (2-13) (flow) and (2-17) (heat), together with the constitutive thermo-elastoplastic law, constitute a coupled system of equations to be solved. To be able to resolve this formulation for complex geometries and boundary conditions, a finite element approach is adopted. The weak form of the governing equations was obtained using a variational formulation.

Initial/boundary conditions

Let Ω be the domain occupied by the solid skeleton, and Γ its boundary. The problem is to find $\mathrm{u}_s(x,t), p(x,t)\ and\ T(x,t)$ where x is the position vector and t the time such that Equations (2-12), (2-13) and (2-17) are satisfied on Ω, and such that

$$\begin{array}{llll} u_s = u^* & \text{on } \Gamma_u, & \sigma.\text{n=t} & \text{on } \Gamma_\sigma \\ p = p^* & \text{on } \Gamma_p, & \partial_t u_{rf}.\text{n=t} & \text{on } \Gamma_\phi \\ T = T^* & \text{on } \Gamma_T, & q_T.\text{n} = \Theta & \text{on } \Gamma_{\phi T} \end{array}$$

together with the initial conditions

$$\mathrm{u}_s(x,0) = \mathrm{u}_{s0}(x), \qquad p(x,0) = p_0(x), \qquad T(x,0) = T_0(x)$$

where q_T is the heat flow given by Fourier's law. $\Gamma_u, \Gamma_\sigma, \Gamma_p, \Gamma_\phi, \Gamma_T, and\ \Gamma_{\phi T}$ are the parts of the boundary on which the solid displacements, the total stress vector, the pore water pressure, the fluid flux, the temperature and the thermal flux, respectively, are prescribed.

Weak formulation and finite element discretization

Let V, Q and F be the spaces of admissible virtual displacements, pressures and temperatures, respectively,

$$V = \{v/v \quad \text{smoooth on } \Omega/v=0 \text{ on } \Gamma_u\}$$
$$Q = \{q_v/q_v \quad \text{smoooth on } \Omega/q_v=0 \text{ on } \Gamma_p\}$$
$$F = \{\theta/\theta \quad \text{smoooth on } \Omega/\theta=0 \text{ on } \Gamma_T\}$$

Thus, Equations (2-12), (2-13) and (2-17) of the initial/boundary value (THM) problem, after applying the Green–Gauss theorem with the boundary conditions previously described, become

$$\begin{aligned}&\forall v \in V, \quad (\nabla\{D{:}\varepsilon(u_s)\}, v)_\Omega - (\beta' T, \nabla(v))_\Omega - (p, \nabla(v))_\Omega \\ &= (\rho_{sat}(u_s, T)g, v)_\Omega + \langle t, v\rangle_{\Gamma_\sigma}\end{aligned} \qquad \text{Eq.2-23}$$

$$\begin{aligned}&\forall q \in Q, \ (\nabla(\partial_t u_s), q_v)_\Omega + (K^* grad\ p, grad\ q_v)_\Omega + (\partial_t p / Q, q_v)_\Omega \\ &-(\partial_t T / Q', q_v)_\Omega = (K^* grad(\rho_f g.x), grad\ q_v) + \langle \phi, q_v\rangle_{\Gamma\phi}\end{aligned} \qquad \text{Eq.2-24}$$

$$\forall \theta \in F, \quad (\rho c \partial_{t,} \theta)_\Omega + (\Lambda\ grad\ T, grad\ \theta)_\Omega = \langle \Theta, \theta\rangle_{\Gamma\phi T} \qquad \text{Eq.2-25}$$

where $(,)_\Omega$ denotes the integration over the domain Ω and $\langle , \rangle_\Gamma$ the integration on its boundary Γ

With the semi-discretization in space by means of isoparametric finite elements, displacements, pore water pressures and temperatures (respectively u_s; p and T) defined in spaces V, Q and F,can be, respectively, approximated by u_{sh}; p_h and T_h; and expressed as follows on V_h; Q_h and F_h; subspaces of V; Q and F

$$\begin{aligned}u_{sh} &= \sum\nolimits_I \left(\sum_{j=1}^{N} u_{SI}^j(t) W_{SI} e_j\right)\\ p_h &= \sum\nolimits_I p_I(t) W_{fI}\\ T_h &= \sum\nolimits_I T_I(t) W_{fI}\end{aligned} \qquad \text{Eq.2-26}$$

where N is the dimension of V_h and $\{\varepsilon_i\}_{i=1,N}$ is a basis of V_h, W_I, W_{fI} and W_{SI} are the interpolation functions on node I of temperature, pore water pressure and displacement, respectively. Hence, the semi-discretized system derived from Equations (2-23) to (2-25) can be written in matricial form

$$\forall j, \forall J, \quad \sum_I (\sum_i K_{IJ,ij} u_{sI}^i - L_{IJ,j} p_I - L'_{IJ,j} T_I) = F_{SJ,j}$$
$$\forall J, \quad \sum_I (\sum_i L_{IJ,ij} \partial_t u_{sI}^i + H_{IJ,} p_I + M_{IJ} \partial_t p_I - M_{TIJ} \partial_t T_I) = F_{PJ} \qquad \text{Eq.2-27}$$
$$\forall J, \quad \sum_I (M'_{TIJ} \partial_t T_I + H_{TIJ} T_I) = F_{TJ}$$

Laloui implemented this three-dimensional formulation of thermo-hydro-mechanical model in a general-purpose finite element code Gefdyn and the thermo-mechanical behaviour of the pile is presented with the following figure.

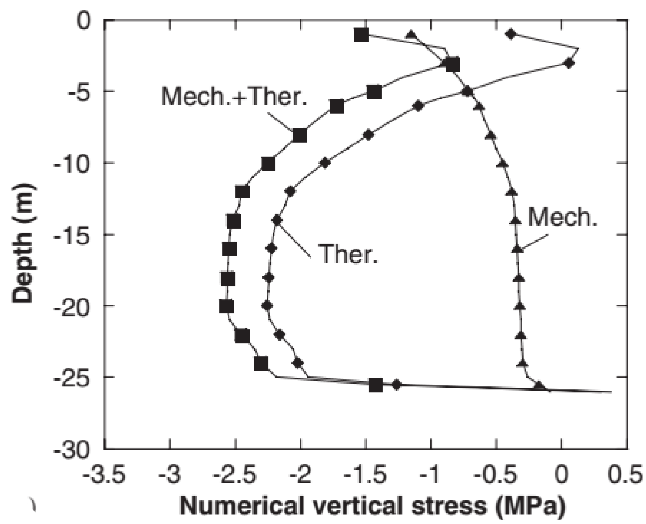

Figure 2-9 Numerical Vertical Stress for 15^{0}C (After Laloui 2006)

CHAPTER 3: METHODS AND MATERIALS

3.1. General

This study evaluate the performance of energy piles foundation by investigating the behaviour in response to thermo-mechanical loading condition in layered soil and also evaluating the expected amount of energy that can be extracted with energy piles. To achieve such objectives, the research is conducted per the methodology described below. Figure 3-1 illustrates the procedure followed in conducting the research.

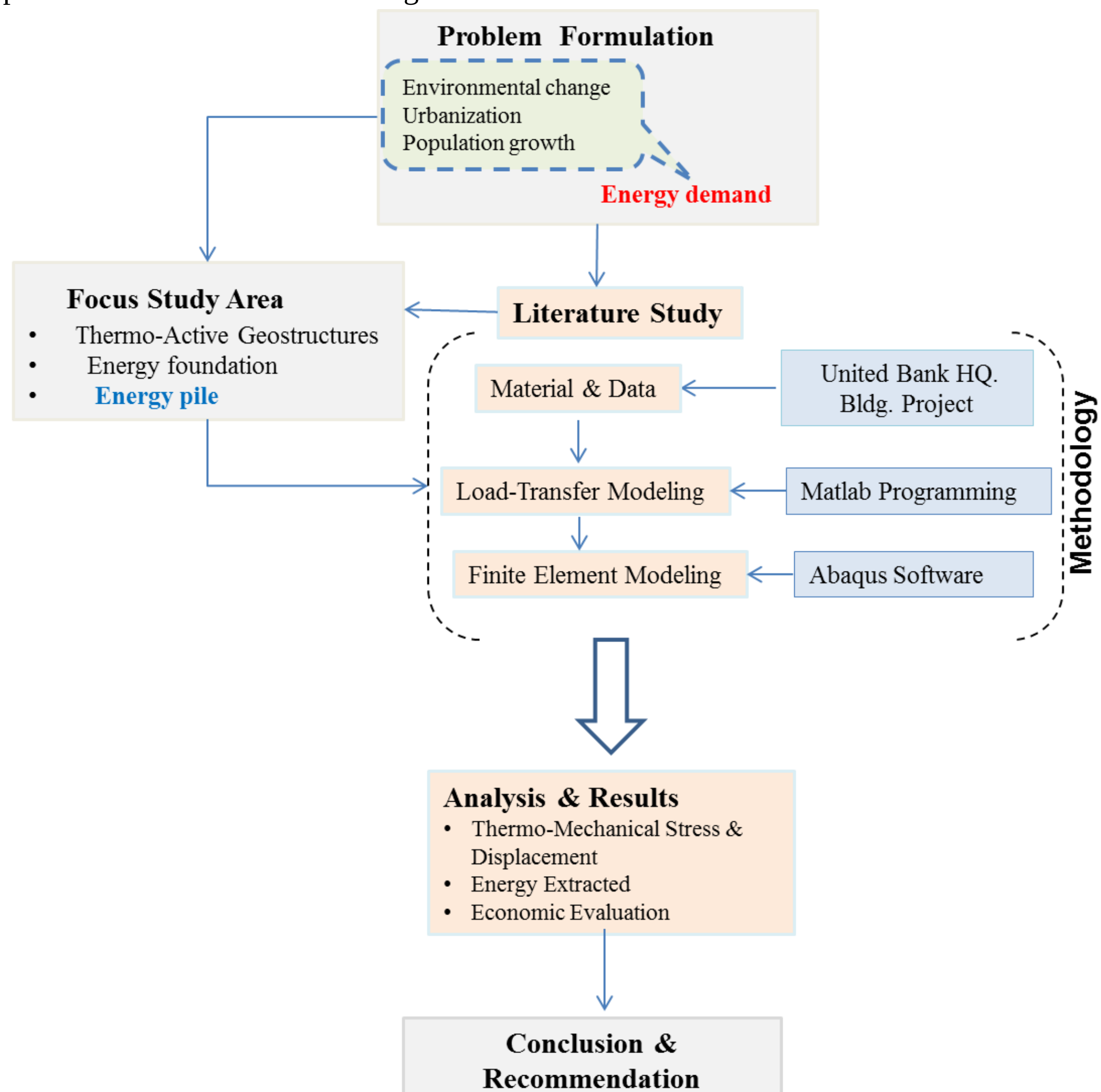

Figure 3-1: Research Framework

As we can see from figure 3-1, due to the rapid growth of population, urbanization and environmental changes, there is a critical energy demands in the country. Owing to this, problem formulation of the study was made on such important issues. In order to finding novel solutions to the new problems related to environmental issues and energy demands, the study focused on thermo-active geo-structure like energy piles foundation: Since they provide a dual purpose for structural stability and alternative energy sources for the building.

Comprehensive literature reviews are made to understand the previous efforts in regarding to the concept, the behaviour and design methods of energy piles. For evaluating, the performance of energy piles under thermo-mechanical loading conditions, load transfer modeling and finite element modeling of energy piles was performed using Matlab programming code and Abaqus Software respectively. The necessary materials and data for numerical study were gathered from (4B+G+30) United Bank Headquarter Building Project, around Mexico Addis Ababa.

From the analysis, a discussion was made to evaluate thermo-mechanical stress and displacement of energy piles foundation under thermo-mechanical loading condition. In addition, evaluation of economic analysis was also made along with the expected amount of energy extracted. Finally, conclusions and recommendations were made based on the outcome of the study.

3.2. Materials

Soil investigation and detailed material report data are the basic input, for the FEM analysis of different geotechnical problems. Most of geotechnical reports that are usually available and/or used in current design and construction practices are commonly done with the intention of determining only the basic soil parameters like cohesion and angle of internal friction. However, other important parameters should be determined to get sufficient input parameters for the FEM model.

Availability of such soil data is the main factor governing the selection of the study area of this thesis. To investigate the performance of energy pile foundation, the data were gathered from

Addis Ababa, around Mexico (4B+G+30) United Bank Headquarter Building Project. The necessary soil and concrete strength parameters were extracted from the project.

3.2.1. Location

Addis Ababa, the capital of Ethiopia, is located in the central highlands of Ethiopia. With an elevation ranging from 2000-2800masl, is the highest capital in Africa. Its topography is constituted by hills, rivers and streams. City Government of Addis Ababa bounded by 9° 00'N and 10° 00'N Latitudes, 37° 30'E and 39° 00'E Longitudes. It is the seat of International Organization, (UNDP, UNICEF, ECA, AU, etc.), high level of governmental and Non-governmental organizations.

3.2.2. Climate

The Climate of Addis Ababa is Woina Dega type Gemechu(1974).The Rainfall has unimodal pattern, one distinct rainy and dry season. The dry season is October through May, the wet season is from June to September and the highest rainfall peakbeing in August. The long-term mean annual rainfall observed at Addis Ababa Observatory is 1254mm (Berhanu, 2002).

The maximum temperature of Addis Ababa ranges between 20^{0}c (in wet season) to 25^{0}c (in dry season), while the minimum falls between 7 - 12^{0}c in the year. This indicates that daily variation of temperature is highly pronounced. Wind speed is generally moderate, ranging between 0.5 to 0.9 m/s. The average daily sunshine hours are 9.5 hours in November & December, and far low, 3 hours, in July and August. Pan-evaporation records at Addis Ababa Observatory showed that the average monthly pan-evaporation during dry season (November) is about 180mm and in wet season (July) falls to 75mm Gemechu, (1974).

3.2.3. Regional Geology

Addis Ababa generally lies in the western margin of the Ethiopian rift and consists of different volcanic rocks that range from basic to acidic composition, belonging to the trap series (Tamiru et.al. 2003).

The north and northeastern area (the Entoto Mountain, the northern and northeastern Addis Ababa) is covered with trachyte, rhyolites, basalts and several episodes of pyroclastic materials of older volcanism occur on the upper part and foothill sides of Entoto ridge. Overlying these, younger basaltic rocks (Addis Ababa Basalt) are found covering the central and southern part of the city.

Outcrops of ignimbrites north of Bole area (Eastern Addis) and Lideta area (Central Addis) have been observed underlying the Addis Ababa basalt. Younger volcanic of trachy-basalt, trachytes, ignimbrites and tuff belonging to the Wochecha, Furi and Yerer volcanoes are recognized overlying un-conformably on the Addis Ababa basalt in the western, south-western and eastern part.

Akaki, Dukem and Debrezeit area are covered with olivine basalt, scoria, scoriaceous basalts and vesicular basalts (Tamiru et.al. 2003). In the upper part, in some places, intercalation of tuffs, sand and gravels are also recognized. In north-east, east and in smaller extent in the western part of DebreZeit, outcrops of trachytes, rhyolitic ignimbrites and tuffs are recognized covering the area. The lacustrine covers Bole, Lideta, Mekanisa, Akaki-Aba Samuel area and Dukem-DebreZeit area. Some alluvial deposit also occur along Big & small Akaki rivers in the southern and south-western part of Addis and minor deposit also occur along Kebena river in the area north-west of Bole.

3.2.4. Site Geology

This report represents the result the geotechnical investigation works for United Bank Share Company Headquarter Building Project, which is located in Addis Ababa, Lideta sub city around Mexico Sengatera. The proposed development consists of the construction of thirteen story building complex with four basement and ground floor (4B+G+30).

Topographically, the site is undulating and partly flat with an elevation difference of about 4m. Eight boreholes were drilled to explore the subsurface geology of the project site. Borehole BH2 & BH5 were drilled to a depth of 50m. Borehole BH1, BH3 & BH4 were drilled to a depth of 45m and the rest of boreholes (BH6, BH7 & BH8) were drilled to 30m depth. The drilling result showed that the project site is constituted by highly weathered basalt intercalated with over consolidated clay. The various geotechnical units that make up the project site can be treated as five major layers, described below.

Layer 1

This is the top firm, expansive clay layer, which original extends to an average depth of 3.6m below the natural ground level and has an average thickness of 1.5m considering an average of 2.25m fill material overlying expansive clay layer. The standard penetration test (SPT) performed gave N-value of 8 to 11 blows for 30cm penetration. The average N-value of the layer is 10. It is surficial covered by about 1.2m to 3.3m thick fill and demolished materials.

Layer 2

This is a thick dense to very dense, pinkish to grayish sandy gravel layer with occasional rock core. The layer is found within average depth interval of 3.6m to 19.50m below the ground level and has an average thickness of 16m. The standard penetration test conducted in the layer resulted in a range of 24 to greater than 50 blows for 30cm depth penetration. The average Nvalue is 48 blows for 30cm penetration.

Layer 3

This very stiff to hard, consolidated silty clay soil layer found below the top highly weathered rock layer and averagely extends from 19.50m to 28.50m below the ground level and has an average thickness of 9m. It is very hard soil layer with an average standard penetration N-value of 45 blows for 30cm depth penetration. This layer is a competent soil layer found underneath the basement floor level.it is underlain by very dense highly weathered basalt (sandy gravel material).

Layer 4

This is the second highly weathered rock (sandy gravel) layer with very stiff reddish silty clay. It is found within an average depth of 28.50 m to 41.80 m below the ground level and has an average thickness of 13m. The standard penetration test conducted inside the layer is in the range of 39 to greater than 50 blows for 30cm depth penetration and the average N-value is 48.

Layer 5

This is moderately weathered, intensively fractured and fragmented rock layer found at variable depth intervals.in boreholes BH2 & BH5,it is encountered beneath layer 4, where as in

BH7 & BH8, it appears overlying the hard reddish brown silty clay layer. In general, the layer is weak to medium strong rock with very poor RQD value (0 to 19%). The range of the SPT value is generally from 19 to greater than 50 and the average N-value is 45.

3.3. Determination of Basic Soil Parameter for the Numerical Model

The soil investigation results, that have been obtained and are used in this study are tabulated and shown in the preceding sections. Parameters necessary for the numerical study have been determined in two ways; by taking directly from the field and laboratory test results. The remaining, perhaps most of the parameters which could not be obtained directly from the laboratory tests, have been indirectly derived by using empirical correlations based on the recommendations of different literature, international geotechnical codes and standards.

3.3.1. Atterberg Limits

Table 3-1: Atterberg limits and unit weight of silty clay layer (19.50-28.50m)

Item No.	BH No.	Depth (m)	Liquid limit (%)	Plastic Limit (%)	Plasticity Index (%)	Unit weight (kN/m^3)	Specific Gravity (Gs)
1	1	20.20	58.46	32.91	25.49	18.07	2.50
2	2	23.10	54.53	35.29	19.24	17.57	2.47
3	3	25.00	49.35	30.73	18.65	16.82	2.50
4	8	28.00	53.80	28.19	25.61	17.38	2.55

3.3.2. Poisson's Ratio, ν

Poisson's ratio is a property that describes the volume change of a material in a direction perpendicular to the application of a load. It is defined as the ratio of the axial compression to the lateral expansion of soils. Teffera & Leikun (1999) recommends a range of values of Poison's ratio between 0.4 and 0.5 for clay and 0.2 to 0.4 for dense cohesion less soil. Hence, typical values of 0.4 and 0.3 have been taken for the numerical analysis of this study respectively.

3.3.3. Stiffness Modulus (Es)

The stiffness modulus Es is a basic parameter that describes the load-settlement behavior of soils and governs the results of settlement related problems. The use of a practical and reasonable stiffness values representing the in situ conditions that has great importance in finite element analysis for better simulation of the actual condition of the soil.

Several methods are available for estimating the stiffness modulus of a soil as described by Bowles (1996). Unconfined compression tests, tri-axial compression tests and in situ tests are among the test methods. While unconfined compression tests tend to give conservative values, tri-axial tests tend to produce more usable values of Es since any confining stress "stiffens" the soil so that a larger initial tangent modulus is obtained.

For United Bank HQ project the geotechnical investigation report has not include E values for the different layers. Therefore, for this study typical range values provided by Teffera & Leikun (1999) was taken.

Once Es has been found, E is determined using the formula based on EVB (1996), it is used as input for ABAQUS software.

$$E = E_s\left(\frac{1-v-2v^2}{1-v}\right) \qquad \text{Eq. 3-1}$$

Where, v = poison's ratio

Based on Eq.3-1 values of stiffness modulus of different soil layers for the projects computed and summarized in Tables 3-2.

Table 3-2: Summary of soil stiffness modulus of united bank HQ building project

Layer	Depth	Description	SPT	Bulk unit weight (γ)	Submerged unit weight (γ')	E_s(MPa)	Poisson's ratio (v)	E(MPa)
1	0-3.60	Expansive Clay	10					
2	3.60-19.50	Dense to Very Dense Sandy Gravel	48	19.50	9.50	150.00	0.3	110.00
3	19.50-28.50	Very Stiff to Hard OC Silty Clay	45	17.93	7.93	80.00	0.4	40.00
4	28..50-41.80	Highly Weathered Rock(Sandy Gravel)	48	20.50	10.50	150.00	0.3	110.00
5	>41.80	Moderately Weathered Fractured Rock	45	20.50	10.50	170.00	0.3	130.00

3.3.4. Shear Strength Parameters

Shear strength parameters, namely, angle of internal friction (∅') and cohesion (c') are determined mostly from the direct shear test result that are taken from samples obtained from shallow depth. But for deeper layers, where laboratory test results are not available, correlation method provided by Bowles (1996), taken from Shioi and Fukui (1982) Japanese standard, has been used to determining angle of internal friction.

$$\phi = \sqrt{18N} + 15 \qquad \text{Eq. 3-2}$$

For sandy and granular soil layers values of internal friction angle are determined using Eq. 3-2 and results are summarized in Tables 3-3. For cohesive soil layers values of internal friction angle (*) and cohesion (*) are directly taken from the respective soil investigation reports.

Table 3-3: Summary of shear parameters of united bank HQ project

Depth (m)	**Description**	**SPT**	Angle of internal friction (Ø')	Cohesion (c), KPa
0-3.60	Expansive Clay	10		
3.60-19.50	Dense to Very Dense Sandy Gravel	48	44.39	0.5
19.50-28.50	Very Stiff to Hard OC Silty Clay	45	33.00*	68*
28..50-41.80	Highly Weathered Rock(Sandy Gravel)	48	44.39	0.5
>41.80	Moderately Weathered Fractured Rock	45	43.46	0.5

3.3.5. Initial stress coefficient, k_0

The initial stress condition of the soil mass is the ratio of the horizontal stresses to the vertical stresses that is called coefficient of earth pressure at rest, k_0. Empirical correlations have been used to determine the value of k_0.

For normally consolidated clays, and for granular soils, Holtz and Kovacs (1981) and Jacky(1944) empirical correlation formulas have been taken respectively as follows:

$$K_o = 0.44 + .0042 \text{ x } I_p$$
$$K_o = 1 - \mathrm{Sin}(\phi) \qquad \text{Eq. 3-3}$$

Where: K_o = coefficient of earth pressure at rest and I_p= plasticity index

Based on Eq. 3.3, values of initial stress coefficient are summarized in Tables 3-4.

Table 3-4: Initial stress coefficient for United Bank HQ building Project

Depth (m)	Description	SPT	Initial stress coefficient (K_o)
0-3.60	Expansive Clay	10	
3.60-19.50	Dense to Very Dense Sandy Gravel	48	0.30
19.50-28.50	Very Stiff to Hard OC Silty Clay	45	0.56
28..50-41.80	Highly Weathered Rock(Sandy Gravel)	48	0.30
>41.80	Moderately Weathered Fractured Rock	45	0.31

3.3.6. Thermal conductivity

In the design of energy pile foundation, accurately, it is important to model the heat transfer process between the pile and the soil, which is largely governed by the soil thermal conductivity. As described earlier, soil thermal conductivity is significantly influenced by its saturation and dry density. An increase in either the saturation or dry density of a soil will result in an increase in its thermal conductivity. Other factors that have a secondary effect upon soil thermal conductivity include mineral composition, temperature, texture, and time. For the preliminary design of complex energy foundations, it can be taken with sufficient accuracy from figures 3-2.by considering water content, saturation density and texture of the soil (Brandl, 2006).The coefficient of thermal expansion of clay and sand adapt $3.4*^{-5}$and $10*^{-4}$°/C respectively,(McTigue, 1986),Tarnawski et al. (2009). In addition, the specific heat capacity of clay and sand is used 880 and 1200 (J/kg C) respectively.

Table 3-5: Thermal conductivity soil parameters for United Bank HQ building Project

Depth (m)	**Description**	**Water content (%)**	**Dry density (t/m^3)**	**Thermal Conductivity (W/mK)**	**Specific heat (J/kg C)**	**Coefficient of thermal expansion, α**
3.60-19.50	Dense to Very Dense Sandy Gravel	24.30	1.57	1.76	1200	10*$^{-4}$
19.50-28.50	Very Stiff to Hard OC Silty Clay	27.24	1.41	1.32	880	3.4*$^{-5}$
28.50-41.80	Highly Weathered Rock(Sandy Gravel)	23.49	1.66	1.81	1200	10*$^{-4}$
>41.80	Moderately Weathered Fractured Rock	21.53	1.69	1.82	1200	10*$^{-4}$

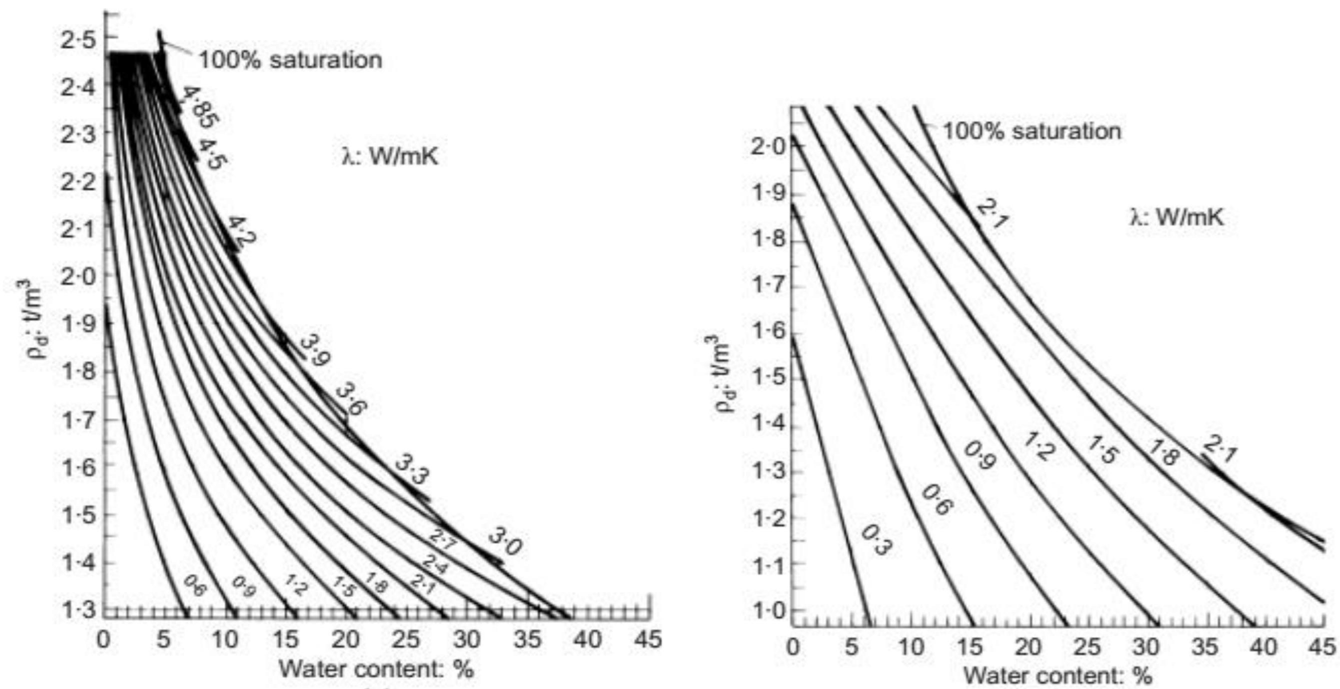

Figure 3-2: Thermal conductivity against dry density and water content for coarse-grained soil &fine-grained soil, (Jessberger & Jagow-Klaff, 1996): (a) coarse-grained soil (b) fine-grained soil

3.4. Load-Transfer Method

3.4.1. Load Transfer Model for Energy piles

McCartney & Chen, (2016) proposed a load transfer model to predict behavior of energy piles subject to combined mechanical and thermal loading. The thermo-mechanical load transfer analysis is based on the following assumptions:

1. The properties of the pile namely its Young's modulus (E) and coefficient of thermal expansion (αT) remain constant along the length of the pile.
2. Downward and upward movements are taken as positive and negative respectively. Compressional stresses are also taken to be positive.
3. Foundation expands and contracts about a point referred to as the null point when it is heat or cool (Bourne-Webb et al. 2009). Expansion strains are assumed negative.
4. Depending on the particular details of the soil profile, the ultimate side shear resistance can be assumed to be constant with depth in a soil layer (i.e., the α method) (Tomlinson, 1957) or it can be assumed to increase linearly with depth in a soil profile (i.e., the β method) (Rollins et al. 1997).

In this approach, discretizing the pile into a series of elements is one of the important tasks in load transfer analysis of energy pile. Accordingly, the typical geometric variables and a schematic of the discretized energy pile and a typical element *i* as presented in Figure 3-3.
The behavior of each pile elements are represented by a spring with stiffness of K^i. The spring stiffness K^i is defined by the following equation:

$$K^i = \frac{E^i A^i}{L^i} \qquad \text{Eq. 3-4}$$

Where A^i is the cross section area of element i, E^i is the Young's modulus of the reinforced concrete in element i, and L^i is the length of the pile element i.

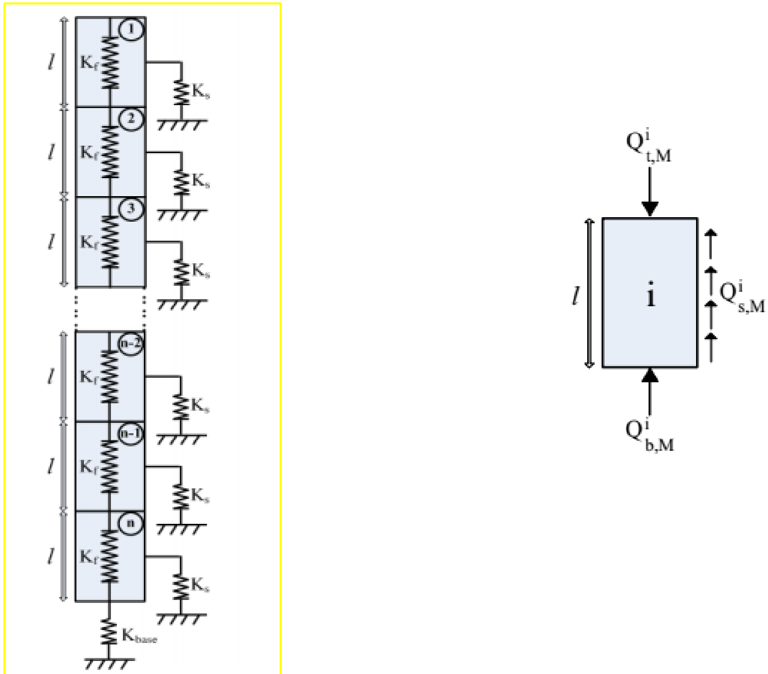

(a) (b)

Figure 3-3:(a) Discretized energy pile used in the load transfer analysis and (b) Typical pile element i (after McCartney & Chen, 2016)

The upward soil reaction force at the pile tip (or base) is modeled using a nonlinear spring (K_b). The spring response is specified as dimensionless tip stress (ratio of tip stress to tip bearing capacity) versus the relative displacement of the foundation toe, referred to as the Q-z curve. Likewise, the mobilization of side shear resistance with displacement defined using a curve of dimensionless side shear versus relative movement between the element and the soil. The dimensionless side shearing stress is typically expressed as the ratio of the actual shearing stress to the shearing stress at failure, and dimensionless movement is the ratio of actual movement to the movement at failure. The dimensionless shearing stress versus displacement is usually referred to as the T-z curve. An example of Q-z and T-z curves for a drilled shaft foundation developed by O’Neill and Reese (1998) are presented in Figure 3-4.

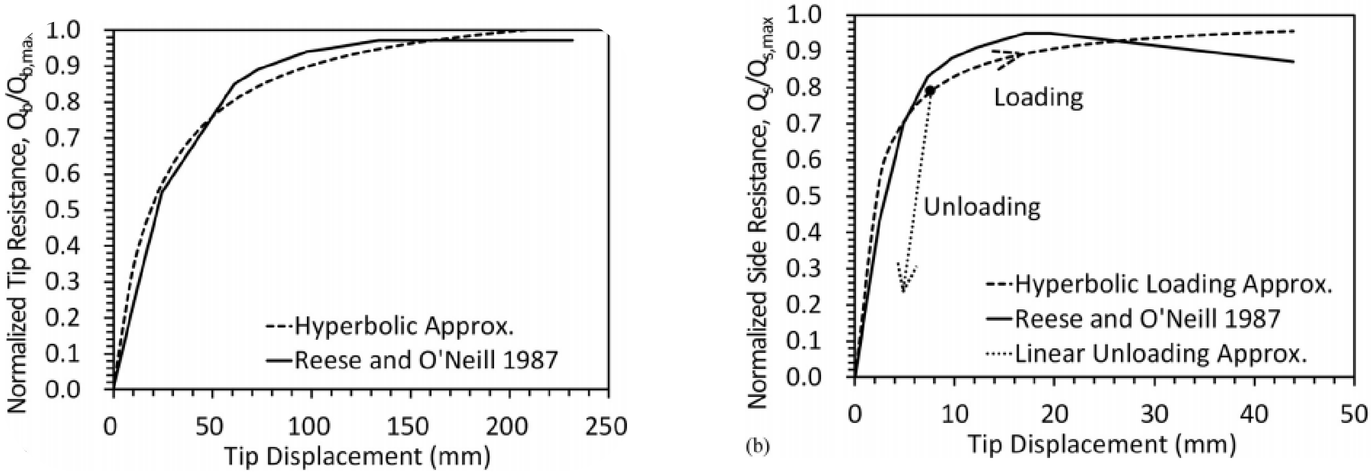

(a) (b)

Figure 3-4: Typical nonlinear spring inputs for the load transfer analysis: (a) Q-z curve; (b) T-z curve (Reese and O'Neill 1988)

The Q-z and T-z curves in Figure 3-4 are nonlinear, and have approximately hyperbolic shape. The normalized side shears resistance (f_{T-z}) and the normalized base reaction (f_{Q-z}) at any relative displacement can be obtained using following equations:

$$f_{T-Z}(\rho_S^i) = \frac{Q_{s,M}^n}{Q_{s,\max}^n} = \frac{\rho_S^i}{a_s + b_s \rho_s^i} \qquad \text{Eq.3-5}$$

$$f_{Q-Z}(\rho_b^n) = \frac{Q_{b,M}^n}{Q_{b,\max}^n} = \frac{\rho_b^n}{a_b + b_b \rho_b^n} \qquad \text{Eq.3-6}$$

Where: $Q_{s,\max}$ is the ultimate end bearing resistance, $Q_{s,\max}^n$ is represents the initial side shear resistance after the mechanical loading is applied and f_{T-Z} is normalized force values that depend on the displacement of side elements ρ_s^n.

$Q_{b,\max}$ is ultimate end bearing resistance, $Q_{b,M}^n$ is mobilized values of base reaction and f_{Q-Z} is normalized force values that depend on the displacement of toe elements ρ_b^n.

a_s & b_s and a_b & b_b are parameters that determine the shape of the T-z curve and Q-z curve respectively.

3.4.2. Mechanical Load Transfer Analysis

First assume a pile under mechanical loading; the pile is first discretized into n elements. The value of the displacement at the bottom of the pile ρ_b^n is assumed for initiating the analysis. The value of $Q_{base,M}$ can be defined as a function of the base displacement ρ_b^n using the Q-z curve. From the relationship in equation 3-6, the axial forces at the base and top of the i^{th} element are defined as follows.

$$Q_{b,M}^n = Q_{b,\max}^n \cdot f_{Q-Z}(\rho_{b,M}^n) \qquad \text{Eq.3-7}$$

The average axial force in the element can be calculated by averaging the axial force at the top $Q_{t,M}^n$ (initially zero) and bottom $Q_{b,M}^n$ for element *n*, as follows:

$$Q_{avg,M}^n = (Q_{b,M}^n + Q_{t,M}^n)/2 \qquad \text{Eq.3-8}$$

Next, assuming a constant shear stress along the lower half side of the element, the direct application of Hooke's law yields an elastic compression, (Δ_M^n), in the middle of element *i* can be calculated by dividing the average force Q_{avg}^n by the stiffness of the K^n, as follows:

$$\Delta_M^n = Q_{avg,M}^n / K^n \qquad \text{Eq.3-9}$$

The displacement at the side of the element $\rho_{s,M}^n$ is defined by adding the settlement at the bottom of the element plus one-half the elastic compression Δ_M^n /2 of the element, as follows:

$$\rho_{s,M}^n = \rho_b^n + \frac{1}{2}\Delta_M^n \qquad \text{Eq.3-10}$$

Next, the mobilized side shear force on this element $Q_{s,M}^n$ is then defined using the T-z curve and the displacement at the side $\rho_{s,M}^n$, as follows:

$$Q_{s,M}^n = Q_{s,\max}^n \cdot f_{T-Z}(\rho_{s,M}^n) \qquad \text{Eq.3-11}$$

Finally, a new force at the top of the element $Q_{t,M,new}^n$ is defined by adding the force at the base of the element and the force on the side of the element to establish equilibrium, as follows:

$$Q_{t,M,new}^{n} = Q_{b,M}^{n} + Q_{s,M}^{n} \qquad \text{Eq.3-12}$$

If the difference between the new and the assumed forces on the top of the element is not less than a user-defined tolerance , the new axial at the top of the foundation is used to calculate a new average axial stress (Equation 3-8). The process is repeated in sequence until the absolute value of the change in $Q_{t,M}^{i}$ between different iterations becomes less than a user-specified criterion.

When the axial force values for a current element have converged, the same process used for the i^{th} element is used for the $(i-1)^{th}$ element, and so on. The force on the bottom of a subsequent element $Q_{b,M}^{i-1}$ is equal to the new force on the top of the element $Q_{t,M}^{i}$ and the settlement on the bottom of subsequent element $\rho_{b,M}^{i-1}$ is equal to the base settlement plus the elastic compression $\triangle_{M}^{i}$ of the element, as follows:

$$Q_{b,M}^{i-1} = Q_{t,M}^{i} \qquad \text{Eq.3-13}$$

$$\rho_{b,M}^{i-1} = \rho_{b,M}^{n} + \triangle_{M}^{i} \qquad \text{Eq.3-14}$$

When the stresses within the whole pile have converged, the equilibrium, compatibility and the constitutive laws of materials are satisfied in all the pile elements.

However, the load applied to the head of the pile P is not necessarily equal to the force at the top of the head element $Q_{t,M}^{1}$. Thus, Newton's method can be used for quickly finding the toe displacement $\rho_{b,.M}^{n}$ that makes the calculated force at the head of pile turns out to be the actual load from the supper structure ($Q_{t,M}^{1} = P$). To perform Newton's method, $\rho_{b,.M}^{n}$ is assumed and a new value of $Q_{t,M}^{1}$ is calculated. Then, the secant stiffness that passes through origin is calculated using Eq.3-12, as follows:

$$k_{\sec} = Q_{t,M}^{1} / \rho_{b,.M}^{n} \qquad \text{Eq.3-15}$$

Then, the new displacement at the base of pile $\rho_{b,M(new)}^{n}$ is calculated using En.3-16, as follows:

$$\rho^{n}_{b,M(new)} = \rho^{n}_{b,M} + k_{\sec}(P - Q^{1}_{t,M}) \qquad \text{Eq.3-16}$$

Where, P is the applied mechanical axial load from the structure. Finally, after several iterations, the acceptable solution will be achieved as the value of the unbalanced force falls within the desired tolerance.

3.4.3. Thermal Load Transfer Analysis

The load transfer analysis can also be used to predict the settlement and stress distribution in energy piles subject to thermal loading (i.e., without mechanical loading). In this regard, a spring should be added to the top of the pile, which represents the pile head-structure stiffness (Knellwolf et al. 2011). The “null point” location is a very important to determine the thermal response of the energy pile during heating/cooling process (Figure 3-5).

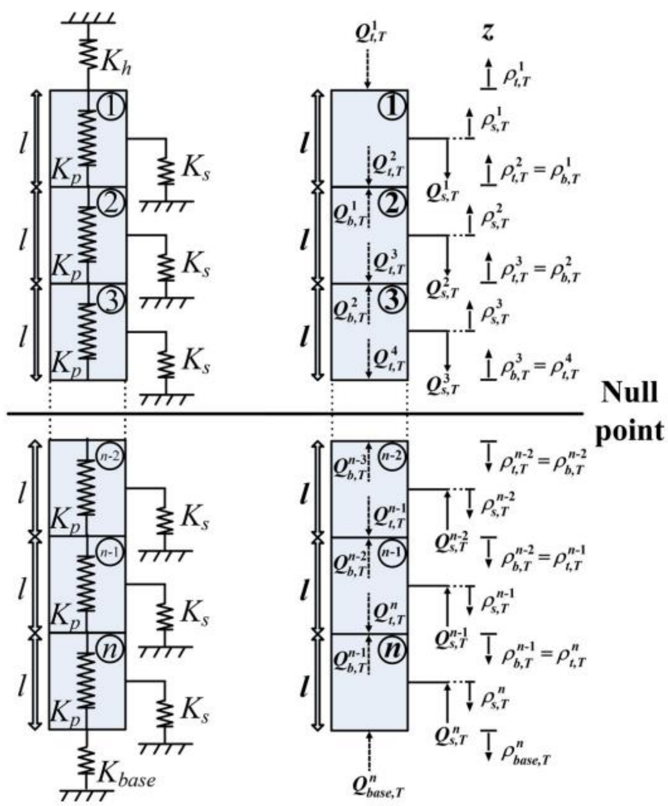

Figure 3-5: Finite-difference model for energy pile, heating (after Knellwolf et al. 2011)

When an energy pile is heated or cooled, it begins to expand or contract about its NP (Bourne-Webb et.al.2009), which is defined as the location in the pile in which there is no thermal expansion or contraction, assuming that the temperature change occurs uniformly throughout the pile.

In order for the displacement at the null point (denoted as NP) to be zero, the sum of the mobilized shear resistance and the structure reaction for the upper section of the null point should be equal to the sum of the mobilized shear resistance and the base reaction in the lower one (Knellwolf et al. 2011). Eq.3-17 through Eq.3-20 can be used to define the null point location along the foundation.

$$\sum_{i=1}^{NP} Q_{s,T}^{i} + Q_{t,T}^{1} = \sum_{i=NP+1}^{n} Q_{s,T}^{i} + Q_{b,T}^{n} \qquad \text{Eq.3-17}$$

$$Q_{t,T}^{1} = K_h \cdot \rho_{t,T}^{1} \qquad \text{En.3-18}$$

$$Q_{b,T}^{n} = Q_{b,\max}^{n} \cdot f_{Q-Z}(\rho_{b,T}^{n}) \qquad \text{Eq.3-19}$$

$$Q_{s,T}^{i} = Q_{s,T,\max}^{i} \cdot f_{T-Z}(\rho_{s,T}^{n}) \qquad \text{Eq.3-20}$$

Where, $Q_{b,T}^{n}$ represents the base response to the thermal expansion and contraction is defined using Q-z curve. $Q_{t,T}^{1}$, represent that the structure response is linearly proportional to the relative displacement of the head of the foundation. $Q_{s,T}^{i}$, is the shear resistance of the foundation and can be determined by T-z curve. K_h represents the pile head-structure stiffness, which depends on several factors including the rigidity of the supported structure, the type of contact between the foundation and the mat or raft, and the position and the number of energy piles (Knellwolf et al. 2011).The values of $\rho_{t,T}^{1}$ and $\rho_{b,T}^{n}$ represents the relative displacements at the head and the base of the foundation, respectively. $\rho_{s,T}^{i}$, is the relative thermal displacement at the side of the element i.

To calculate the settlement and stress distribution of the energy pile (under heating load for example), the first step is to assume the null point location, NP. Then, appropriately divide the pile above the NP into n_1 elements and the pile below the NP into n_2 elements. The pile is assumed to be totally free to move (Knellwolf et al. 2011).

The mechanical load transfer analysis is performed, and the displacements and forces on each element of the pile under mechanical loading are used as the initial condition for heating the energy pile. After this preprocessing is done, the energy pile is initially assumed to be totally free to move, similar to the approach of Knellwolf et al.(2011), in which case an initial estimate of the thermal elongations of each element can be obtained from the following expression:

$$\Delta_T^i = L^i \alpha_T \Delta T \qquad \text{Eq.3-21}$$

Where L^i is the length of pile element and the superscript, i represent the element number along the energy pile.

For the part of the energy pile below the NP, these elements move downward. Thus, the thermal displacement at the top, middle, and base of the element (n_1+1) downward to element, n can be calculated as follows:

$$\begin{aligned} \rho_{t,T}^i &= \{ \ 0 \qquad for\ i \neq n1+1 \\ &= \{ \ \rho_{t,T}^{i-1} \qquad for i \neq NP \end{aligned} \qquad \text{Eq.3-22}$$

$$\rho_{s.T}^i = \rho_{t,T}^i + \frac{1}{2}\Delta_T^i \qquad \text{Eq.3-23}$$

$$\rho_{b.T}^i = \rho_{t,T}^i + \Delta_T^i \qquad \text{Eq.3-24}$$

Next, the thermal force at the base, side, and top of the elements from n upward to the element (n_1+1) can be calculated using the following equations:

$$Q_{b,T}^i = Q_{b,\max} \cdot f_{Q-z}(\rho_{b.T}^i) \qquad for\ i = n \qquad \text{Eq.3-25}$$

$$Q_{s,T}^i = Q_{s,T,\max} \cdot f_{T-z}(\rho_{s.T}^i) \qquad \text{Eq.3-26}$$

$$Q_{t,T}^{i} = Q_{s,T}^{i} + Q_{b,T}^{i} \qquad \text{Eq.3-27}$$

In addition, the thermally induced axial stress at the middle of each element can be calculated as follows:

$$\sigma_{T}^{i} = \frac{Q_{t,T}^{i} + Q_{b,T}^{i}}{2A_{b}} \qquad \text{Eq.3-28}$$

After the forces acting on these elements are defined, the actual thermal elongation of each element is calculated as follows:

$$\Delta_{T,actual}^{i} = \Delta_{T}^{i} - \frac{\sigma_{T}^{i} \cdot L^{i}}{E} \qquad \text{Eq.3-29}$$

The actual thermal elongation in each element will be lower than that present when the energy pile is free to move from the bottom. This actual thermal elongation should be replaced with the initial thermal elongation (free boundary), the process from Eq.3-22 to 3-28 should be repeated in order to get a new actual thermal elongation from Eq.3-29, and this process should be repeated until the values of actual thermal elongation reasonably converge to a desired tolerance.

For the part of pile above the null point, heating leads to these elements move upward. Thus, from the element above and adjacent the null point to the top element, the displacement can be calculated using Eq.3-30 through 3-32, as follows:

$$\begin{aligned} \rho_{b,T}^{i} &= \{ \ 0 \qquad for \ i = n_{1} \\ &= \{ \ \rho_{t,T}^{i-1} \qquad for \ i \neq NP - 1 \end{aligned} \qquad \text{Eq.3-30}$$

$$\rho_{s.T}^{i} = \rho_{t,T}^{i} - \frac{1}{2}\Delta_{T}^{i} \qquad \text{Eq.3-31}$$

$$\rho_{t.T}^{i} = \rho_{t,T}^{i} - \Delta_{T}^{i} \qquad \text{Eq.3-32}$$

3.4.4. Thermo-Mechanical Load Transfer Analysis

The most accurate representation of energy piles can be obtained using a thermomechanical T-z analysis, in which the thermal loading is applied to an energy pile under an initial mechanical load. To calculate the thermo-mechanical response of the energy pile, the first step is to calculate the distribution in axial and interface displacements and forces along the pile for a given initial mechanical loading. Then the energy pile response due to thermal loading (heating for example) will be applied subsequently to define the overall response of an energy pile subject to thermo-mechanical loading.

The thermo-mechanical process should be started from the "null point" which represents the zero thermal displacement point (not necessarily the point of zero thermo-mechanical displacement). The location of the null point is first assumed to start the analysis, and the part of pile above and below the null point is equally and appropriately meshed into $n1$ and $n2$ elements, respectively (totally N elements). Then, similar to the thermal algorithm, the initial displacements are considered to be the same as the free boundary condition ($\Delta^i{}_T$ = $\mathrm{L}^i\alpha\Delta T$). After the mechanical T-z analysis, a similar thermal T-z analysis is performed to calculate the response of energy pile under the combined thermo-mechanical load.

The thermo-mechanical displacement can be calculated using Eq.3-33through 3-36, as follows

$$\rho^i_{t.MT} = \rho^i_{t,M} + \rho^i_{t,T} \qquad \text{Eq.3-33}$$

$$\rho^i_{s.MT} = \rho^i_{s,M} + \rho^i_{s,T} \qquad \text{Eq.3-35}$$

$$\rho^i_{b.MT} = \rho^i_{b,M} + \rho^i_{b,T} \qquad \text{Eq.3-36}$$

Where, the subscript "MT" represents the combined thermal and mechanical loading. While the base of the energy pile is reached, the thermo-mechanical force in each element can be calculated using Eq.3-37 through 3-41 from the element N down to the element $n1$ +1, as follows:

$$Q^i_{b,MT} = \begin{cases} Q_{b,\max} \cdot f_{Q-z}(\rho^i_{b.MT}) & for\ i = n \\ Q^{i+1}_{t,MT} & for\ i \neq n \end{cases} \quad \text{Eq.3-37}$$

$$Q^i_{s,MT} = Q_{s,T,\max} \cdot f_{T-z}{}^{loading}(\rho^i_{s.MT}) \quad \text{Eq.3-38}$$

$$Q^i_{t,MT} = Q^i_{s,MT} + Q^i_{b,MT} \quad \text{Eq.3-39}$$

$$\sigma^i_T = \frac{Q^i_{t,MT} + Q^i_{b,MT}}{2A_b} - \sigma^i_M \quad \text{En.3-40}$$

Where

$$\sigma^i_M = \frac{Q^i_{avg,M}}{A_b} \quad \text{Eq.3-41}$$

After the forces acting on these elements are defined, the actual thermal elongation of each element is calculated using Eq.3-29 as mentioned before. Again, the actual thermal elongation in each element will be lower than that present when the energy pile is free to move from the bottom. This actual thermal elongation should be replaced with the initial thermal elongation (free boundary) and the process for computing the response for the part of pile elements below the null point should be repeated until the values of actual elongation reasonably converge to desired toleration.

A similar process for solving for the behavior of the part of the energy pile below the NP can be applied for the part above the NP, considering the boundary conditions at the head of the pile instead. It should be noted that in the region of the pile above the NP the pile will move upward and the side shear stress will decrease following the unloading path.

3.5. Finite Element Method

Finite element method is a common tool used for advanced numerical modelling within various fields of engineering. This technique is utilized by numerous engineering disciplines because it can provide numerical approximations to very complex systems. The FEM is carried out by discretizing a body into smaller parts called elements. Each element has a system of equations that are continuous across the entire element and described by the element nodes. Elements are connected to other elements by nodes and are where evaluation of the system takes place. Applied loadings to the element result in displacements, which are then transformed back to a global coordinate system where the solutions can be viewed.

There are numerous FE software programs available. To simulate the behaviour of energy pile foundation, finite element software ABAQUS was used in this paper. Abaqus is general-purpose software that can perform both linear and nonlinear analyses. Moreover, it is used to investigate mechanical and thermal geotechnical problems under static and dynamic loadings. The package has the capability to model complex interaction between different bodies and to account the initial stress states of the material.

3.3.1 General Steps of the Finite Element Method

Finite element methods are at present very widely used in engineering analysis for solving problems of engineering and mathematical models. This method can readily handle complex geometries and complex loadings like point loads, element load (pressure, thermal, inertial forces) and time or frequency dependent loading.

As described on Potts and LidijaZdravkovic (1999), the finite element method involves the following steps.

Element discretization: this is the process of modeling the geometry of the problem under Investigation by assemblage of small regions, termed finite elements. These elements have nodes defined on the element boundaries, or within the element.

Primary variable approximation: a primary variable must be selected (e.g. displacements, stresses etc.) and rules as to how it should vary over a finite element established. This variation is expressed in terms of nodal values. In geotechnical engineering it is usual to adopt displacements as the primary variable.

Global equations: Combine element equations to form global equations

$$\{M_d\} = [K_G]\{D_{dG}\} \qquad \text{Eq.3-42}$$

Where $[K_G]$ is the global stiffness matrix, $\{D_{dG}\}$ is the vector of all incremental nodal displacements and $\{M_d\}$ is the vector of all incremental nodal forces.

Boundary conditions*:* Formulate boundary conditions and modify global equations. Loadings (e.g. line and point loads, pressures and body forces) affect $\{M_d\}$, while thedisplacements affect $\{D_{dG}\}$

Solve the global equations: The global Equations 3-42 are in the form of a large number of simultaneous equations. These are solved to obtain the displacements $\{D_{dG}\}$ at all the nodes. From these nodal displacements, secondary quantities, such as stresses and strains, are evaluated.

3.3.2 Finite Element Modelling of Energy Piles

The pile is installed and is assumed to be perfectly bounded with the surrounding soil.The pile and soil geometries are created as separate parts. Then a finite element model was developed to simulate the energy pile under mechanical and thermal loading conditions. Due to axisymmetric of this problem, only one-half of the cross section is meshed using an 8 node, biquadratic, axisymmetric quadrilateral (CAX8) type element. As shown in figure 3-2.the vertical soil boundary at the right side of the model is placed at a distance of 1.5 pile length from the pile-soil interface. The soil boundary at the bottom is placed at a distance of one pile length from the base of the pile. The base of the mesh is fixed and only vertical movement is allowed along right hand side of the mesh and the axis of symmetry (the left hand side of the mesh). The pile is modeled with linearly elastic elements with a Young's modulus E= 29GPa and Poisson's ratio v=0.2.A constant temperature of 15°C is assumed at the top soil boundary. The ambient ground temperature is assumed 15°C (Laloui et al. 2006). The thermal load ΔT is applied uniformly over the entire length of the pile using a temperature boundary condition.

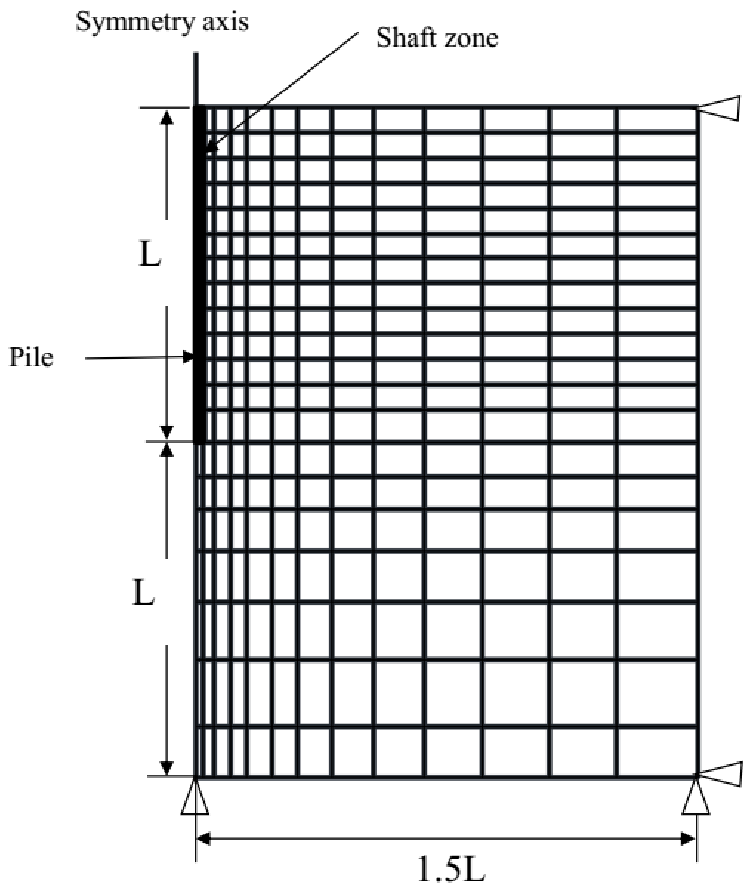

Figure 3-6: Typical discretization of the computational model (Helwany, 2007)

3.5.1. Constitutive Models

When an elastic material is subjected to load, it sustains elastic strains. Elastic strains are reversible in the sense that the elastic material will spring back to its un-deformed condition if the load is removed. On the other hand, if a plastic material is subjected to a load, it sustains elastic and plastic strains. If the load is removed, the material will sustain permanent plastic (irreversible) strains, whereas the elastic strains are recovered. Hooke's law, which is based on elasticity theory, is sufficient (in most cases) to estimate the elastic strains. To estimate the plastic strains, one needs to use plasticity theory.

Plasticity theory was originally developed to predict the behavior of metals subjected to loads exceeding their elastic limits. Similar models were developed later to calculate the irreversible strains in concrete, soils, and polymers.(Sam Helwany 2007). A plasticity model includes (1) a yield criterion that predicts whether the material should respond elastically or plastically due to a loading increment, (2) a strain hardening rule that controls theshape of the stress–strain response during plastic straining, and (3) a plastic flow rule thatdetermines the direction of the plastic strain increment caused by a stress increment.In this study only two plasticity models (Mohr-Coulomb model and Cap model) that are frequently used in geotechnical engineering applications will be reviewed and used in thesimulation of the energy pile with finite element method.

3.5.1.1. Mohr-Coulomb Model

The Mohr-Coulomb failure or strength criterion has been widely used for geotechnical applications. Indeed, a large number of the routine design calculations in the geotechnical area are still performed using the Mohr- Coulomb criterion. The Mohr-Coulomb criterion assumes that failure is controlled by the maximum shear stress and that this failure shear stress depends on the normal stress, (Abacus software manual). This can be represented by plotting Mohr's circle for states of stress at failure in terms of the maximum and minimum principal stresses. The Mohr-Coulomb failure line is the best straight line that touches these Mohr's circles.

The failure envelope, being dependent on the major and minor principle stresses (σ_1 σ_3) as shown in Fig. 3-3, is defined by cohesion, *c* and internal frictional angle, φ

$$\frac{1}{2}(\sigma_1-\sigma_3)\ +\frac{1}{2}(\sigma_1+\sigma_3)\sin\phi-c\cos\phi=0 \qquad \text{Eq.3-43}$$

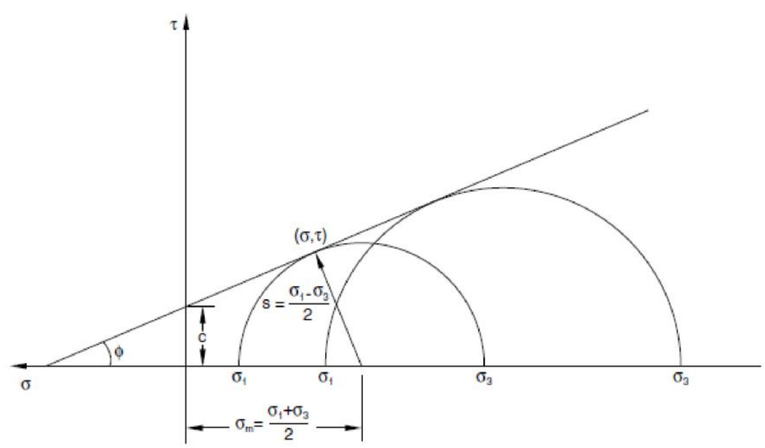

Figure: 3-7: Mohr-Coulomb failure criterion (Adapted from ABAQUS, 2002.)

The failure of typical geotechnical materials generally includes some small dependence on the intermediate principal stress, but the Mohr-Coulomb model is generally considered to be sufficiently accurate for most applications. This failure model has vertices in the deviatoric stress plane.

The constitutive model described here is an extension of the classical Mohr-Coulomb failure criterion. It is an elasto-plastic model that uses a yield function of the Mohr- Coulomb form; this yield function includes isotropic cohesion hardening/softening. However, the model uses a flow potential that has a hyperbolic shape in the meridian stress plane and has no corner in the deviatoric stress space. This flow potential is then completely smooth and, therefore, provides a unique definition of the direction of plastic flow.

3.5.1.2. Modified Drucker-Prager/Cap Model

The Drucker–Prager/cap plasticity model has been widely used in finite element analysis programs for a variety of geotechnical engineering applications. The cap model is appropriate to soil behavior because it is capable of considering the effect of stress history, stress path, dilatancy, and the effect of the intermediate principal stress. The yield surface of the modified Drucker–Prager/cap plasticity model consists of three parts: a Drucker–Prager shear failure surface, an elliptical *cap*, which intersects the mean effective stress axis at right angle, and a smooth transition region between the shear failure surface and the cap, as shown in Figure 3-8.

The cap serves two main purposes: it bounds the yield surface in hydrostatic compression thus providing an inelastic hardening mechanism to represent plastic compaction, and it helps to control volume dilatancy when the material yields in shear by providing softening as a function of the inelastic volume increase created as the material yields on the Drucker-Prager shear failure and transition yield surfaces (Abacus tutorial, 2002).

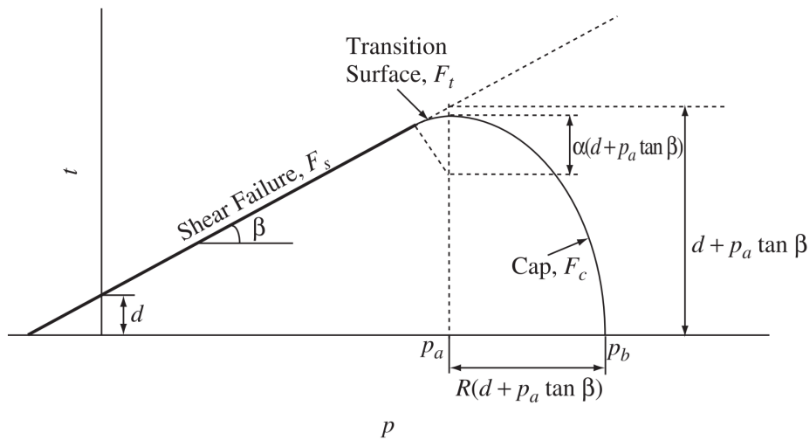

Figure 3-8: Yield surfaces of the modified cap model in the p–t plane. (Adapted fromABAQUS, 2002.)

Where β is the soil's angle of friction and *d* is its cohesion in the *p*–*t* plane, as indicated in Figure 3-8.

The model uses associated flow in the cap region and non-associated flow in the shear failure and transition regions.

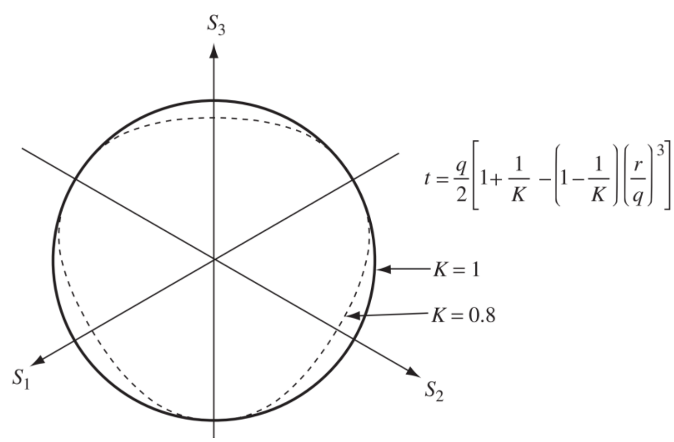

Figure 3-9: Projection of the modified cap yield/flow surfaces on the -plane. (Adapted fromABAQUS, 2002.)

Elastic behavior is modeled as linear elastic using the generalized Hooke's law. Alternatively, an elasticity model in which the bulk elastic stiffness increases as the material undergoes compression can be used to calculate the elastic strains. The onset of plastic behavior is determined by the Drucker–Prager failure surface and the cap yield surface. The Drucker–Prager failure surface is given by Eq.3-44.

$$F_s = t - p\tan\beta - d = 0 \qquad \text{Eq.3-44}$$

Where,t=deviatoric stress with a distinction between compression and extension by

$$t = \frac{q}{2}\left[1 + \frac{1}{K} - \left[1 - \frac{1}{k}\right]\left[\frac{r}{q}\right]^3\right] \qquad \text{Eq.3-45}$$

$$q = \sqrt{\frac{1}{2}((\sigma_1 - \sigma_2)^2 + (\sigma_2 - \sigma_3)^2 + (\sigma_3 - \sigma_1)^2} \qquad \text{En.3-46}$$

$$p = \frac{1}{3}(\sigma_1 + \sigma_2 + \sigma_3) \qquad \text{Eq.3-47}$$

q = deviatoric stress (Misses equivalent stress)

d = cohesion in the p-t-plane

p = hydrostatic stress

b = slope of the yield surface FS in the p-t-plane

K = shape parameter of the yield surface FS determined from tri-axial

compression and extension tests with usual values, 0.778 < K < 1

The cap yield surface is an ellipse with eccentricity = *R* in the *p–t* plane. The cap yield surface is dependent on the third stress invariant, *r*, in the deviatoric plane as shown in Figure 3-9. The cap surface hardens (expands) or softens (shrinks) as a function of the volumetric plastic strain. When the stress state causes yielding on the cap, volumetric plastic strain (compaction) results, causing the cap to expand (hardening). But when the stress state causes yielding on the Drucker–

Prager shear failure surface, volumetric plastic dilation results, causing the cap to shrink (softening). The cap yield surface is given with Equation 3-48.

$$F_c = \sqrt{(p - p_a)^2 + \left(\frac{Rt}{1 + a - a/\cos\beta}\right)^2} - R(d + p_a\tan\beta) = 0 \qquad \text{Eq.3-48}$$

Where R is a material parameter that controls the shape of the cap and α is a small number (typically, 0.01 to 0.05) used to define a smooth transition surface between the Drucker–Prager shear failure surface and the cap defined by Eq. 3-49.

$$F_t = \sqrt{(p - p_a)^2 + \left[t - \left(1 - \frac{a}{\cos\beta}\right)(d + p_a \tan\beta)\right]^2} - a(d + p_a \tan\beta) = 0 \qquad \text{Eq.3-49}$$

P_a is an evolution parameter that controls the hardening–softening behavior as a function of the volumetric plastic strain. The hardening–softening behavior is simply described by a piecewise linear function relating the mean effective (yield) stress p_b and the volumetric plastic strain as shown in Figure 3-8. This function can easily be obtained from the results of one isotropic consolidation test with several unloading–reloading cycles. However, in this study since no triaxial tests are performed, methods specified by Sam Helwany 2007, are used for the computation Equation 3-50.

$$\varepsilon_v^p = \frac{\lambda - k}{1 + e_o} \ln \frac{p'}{p_o} = \frac{c_c - c_s}{2.3(1 + e_o)} \ln \frac{p'}{p_o} \qquad \text{Eq.3-50}$$

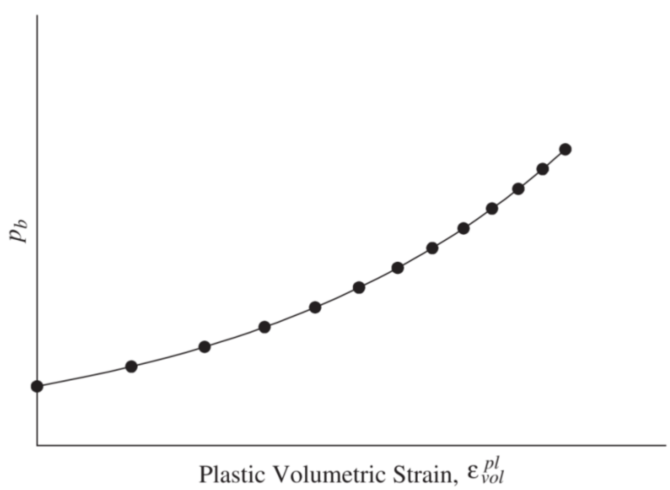

Figure 3-10: Typical cap hardening behavior. (Adapted from ABAQUS, 2002.)

The cap hardening behavior of the different soil layers in all cases of piles are summarized in table 3-6.

Table 3-6:Cap hardening behavior for United Bank HQ building

Soil parameter	**Sym.**	**Unit**	**Dense to Very Dense Sandy Gravel**	**Very Stiff to Hard OC Silty Clay**	**Highly Weathered Rock(Sandy Gravel)**	**Moderately Weathered Fractured Rock**	**Pile**
Modulus of Elasticity	**E**	[MN/m2]	110	40	110	130	29000
Poisson's ratio	**ν**	[-]	0.3	0.4	0.3	0.3	0.2
Unit weight	**γ**	[kN/m3]	19.5	17.93	20.5	20.5	24
Angle of friction	$\emptyset'$	[o]	44.39	33	44.39	43.46	-
Slope of yield surface Fs in the p-t plane	b	[o]	61.27	53.08	61.27	60.74	-
Cohesion	**c**	[kN/m2]	0.5	68	0.5	0.5	-
Intersection of yield surface Fswith t-axis	**d**	[kN/m2]	2.80	418.08	2.80	2.83	-
Initial cap position	ε_v^p	[-]	0	0	0	0	-
Cap Eccentricity	**R**	[-]	0.8	0.1	0.8	0.8	-
Flow stress ratio	**K**	[-]	0.788	0.788	0.788	0.788	-

3.5.2. Interface Modeling

Soil-structure interface modelling is a key issue for many geotechnical analyses. Using the finite element simulation of displacement pile requires application of appropriate modelling of pile elements interactions with the surrounding soil. In computer simulation, one can use the case without a contact (the soil elements and adjacent pile elements are forced to move together) or the case with a contact. The main advantages of using the contacts are: 1) frictional behaviour of a pile with soil is fully represented in the model; 2) different movements of the pile elements and soil (slip) are possible (Wrana, 2013). It should be noted that pile elements are relatively rigid to the surrounding soil deformations. The surface of pile elements that are in contact with the soil elements is referred to as the main surface (*master*). The surface of the soil elements in contact is set as the secondary surface (*slave*). In the ABAQUS program, these surfaces are called *contact pairs*. The contact pair representing the interaction of a pile with the soil is shown in Fig. 3-10.

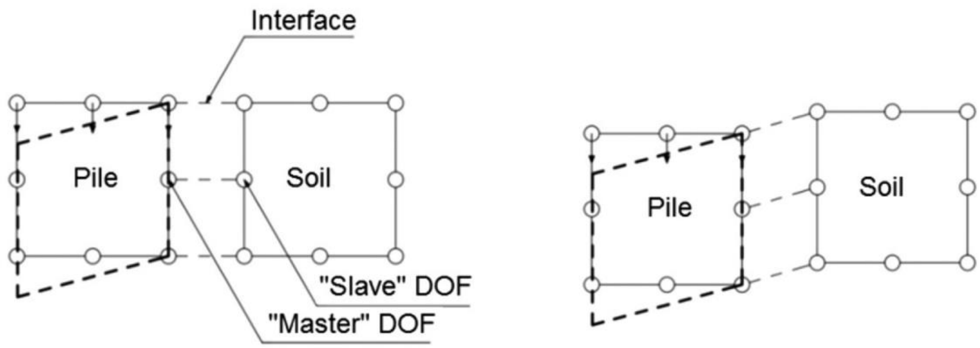

Figure 3-11:The contact pair scheme in ABAQUS

However, in other research, According to Potts and Zdravkovic (2001), it ispreferable not to use interface elements for the case of vertical loading. Researchers in theUniversity of Delaware have shown that, “with interface element lower capacity ofpile is always predicted. They also noted that computational costs and numerical instabilityincrease considerably in simulation with interface elements. Gang Wang et. Al.(2004)

Gebreziabher H.F. (2011) on his Ph.d dissertation had used an ideal contact without interface element and shown that an ideal contact can simulate the soil-pile interaction in FEM model. It is assumed that the pile is in perfect contact with the surrounding soil and hence the concept of ideal contact (as usually referred as “shear bands or shaft zone elements”), on studies made by Rolf Katzenbach et. al. 2000) is used throughout the analysis of this study. Fig 3-8. shows typical section of the shaft zone.

The shear band zones are continuum elements, with specified width normal the shaft surface and exhibit the same material behavior as the soil elements. Rolf Katzenbach et. Al. 2000, has further studied, effect of the width of the shaft zone elements on the pile resistance- settlement relationship. Continuum elements of thickness 0.1D at the pile-soil interface have been applied throughout the numerical studies as recommended by Reul (2000) and de Sanctis and Mandolini (2003, 2006)

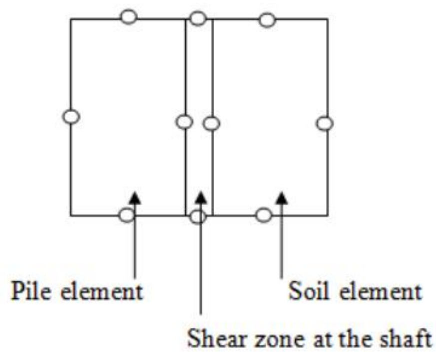

Figure 3-12: Enlarged mesh at the shear zone between the pile and soil

3.5.3. Choice of Meshing Techniques

Abacus uses a number of different meshing techniques and it assigned to a region to generate a mesh for the region. Abacus assigns a default top-down meshing technique to each meshable region of a model based on the geometry of the region and the current element shape selection for that region. Among different meshing techniques, in this study structured meshing technique was used that generates structured meshes using simple predefined mesh topologies. In this technique, Abaqus transforms the mesh of a regularly shaped region, such as a square or a cube, onto the geometry of the region to mesh.

The effect of mesh types applied just beneath the pile tip is another important issue in numerical modeling. In this study, by considering this issue, in figure 3-13, finer mesh is used just below the tip of the pile and meshed vertically aligned with the bottom soil mesh elements.

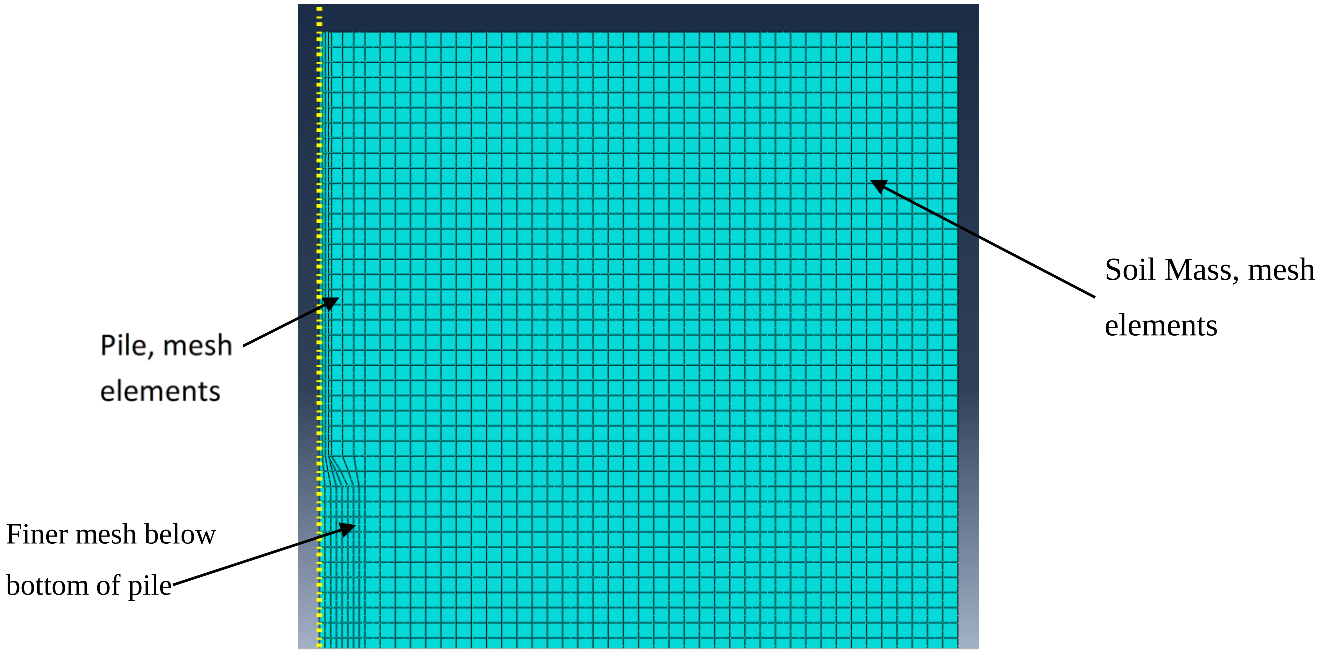

Figure 3-13: Finer Meshing technique below bottom of pile

3.5.4. Analysis Steps

The general analysis step, which can be used to analyze linear and or non-linear response, is selected for the analysis, (Abaqus tutorial, 2013).

Analysis steps can be broadly categorized as initial step and analysis step. Abaqus creates a special initial step at the beginning of the model's step and allows defining boundary condition, predefined fields. Whereas the analysis step is followed by one or more subsequent analysis steps where each subsequent step is associated with a specific procedure that define the type of the analysis to be performed. In this study, different analysis steps have been followed to simulate the energy pile performance.

Axisymmetric finite element analyses of piles have been performed in two steps- (i) a static step to apply the gravity loading and to bring the model in geostatic equilibrium and (ii) a coupled temperature-displacement step to apply the thermal loading. The thermal load is applied uniformly over the entire length of the pile as temperature time-history with ΔT = 15°C, same as that applied in Laloui et al. (2006).

3.5.5. Fully coupled thermal-stress analysis

Fully coupled thermal-stress analysis is needed when the stress analysis is dependent on the temperature distribution and the temperature distribution depends on the stress solution. For such cases, the thermal and mechanical solutions must be obtained simultaneously rather than sequentially.

In Abaqus, the temperatures are integrated using a backward-difference scheme, and the nonlinear coupled system is solved using Newton's method. Abaqus offers an exact as well as an approximate implementation of Newton's method for fully coupled temperature-displacement analysis (Abaqus tutorial, 2013).

3.5.5.1. Exact implementation

An exact implementation of Newton's method involves a non-symmetric Jacobian matrix as is illustrated in the following matrix representation of the coupled equations:

$$\begin{bmatrix} K_{uu} & K_{u\theta} \\ K_{\theta u} & K_{\theta\theta} \end{bmatrix} \begin{Bmatrix} \Delta u \\ \Delta\theta \end{Bmatrix} = \begin{Bmatrix} R_u \\ R_\theta \end{Bmatrix} \qquad \text{Eq.3-51}$$

Where Δu and $\Delta\theta$ are the respective corrections to the incremental displacement and temperature, K_{ij} are sub-matrices of the fully coupled Jacobian matrix, R_u and R_θ are the mechanical and thermal residual vectors, respectively. Solving this system of equations requires the use of the un-symmetric matrix storage and solution scheme. Furthermore, the mechanical and thermal equations must be solved simultaneously. The method provides quadratic convergence when the solution estimate is within the radius of convergence of the algorithm.

3.5.5.2. Approximate implementation

Some problems require a fully coupled analysis in the sense that the mechanical and thermal solutions evolve simultaneously, but with a weak coupling between the two solutions. In other words, the components in the off diagonal sub-matrices $K_{u\theta}, K_{\theta u}$ are small compared to the components in the diagonal sub-matrices K_{uu} , $K_{\theta\theta}$.

For these problems, a less costly solution may be obtained by setting the off-diagonal sub matrices to zero so that we obtain an approximate set of equations:

$$\begin{bmatrix} K_{uu} & 0 \\ 0 & K_{\theta\theta} \end{bmatrix} \begin{Bmatrix} \Delta u \\ \Delta \theta \end{Bmatrix} = \begin{Bmatrix} R_u \\ R_\theta \end{Bmatrix} \quad \text{Eq.3-52}$$

As a result of this approximation the thermal and mechanical equations can be solved separately,with fewer equations to consider in each sub problem. The savings due to this approximation, measured as solver time per iteration, will be of the order of a factor of two, with similar significant savings in solver storage of the factored stiffness matrix. Further, in many situations the sub problems may be fully symmetric or approximated as symmetric, so that the less costly symmetric storage and solution scheme can be used. The solver timesaving for a symmetric solution is an additional factor of two.

3.6. Method of Calculation for Heat Extraction with Energy Pile

In the design and analysis of energy foundation, one of the first important tasks is analyzing the energy demands of the building in related to heating and cooling requirement (HVAC system). As such, this value was used to measure the total pile length needed. However, for this study, already constructed 4B+G+30 United Bank Head Quarter Building was chosen for the analysis. The pile foundation of the building was only designed to carry structural load. The design does not include any special features to use as an energy foundation.

Although the pile foundation of the building was designed only by considering the structural load, the existing foundation was also used to evaluate how much energy can be extracted if current pile spacing and pile length are used.

Main characteristics of the building:

- Total area: 3,338m^2
- Number of energy piles: 282
- Length of the piles: 28 m
- Thermal conductivity of the ground: 1,6 W/mK (Average Value)
- Diameter of piles :0.8 m

Table 3-7:Total energy demands Vs. HVAC system of United Bank HQ building

Building	Total energy Demand of the Bldg.(kW)	Energy Demand for HVAC system(kW)	% of energy demand for HVAC/Total Energy Demand of the Bldg.
United Bank HQ	2158.40	526.22	24.38

As we can see from table 3-7, the total energy demands of the building is 2,158.40kW, from this 526.22kW is required for heating and cooling (HVAC) load of the building which accounts 24.38% of the total demands.

Different literatures state that method of calculation for heat energy extraction with energy pile foundation. According to Brandl (2006) for ***general feasibility studies and pre-design of energy foundations***, the following assumptions can be made regarding the energy volume that can be extracted from thermo active energy foundations.

(a) pile foundations ,with piles D =0.3–0.5 m: 40–60 W per meter run
(b) pile foundations, with piles D > 0.6 m: 35 W per m^2 earth-contact area
(c) diaphragm walls, pile walls (fully embedding the soil): 30 W per m^2 earth-contact area
(d) base slabs: 10–30 W per m^2 earth-contact area.

Cervera (2013) has maintained Brandl’s assumptions using climate and energy function method. First, this method relied on climate boundary condition that calculated from monthly average temperatures during the last 30 years. The climate function is applied as a boundary condition for the ground temperature. Based on this, reasonable values of average maximum and minimum temperatures of Addis Ababa were taken after comparing the data obtained from two different sources.

The first data was obtained from World Weather and Climate Information and is shown in Figure 3-9.

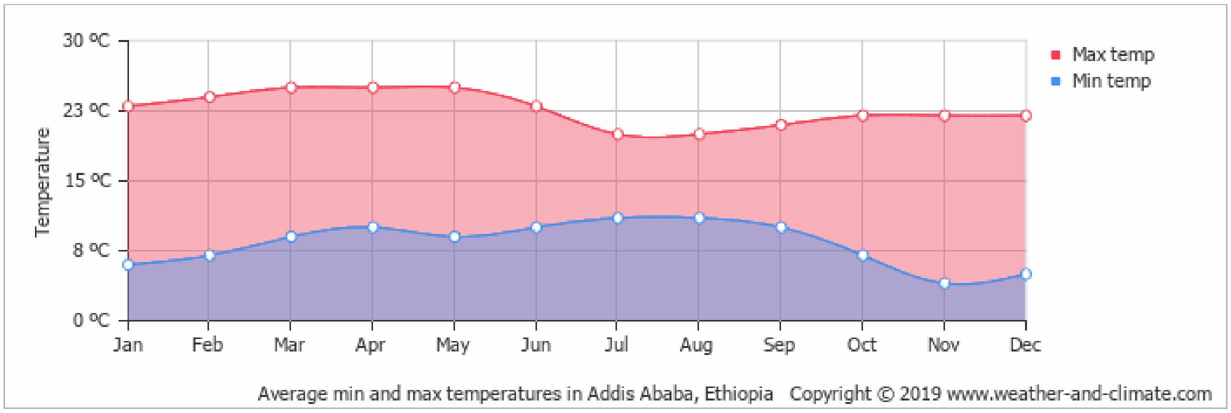

Figure 3-14: Average Maximum and Minimum Temperatures of Addis Ababa (Source: World Weather and Climate Information)

The second data was obtained from World Weather Information Service and the daily minimum and maximum values for each month of the year are shown in Table 3.6.

Table 3-8: Daily Minimum and Maximum Mean Temperatures of Addis Ababa

Month	**Mean Temperature**	
	Daily Minimum	**Daily Maximum**
January	8	24
February	9	24
March	10	25
April	11	24
May	11	25
June	10	23
July	10	21
August	10	21
September	10	22
October	9	23
November	7	23
December	7	23
Average	**9**	**23**

Climatological information is based on monthly averages for the 30-year period 1990-2019 (Source: World Weather Information Service)

Based on the above data, the following design temperatures/climate function were defined

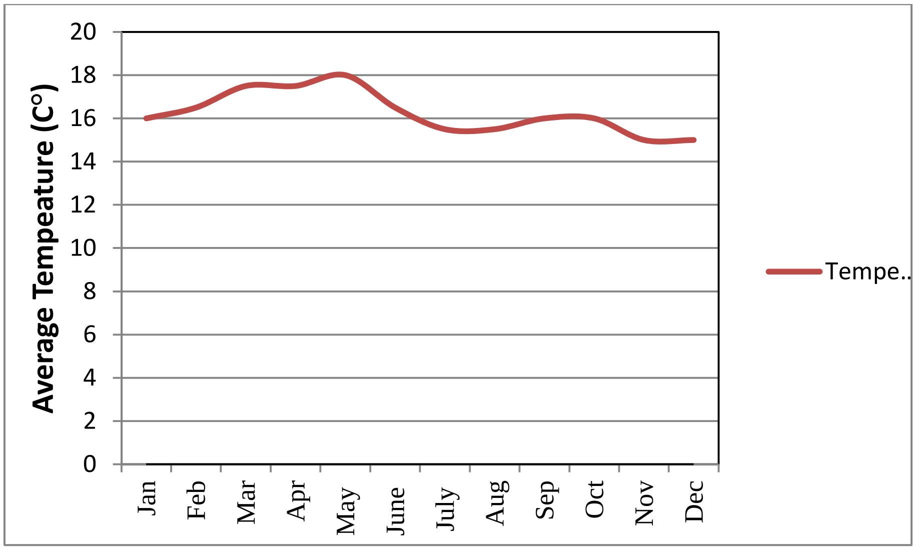

Figure 3-15: Addis Ababa cyclic climate function based on average air temperature

Next, calculate the energy function, which represents the boundary condition of the energy piles for heating and cooling purposes during the different seasons of the year. The energy piles are absorbing or pumping different values of heat flux depending on the energy requirements of the building on each season. Studies show the energy that can be extracted or pumped from the soil depending on the thermal conductivity of the ground (Nyholm, 2011).

Next figure (Figure 3-16) shows the energy function calculated according to the thermal properties of the ground. The energy function for energy piles was calculated by interpolating the average values of thermal conductivity of the clay and sandy gravel soil (λ =1.76 W/mK).

As can be seen in figures 3-16, the minimum and maximum estimated value of heat flow extracted by the energy pile was 23W/m & 31W/m respectively. The values of energy extracted obtained from the energy function are similar to the typical values that can be found in literature (Brandl, 2006). These typical values of heat flux for energy piles were between 20-50 W/pile-meter and applicable for pile diameter 0.3m up to 0.5m. However, due increasing the contact area between the pile and the soil, these typical values may exceed for piles with diameter greater than 0.6m.

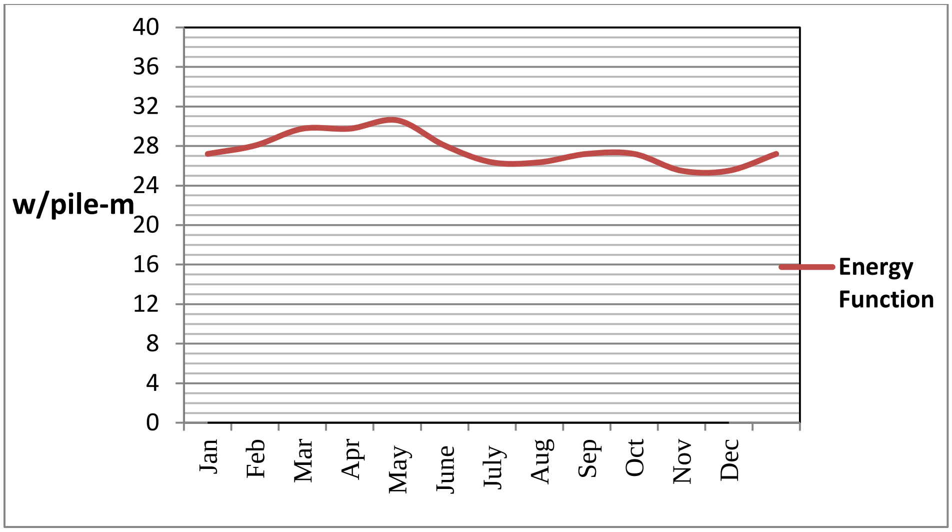

Figure 3-16: Energy functions calculated according to the thermal conductivity of the ground

For this study, the values of 35W per m^2 earth- contact area is adopted to calculate the amount of energy that can be extracted from the ground. Accordingly, the total amount of energy that can be obtained from a single energy pile was calculated by multiplying such typical values with the lateral surface area of the pile (in this study 70.37 m^2 for a pile diameter 0.8 m used).

CHAPTER 4: RESULTS AND ANALYSIS

4.1. General

As a primary objective to evaluate the performance energy pile that subjected to mechanical and thermal loading, load transfer model and finite element method are used. As indicated in earlier chapter, Matlab program code was developed for load transfer model and Abaqus software used for finite element method. Results from both software, are presented in a separate graph since those tools uses different nodal points. Moreover, the results from load transfer model and finite element method ware not comparing here. Nevertheless, a general evaluation is made just to show performance of the foundation in terms of axial stress, side shear stress and displacement. The response of energy pile under 1000kN mechanical load is analyzed first and then 21°C thermal load. Finally, the analysis for thermo-mechanical loading response of energy pile foundation is presented.

4.2. Mechanical Loading Only

First, a simulation of mechanical loading without temperature change is conducted. A force, 1000kN is applied to the top of pile and the results are presented on the following section:

4.2.1. Axial stress distribution

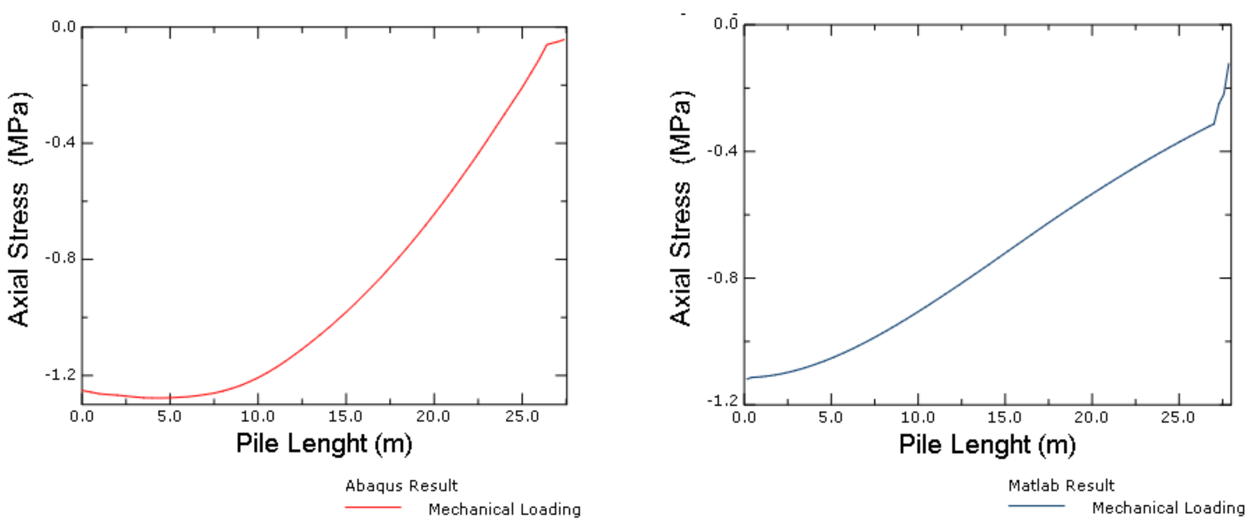

(a) (b)

Figure 4-1: Axial Stress for 1000kN Mechanical Loading (a) Finite Element Method (b) Load Transfer Method

The axial stress distribution due to mechanical loading is depicted in Figure 4-1. The maximum stress on pile due to mechanical loading occurs at the top of pile, which decreases towards the bottom. The axial stress at the bottom of pile tends to be zero. This may be the cause of soil pile interaction as the stress is transferred to the ground to from the bottom of pile instead of resisting it.

4.2.2. Shear Stress Distribution

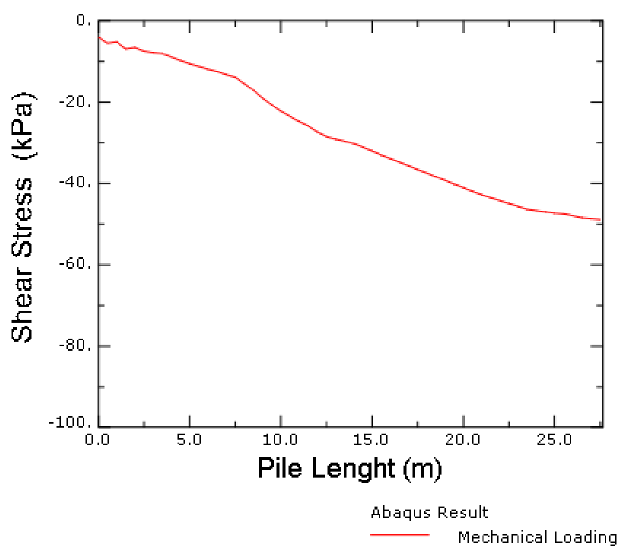

(a)

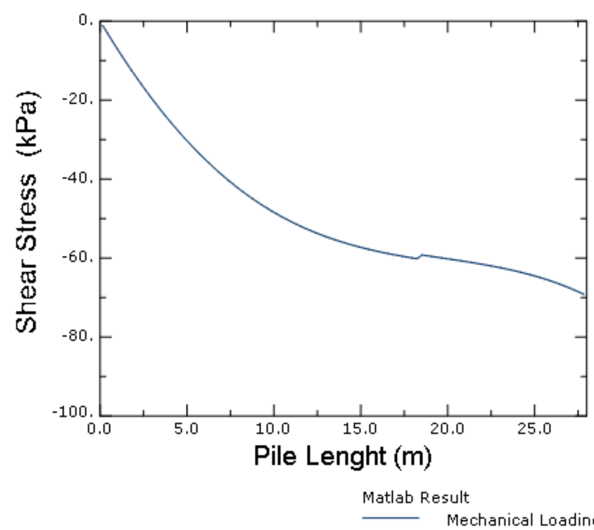

(b)

Figure 4-2: Shear Stress for 1000kN Mechanical Loading (a) Finite Element Method (b) Load Transfer Method

The shear stress distribution during the mechanical loading of a pile can be seen in figure 4-2**.** The increasing of shear stress that the figure shows is due to the reason that the mechanical load is resisted by solely with frictional resistance between the pile and the soil. The higher mobilized side shear stress is at the toe, because the highest downward displacement accumulated from mechanical load.

4.2.3. Vertical displacement

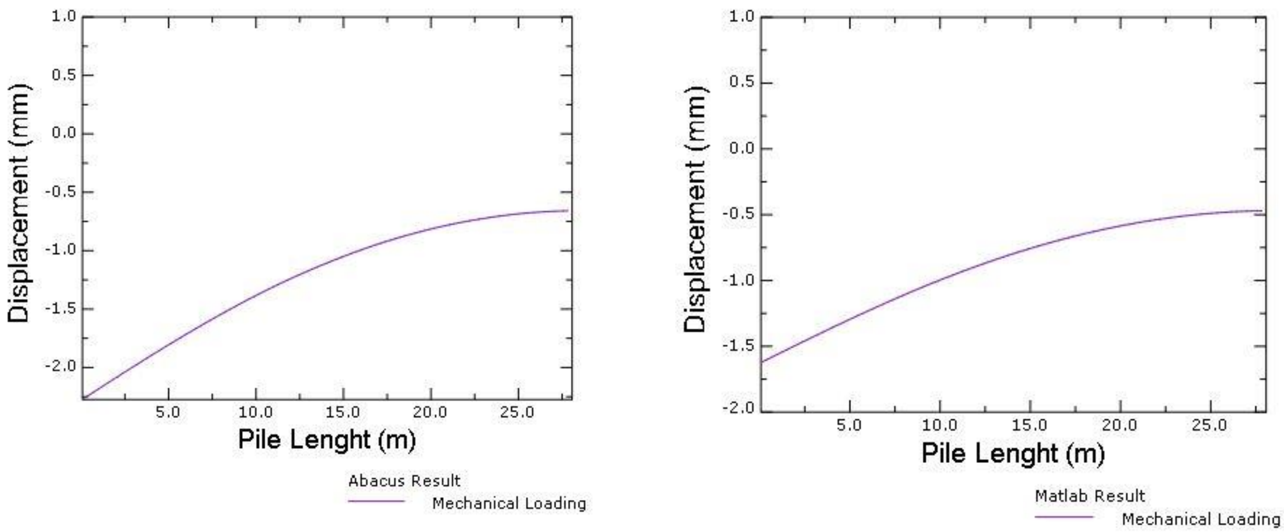

(a) (b)

Figure 4-3: Vertical Displacement for 1000kN Mechanical Loading (a) Finite Element Method (b) Load Transfer Method

Figure 4-3 shows the variation of displacement in vertical direction of pile when mechanical load is applied on the top. The downward displacement is clearly nonlinear across the depth. Since the mechanical loading is applied form the top of pile, the compression on pile is maximum at the top and decreases towards the bottom of pile.

4.3. Thermal Loading Only

Energy pile under thermal loading is shows different response than the convectional pile foundation under mechanical loading condition. The behaviour and the performance of energy pile on thermo-mechanical loading condition are more significant with the presence of temperature. Owing to this, more emphasis will be given for this section. The thermal load is applied uniformly over the entire length of the pile with ΔT = 21°C.

4.3.1. Vertical Stress Distribution

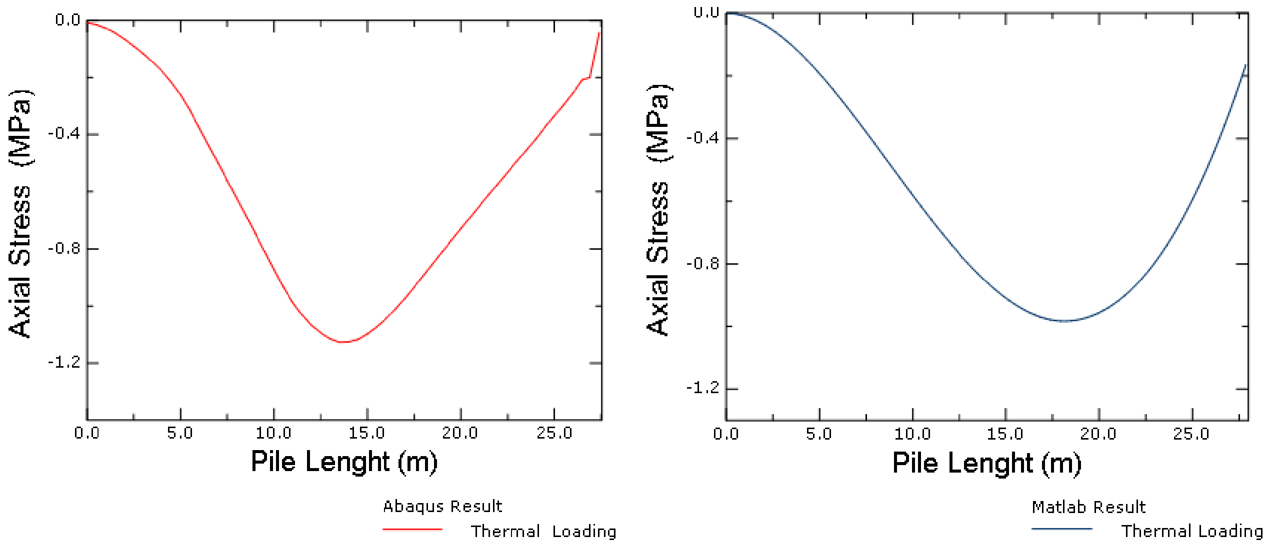

(a) (b)

Figure 4-4: Axial Stress Distribution under 21°C. Thermal Loading (a) Finite Element Method (b) Load Transfer Method

Figure 4-4 shows the vertical stress distribution in pile under thermal loading. During thermal loading, when the temperature of an energy pile increases, it tends to elongate proportional to the coefficient of thermal expansion of the pile material and the magnitude of temperature change. Whenever the pile is constrained, deformations on the pile are prevented, which causes thermal stress in the pile. The stress, which is compressive in nature, is maximum around the mid length of the pile where the expansion was observed to be reversed from upward to downward expansion. The thermal stress distribution would be symmetrical if the pile was set to be free at both.

Accordingly, heating is expected to result in an increase in compressive stress throughout the energy pile, due to the axial expansion. Furthermore, the higher thermal loading in the energy pile causes more upward movement of the pile above the null point and more downward movement below the null point.

4.3.2. Shear stress distribution

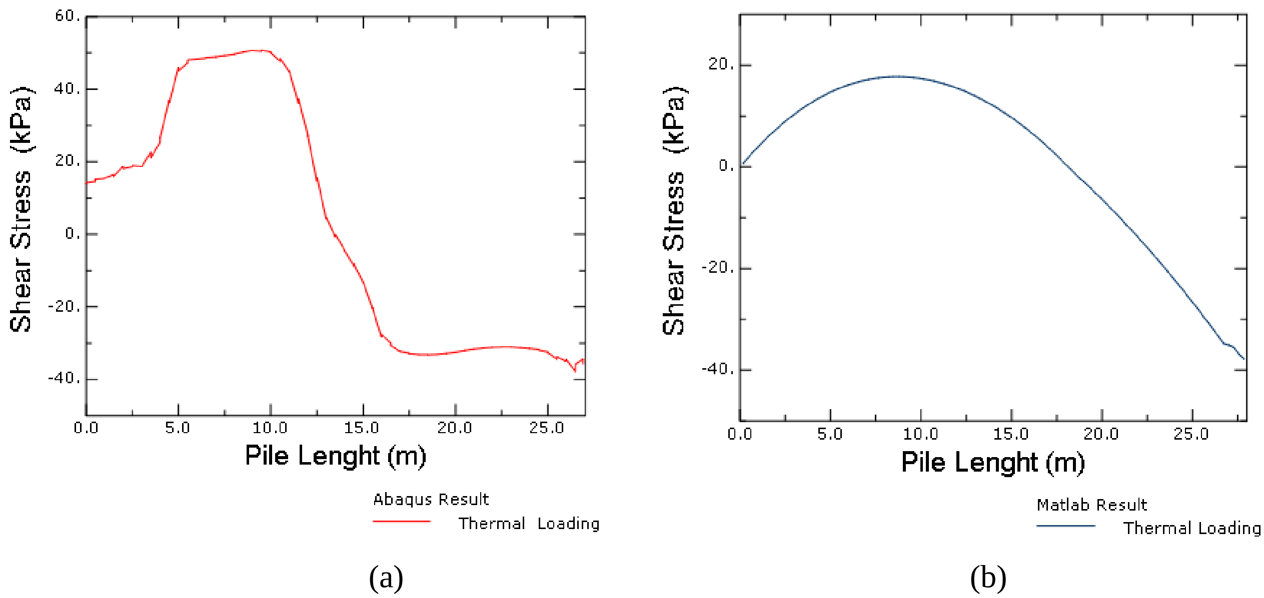

Figure 4-5: Shear Stress Distribution under 21°C. Thermal Loading (a) Finite Element Method (b) Load Transfer Method

The shear stress developed on the soil pile interface during thermal loading condition on the pile is presented in the figure 4-5. Because of the heating, the pile goes on expansion both on the top and bottom of the pile but in opposite direction as shown in the vertical displacement distribution. At the point of maximum shear stress, the compressive stress becomes minimum and vice versa.

As it can see from the figures, the shear stress distribution in the finite element method and load transfer method is shows some different values. In comparing with other literatures, the result of finite element method is more accurate since it is capable of simulating the pile soil interaction than load transfer model.

4.2.3 Vertical displacement

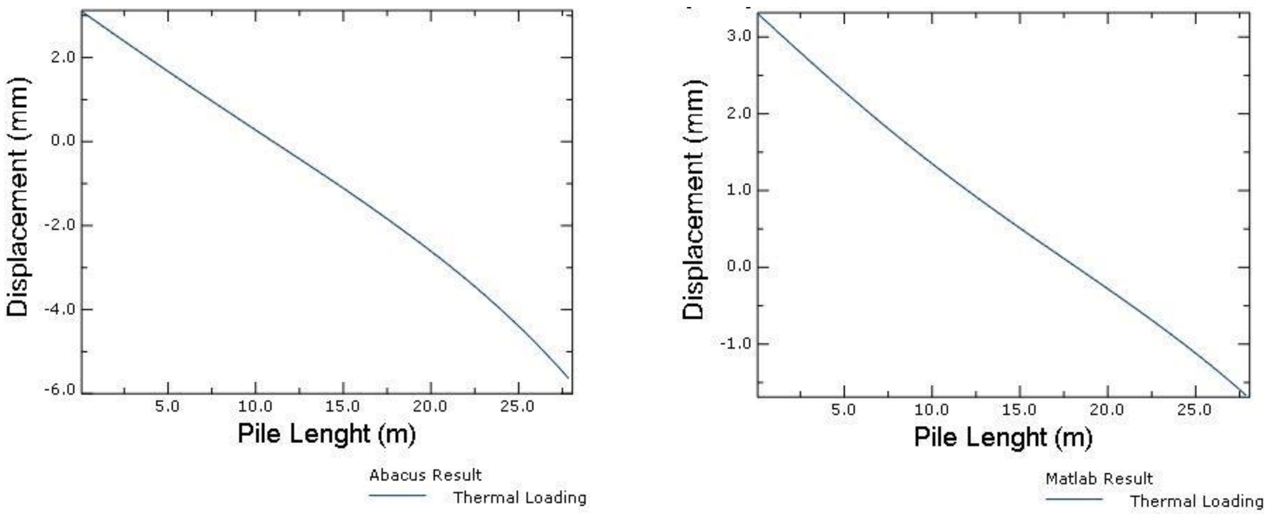

(a) (b)

Figure 4-6: Vertical Displacement under 21°C. Thermal Loading (a) Finite Element Method (b) Load Transfer Method

Figure 4-6 presents the vertical displacement under thermal loading. When the thermal load is applied throughout the pile length, the top part of the pile expands upward whereas the lower part tends to expand downward at the location of null point, the point at which the sign of the mobilized side shear stress and displacement changes.

4.4. Thermo-Mechanical Loading

Both mechanical load and thermal load were applied on the pile during the thermomechanical simulation of the pile. The initial temperature on the pile and soil was maintained constant (and equal), then the pile was uniformly heated to a certain temperature. 1000 kN axial load was applied on the pile head that can be considered as the super structural load of the building.

4.4.1. Vertical Stress Distribution

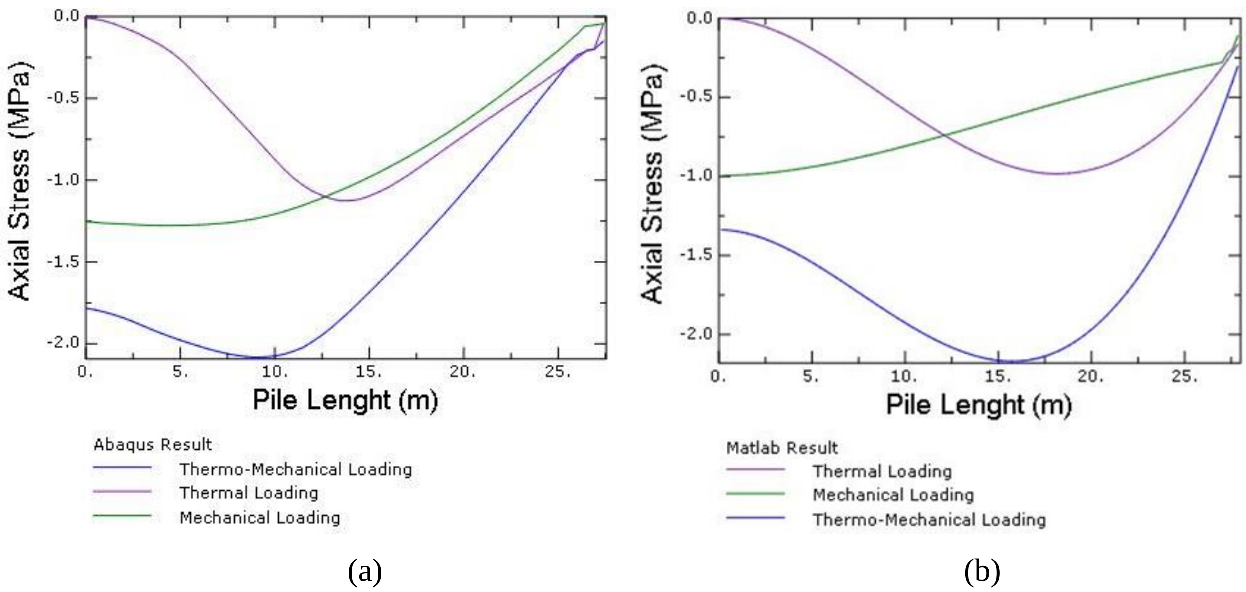

Figure 4-7: Thermo-Mechanical Axial Stress Distribution for 1000 kN mechanical load & 21°C thermal Load (a) Finite Element Method (b) Load Transfer Method

Figure.4-7 shows the stress variation in pile in three different conditions of loading i.e. mechanical loading (M), thermal loading (T) and thermomechanical loading (TM). From the result of vertical stress distribution in the pile under different loading conditions, it can be observed that the stress due to mechanical loading is large at the pile head and diminishes with depth. The bottom of pile carries almost no stress on it since the entire applied load transferred to the soil by side friction. However, in case of thermal loading, the stress on the top is smaller than the mechanical loading. Nevertheless, around the mid-point of the pile , more stress take place compared to mechanical loading.

The axial stress induced by thermal load is maximum at the location of null point (NP). This result coincide with Bourne-Webb (2009) which state the location of the null point is where there is no thermal induced displacement and as a result, the highest compressive axial stresses occur at it. Since the pile is somewhat constrained with soil at the bottom, the curve of thermal loading is not symmetrical about the mid-point of pile. He emphasized that the location of the NP depends on the upper and lower axial boundary conditions and side shear distribution.

Ideally, the effect of thermomechanical loading should be a combined effect of thermal and mechanical loading which can be observed in almost every part of the pile except in the pile head. At some distance from the top of pile, some “anomalous” distribution of stress can be observed in thermomechanical loading of the pile, which is similar with the results presented in Laloui et.al. 2006. The total axial stress (thermo-mechanical axial stress) in the pile has increase with 50 % due to thermally induced axial compressive stresses with temperature. Such phenomena is shown in Laloui (2006) experimental investigation of energy pile at Lausanne, which indicated that a temperature increment of 1^0 C results in approximately 100 kN additional temperature-induced vertical force. As a result, around the null point, the total axial load in the pile is twice as large as the one due to purely mechanical loading.

4.4.2. Shear Stress Distribution

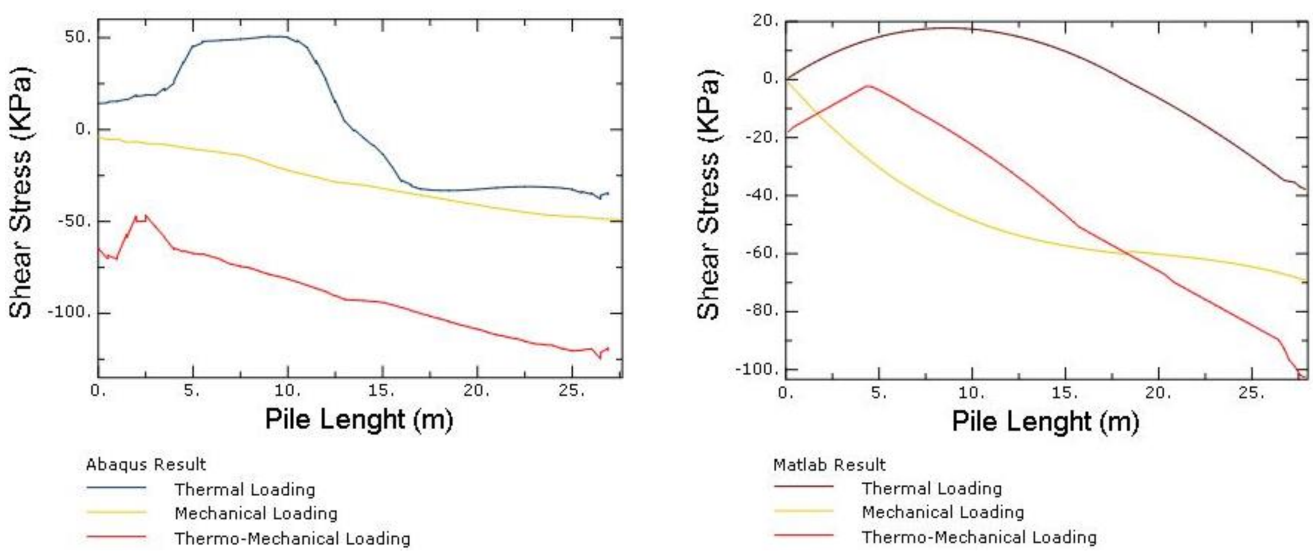

(a) (b)

Figure 4-8:Thermo-Mechanical Shear Stress Distribution for 1000 kN mechanical load & 21^{o}C thermal Load (a) Finite Element Method (b) Load Transfer Method

The mobilized side shear stresses are presented in Figure 4-8 that the thermal load creates more mobilization of friction than the mechanical load. The result indicates that due to the relative upward movement of the pile with respect to the surrounding soil, positive (downward) shaft resistance is mobilized at the upper portion of the pile. Similarly, due to downward movement of the pile, negative (upward) shaft resistance is mobilized at the bottom portion of the pile. The point at which the sign of the mobilized side shear stress change is in the region where the maximum thermal axial stress and the corresponding position of the null point (Knellwolf, 2011; Amatya et al.2012; Murphy, 2015).

4.4.3. Vertical Displacement

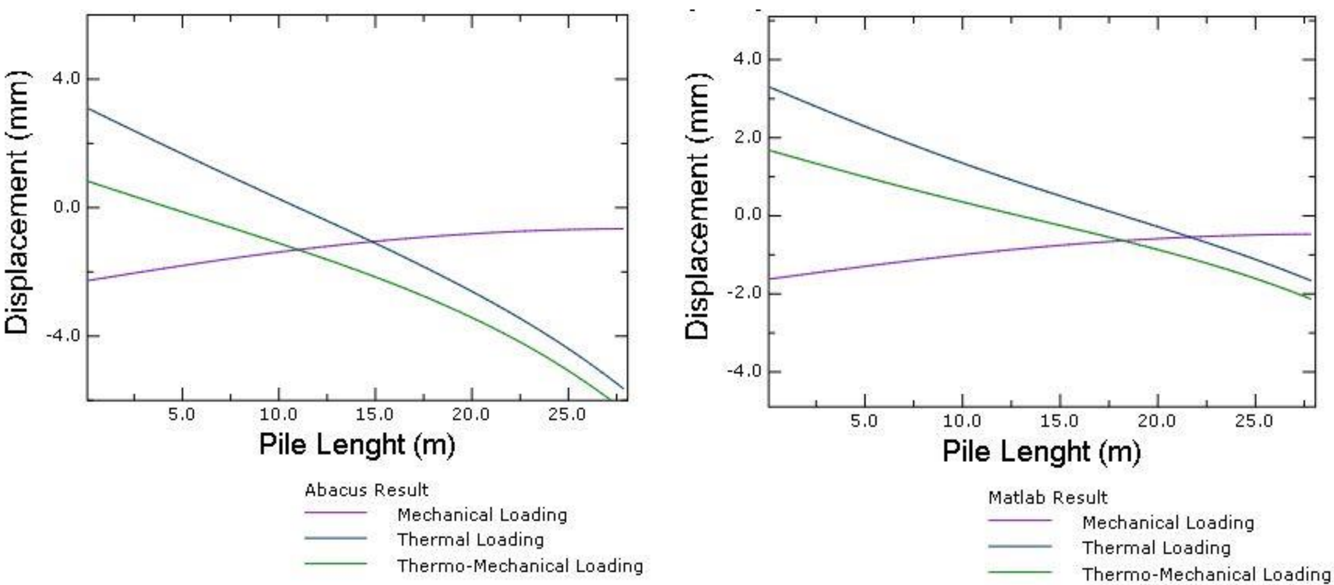

(a) (b)

Figure 4-9: Thermo-mechanical Vertical Displacement under 1000 kN Mechanical loading & 21°C. Thermal Loading (a) Finite Element Method (b) Load Transfer Method

Figure 4-9 presents the vertical displacement distribution during the thermomechanical loading of a pile. Similar to thermal loading, the top part of pile expands upward and bottom part expands downward with changing direction around the midpoint of the pile. The mechanical displacement has shown comparable positive values throughout the pile length as the pile moves downward. Displacement in the downward direction was considered negative.

4.5. The Expected Amount of Energy Production and Financial Evaluation

For this preliminary study, the expected amount of energy that can be extracted with energy pile was calculated by considering the method that stated in chapter three. For structural safety and initial investment cost, it is not recommended to design all piles as an energy pile. Therefore, out of the total number of structural piles, for this study considering the following four scenarios.

Table 4-1: No of energy piles used and the corresponding total earth-contact area

Scenarios	No of Energy piles (x) out of the total no structural piles (282)	Total Earth-contact Area of Energy piles ($70.38m^2$*x)
First	50	3,519
Second	100	7,038
Third	150	10,557
Fourth	200	14,076

As indicated in chapter three, the total energy demand of the building for heating and cooling requirements was 526.22 kW. In order to evaluate yearly energy output, this value should convert in to kWh per year.

The energy consumption per year (E) assuming four hours operation per day is calculated from Equation 4-1 as follows:

$$E = P \times \text{hours/day} \times \text{days/year} \qquad \text{Eq.4-1}$$

$$E = 526.22 \text{ kW} \times 4\text{hrs/day} \times 365 \text{ days/year}$$

$$E = 768{,}281 \text{ kWh/year}$$

The total energy consumption of the building for heating and cooling purpose was 768.281kWh per year. Next, the amounts of energy that can be extracted with energy piles was calculated by multiplying the total earth-contact area of energy piles with the assumed typical value of $35w/m^2$ for each scenarios and are summarized in Table 4-2 below:

The results of economic evaluation for each scenario are also displayed in Table 4-2 .The economic evaluation was calculated based on the current electricity tariff of Ethiopia, *US$ 0.053kWh*

Table 4-2: Expected Energy yield and Economic Evaluation of Each Scenario

Scenarios	Expected Amount of Energy Extracted (kWh/Year)	Energy Demand of the Building for HVAC (kWh/year)	Percentage of Energy Covered by EPs. System (%)	Amount Saved (USD per year)
First	179,820.90	768,281	23.41	9,530.51
Second	359,641.80		46.81	19,061.02
Third	539,462.70		70.22	28,591.52
Fourth	719,283.60		93.62	38,122.03

As we can see from table 4-2, in the fourth scenario, from the total amount of energy that required for heating and cooling of the building, 93.62% of energy was covered by using 200 energy piles, which account 719,283.60kWh/year. In addition, annually $38,122.03 can be saved with such energy geo-structure system. Moreover, it can be also cover 46.81% & 70.22% of energy required for heating and cooling can be by using 100 & 150 energy piles respectively. However, the amount of energy extracted with the corresponding number of energy pile may decrease or increase during the operation since such system depending on the ground condition and the efficiency of the overall system.

CHAPTER 5: CONCLUSIONS AND RECOMMENDATIONS

5.1. Conclusions

Despite the global problem of energy demand, now a day looking for other renewable sources has been necessary. As an alternative, energy pile foundation has a novel solutions to the new problems related to environmental issues and energy demands by providing energy sources while maintain structural stability of the building. To some extent, adopting such innovative mechanism was found to be as a solution for the problem of energy of demands the country.

Therefore, this preliminary study was made to reveal the opportunities of meeting the energy demand of residential or commercial buildings in Ethiopia using pile foundation by taking United Bank Headquarter Building as a case study. Evaluation of the performance of energy piles under thermo-mechanical loading conditions was investigated with Matlab programming code and Abaqus software. In addition, the amount of energy yield and the corresponding economic advantage was also studied. Finally, the following conclusions are made.

The finite element modeling of energy piles verifies that during thermo-mechanical loading, the total axial stress in the pile shows significant increases due to thermal loading that causes axial expansion in the energy pile. Along with this, the load transfer modeling also illustrates that the axial stress induced by thermal load is maximum at the location of null point (NP).

Thermo-mechanical behaviour of energy piles has significant loading response due to temperature as compared with the conventional pile foundation under mechanical loading. Accordingly, the thermal load (temperature) results in an increase in compressive stress throughout the energy pile due to the axial expansion. Furthermore, the higher thermal loading in the energy pile causes more upward movement of the pile above the null point and more downward movement below the null point.

Thermal loading causes significant mobilized side shear stress than the mechanical loading. The results obtained from this study mobilized side shear stress were more simulated with the finite element modeling than the load transfer model.

Regarding the expected amount of energy extracted, the results of the preliminary study indicated that a significant amount of energy, 719,283.60kWh/year, can be generated. This amount could covers 93.62% of the estimated heating and cooling energy demand of the building. In addition, based on the current electricity tariff of Ethiopia, up to 38,122.03 USD can be saved **annually** with such energy geo-structure system. However, the amount of energy extracted with the corresponding number of energy pile may fluctuate during operation since the system depends on the ground condition and the efficiency of the overall system.

In conclusion, the outcomes from this preliminary study indicates that energy piles foundation may be used as an alternative means of energy source by taking the essential design consideration of the additional axial stress due thermal loading.

5.2. Recommendations

Many researchers agreed that, “the first important deed for conducting a sound research is a spirited effort”. However, beyond to these, graduate students usually face enormous challenges in conducting their research due to lack of strong theoretical background, necessary advancing tools, detail data, funding and guidance. Owing to this, the author, forward the following recommendations for future **studies and considerations**.

This preliminary study indicated that use of energy pile have its own economic advantage. Hence, in order to apply such innovative technology to our country, extensive research should be conducted beyond to MSc thesis. This paper focused on thermo-mechanical response of energy pile under monotonic thermo-mechanical loading condition 2D Finite element method. However, the behaviour of thermomechanical energy pile is quite complex. Therefore, further research on three-dimensional finite element modeling should be conducted.

To evaluate the response of the foundation under thermo-mechanical loading conditions and the expected energy yield, this study used performance-based analyses for the thermomechanical design of energy piles. This requires the availability of high level of advancing tools, and detail input data for numerical analysis. Therefore, researchers should be provided with such tools, geotechnical data and funds from the concerned institutions and geotechnical investigation firms.

Due to its economic and environmental advantage, the government policies shall be formulated to integrate energy foundation systems in commercial and residential high-rise buildings by the designer and the construction companies.

Bibliography

Adam, D., & Markiewicz, R. (2009). "Energy from earth-coupled structures, foundations, tunnels and sewers". *Ge ´otechnique*, 229–236.

Amatya, B. L., Soga, K., Bourne-Webb, P. J., Amis, T., & Laloui, L. (2012). "Thermo-mechanical behaviour of energy piles". *Géotechnique*.

Amis, T., Bourne-Webb, P., Davidson, C., Amatya, B., & Soga, K. (2008). "The effects of heating and cooling energy piles underworking load at Lambeth College, UK.". *33rd Annual and 11th International Conference of the Deep Foundation.* New York, USA.

Bourne-Webb. (2013). A framework for understanding energy pile behaviour. *ICE Publishing*, 170-177.

Bourne-Webb, P., Amatya, B., Soga, K., Amis, T., & Davidson, C. (2009). Energy pile test at Lambeth College, London:Geotechnical and thermodynamic aspects of pile response to heat cycle. *Geotechnique*, 56(2), 81–122.

Brandl, H. (1998). " Energy piles and diaphragm walls for heat transfer from and into theground.". *In: Van Impe, Haegeman, editors. Deep foundations on bored and.* Rotterdam: Balkema.

Brandl., H. (2006). Energy foundations and other thermo-active ground structures. *Ge ´otechnique*, 56, (2), 81–122.

Brian, A. F., & Anil, M. B. (2011). Soil Thermal Conductivity:Effects of Saturation and Dry Density. *University of Missouri-Kansas City*.

Burlon, S. H. (2013). Towards a design approach of bearing capacity of thermo-active piles. *European Geothermal Congress Pisa*, 1-6.

Cervera, C. P. (2013). Ground thermal modelling and analysis of energy pile.

Chakraborty, R. S. (2017). "Thermomechanical Analysis and Parametric Study of Geothermal Energy Piles in Sand". *Int. J. Geomech, 17(9).*

Coyle, H. M., & Reese, L. C. (1966). Load transfer for axially loaded piles in clay. *J.Soil Mech. and Found*, 92(2), 1–26.

Di Donna, A., & Laloui, L. (2011). understanding the behaviour of energy geo-structures. (pp. 184–191). ice.

Di Donna, A., Dupray, F., & Laloui, L. (2013). "Numerical study of the heating-cooling effects on the geotechnical behaviour of energy piles". *International Symposium on Coupled Phenomena in Environmental Geotechnics*, 475-482.

Dupray, F. L. (2014). Numerical analysis of seasonal heat storage in an energy pile foundation. *Computers and Geotechnics, 55*, 67-77.

Ebnother. (2008). Energy piles. The European Experience. *GeoDrilling 2008*.

Epstein, C. (1998). "Impact of groundwater flow on the Stockton geothermal well field.". *2nd Stockton International Geothermal Conference.* Pomona, NJ ,USA.

Farouki, O. (1991). *Thermal Properties of Soil.*

GSHP-Association. (2012). *Thermal Pile Design, Installation & Materials Standards* (Vol. Issue 1.0).

Heinz Brandl, D. A. (2006). Ground-Sourced Energy Wells For Heating And Cooling Of Buildings. *Acta Geotechnica Slovenica*.

Helwany, S. (2007). *Applied soil mechanics with ABAQUS applications / Sam Helwany.* John Wiley & Sons, Inc.

Katzenbach, R. R. (2009). “Recent developments in foundation and geothermal engineering.”. *2nd International Conference on New Developments in Soil*, (pp. pp. 464-471.). Nicosia, Cyprus.

Knellwolf, C. P. (2011). Geotechnical analysis of heat exchanger piles. *J. Geotech. Geoenviron. Eng*, 890–902.

Laloui, L., & Donna, D. (2011). “Understanding the behavior of energy geo-structures.”. (pp. pp. 184-191). Proceedings of the Institution of Civil Engineers.

Leong, V. R. (2009). Thermal Conductivity of Standard Sands. Part I. *Int J Thermophys*.

Lyesse, L., Mathieu, N., & Laurent, V. (2006). Experimental and numerical investigations of the behaviour of a heat exchanger pile. *Int. J. Numer Anal. Methods Geomech., 30*(8), 763–781.

McCartney, J., & Chen, D. (2016). Parameters for Load Transfer Analysis of Energy Piles in Uniform Nonplastic Soils. *Int. J. Geomech*, 1532-3641.

Monique, d. M. (2010). Technological advances and applications of geothermal energy pile foundations and their feasibility in Australia. *Renewable and Sustainable Energy Reviews, 14*, 2683–2696.

Murphy, K. D. (2015). "Evaluation of thermo-mechanical and thermal behavior of full-scale energy foundation". *Acta Geotech*.

Nyholm, V. (2011). Energiapaalujen hyödyntäminen taloteknisissä konsepteissa. *Master Thesis, Aalto University*.

Olgun, C. G. (2013). Energy Piles : Background and Geotechnical Engineering Concepts. *16th Annual George F. Sowers Symposium,Atlanta*.

Olgun, C., & McCartney, J. (2014). "Outcomes from International Workshop onThermoactive Geotechnical Systems forNear-Surface Geothermal Energy: from research". *The Journal of the Deep Foundations Institute, 8*.

Ouyang, Y. S. (2011). Numerical back-analysis of energy pile test at Lambeth college. *Proceedings of Geo-Frontiers – Advances in Geotechnical Engineering*, 440-449.

Ouyang, Y. S. (2011). "Numerical back-analysis of energy pile test at Lambeth College, London". *GeoFrontiers*, 440–449.

Pasten, C. a. (2014). Thermally induced long-term displacement of thermoactive piles. *Journal of Geotechnical and Geoenvironmental Engineering, 140*.

Plaseied, N. (2012). Load transfer analysis of energy foundations. *Univ. of Colorado Boulde*.

Rammal, D. M. (2017). "Accounting for transient effects in energy pile design". *Proceedings of the 19th International Conference on Soil Mechanics and Geotechnical Engineering.* Seol.

Rotta, L. A. (2015). Thermo-mechanical analysis of soil characteristics fromenergy piles tests in Richmond. *Texas by Virginia Tech University. LMS/EPFL Internal Report*, p55.

Saggu, R. a. (2015). "hermal Stress and Displacement Response of Geothermal Energy Piles in Sand". *IFCEE*.

Suryatriyastuti, M. E. (2013). "Numerical analysis of the bearing capacitiy in thermo-active piles under cyclic axial loading". *Energy geostructures: Innovation in underground engineering, L. Laloui and A. Di Donna, eds., John Wiley, Hoboken, NJ*, 139–154.

Sutman, M. (2016). *Thermo-Mechanical Behavior of Energy Piles:Full-Scale Field Testing and Numerical Modeling.*

Teffera, A., & Leikun, M. (1999). *Soil Mechanics.*

Tomlinson, M. J. (1957). Adhesion of piles in clay soils. *Proc., 4th Int.Conf. on Soil Mechanics and Foundations Engineerin, 2*, 66–71.

Utility, E. E. (2020). *www.eeu.gov.et*. Retrieved from www.eeu.gov.et/index.php/current-tariff.

Wang, W., Regueiro, R., & McCartney, J. S. (2015). Coupled axisymmetric thermo-poro-mechanical finite element analysis of energy foundation centrifuge experiments in partially saturated silt". *Geotech. Geol.Eng, 33(2), ,* 373–388.

Wrana, B. (2013). Nonlinear Analysis Of Pile Displacement Using The Finite Element Method.

APPENDICES

Appendix A: Matlab Code for Energy Pile

Initialize Variable

```
%% VARIABLES FOR MECHANICAL T-Z ANALYSIS %%
QbM = zeros(N,1);                    % Force at bottom of element (kN)
QtM = zeros(N,1);                    % Force at top of element (kN)
FsM = zeros(N,1);                    % Mobilized side shear force on each element (kN)
pbM = zeros(N,1);                    % Displacement at bottom of each element (m)
ptM = zeros(N,1);                    % Displacement at top of each element (m)
psM = zeros(N,1);                    % Shear displacement at side of each element (m)
QaveM = zeros(N,1);                  % Average force in each element (kN)
deltaM = zeros(N,1);                 % Compression of each element (m)
epsM = zeros(N,1);                   % Axial strain (microstrain)
sigmaM = zeros(N,1);                 % Axial stress (kN/m2)

%% VARIABLES FOR THERMO-MECHANICAL T-Z ANALYSIS %%
QtT = zeros(N,1);                    % Thermal axial force at the top of each element (kN)
FsT = zeros(N,1);                    % Mobilized side shear force due to thermal loading (kN)
QbT = zeros(N,1);                    % Thermal axial force at the bottom of each element (kN)
ptT = zeros(N,1);                    % Thermal displacement at the top of each element (m)
psT = zeros(N,1);                    % Thermal shear displacement (m)
pbT = zeros(N,1);                    % Thermal displacement at the bottom of each element (m)
QaveT = zeros(N,1);                  % Change in average axial force due to heating (kN)
deltaT = zeros(N,1);                 % Constrained thermal expansion of each element (m)
sigmaT = zeros(N,1);                 % Thermal axial stresses in each element (kPa)
epsT = zeros(N,1);                   % Thermal axial strains in each element (microstrain)
QtMT = zeros(N,1);                   % Thermo-Mechanical force at the top of each element (kN)
FsMT = zeros(N,1);                   % Mobilized side shear force due to thermo-mechanical loading (kN)
QbMT = zeros(N,1);                   % Thermo-Mechanical force at the bottum of each element (kN)
ptMT = zeros(N,1);                   % Thermo-Mechanical displacement at the top of each element (m)
psMT = zeros(N,1);                   % Thermo-mechanical shear displacement (m)
```

```
pbMT = zeros(N,1);                    % Thermo-Mechanical displacement at the bottum of each element (m)
QaveMT = zeros(N,1);                  % Change in average axial force due to mechanical loading and heating (kN)
sigmaMT = zeros(N,1);                 % Thermo-mechanical axial stresses in each element (kPa)
epsMT = zeros(N,1);                   % Thermo-mechanical axial strains in each element (microstrain)
```

Definition of load

```
%% LOAD DEFINITION %%
P = 500;                              % Mechanical load (kN)
DT = 15;                              % Change of temperature
```

Definition of Pile Geometry

```
%% Pile GEOMETRY DESCRIPTION %%
L = 28;                               % Length of pile (m)
D = 0.8;                              % Diameter of pile (m)

%% Pile MATERIAL DESCRIPTION %%
gampile = 24;                         % INPUT Unit weight of concrete (kN/m3)
E = 29200000;                         % Young's modulus of pile (kPa)
alphaT = -10e-6;                      % Coefficient of thermal expansion
kappa = 65;                           % Radial expansion
Kh = 2e5;                             % Head stiffness (kN/m)
```

Definition of soil

```
%% SOIL PARAMETERS %%
Undrained=0;
Drained=1;
EndBearing = 1;                       % End Bearing = 1, Not End Bearing

%% DEFINITION OF SOIL LAYER
Soillayer =1;                         % Layer1, Layer2, Layer3, Layer4, Layer5

%% SOILLAYER
Layer1=1;
Layer2=1;
Layer3=1;
Layer4=1;
Layer5=1;
```

Definition of T-z curve parameters

```
%% Q-z PARAMETERS (TIP) %%
ab = 0.002;
bb = 0.9;

%% T-z PARAMETERS (SIDE) %%
as = 0.0035;
bs = 0.9;

%% CHI_T FOR BETA %%
chiT = 1.7;
```

Redefinition of parameters

```
L1=4.5;
gama1=16.92;
alpha1=0.5;
cu1=30;
Phi1=28;

L2=9;
gama2=17.86;
alpha2=0.5;
cu2=35;
Phi2=30;

L3=13;
gama3=18.18;
alpha3=0.5;
cu3=54;
Phi3=35;

L4=1.5;
gama4=19;
alpha4=0.5;
cu4=22;
Phi4=19;

L = 28;
D = 0.8;
gampile = 25;
E = 29.2e6;
alphaT = -10e-6;
kappa = 65;
Kh=2e6;

as = 0.0035;
bs = 0.9;
ab = 0.02;
bb = 0.9;
chiT = 1.7;

P = 500;
DT=15;
```

Ultimate Bearing Capacity Parameters

```
   rad = pi/180;                                    % Degree to Rad

%% EARTH PRESSURE COEFFICIENTS %%
K01 = 1-sin(Phi1*rad);                                  % Coefficient of lateral earth pressure at rest
Ko1 = 1-sin(Phi2*rad);
Ko3 = 1-sin(Phi3*rad);
Ko4 = 1-sin(Phi4*rad);
Kp1  =  (1+sin(Phi1*rad))/(1-sin(Phi1*rad));        %  Coefficient  of  passive earth pressure
Kp2 = (1+sin(Phi2*rad))/(1-sin(Phi2*rad));
Kp3 = (1+sin(Phi3*rad))/(1-sin(Phi3*rad));
Kp4 = (1+sin(Phi4*rad))/(1-sin(Phi4*rad));
Ka1 = (1-sin(Phi1*rad))/(1+sin(Phi1*rad));     % Coefficient of active earth pressure
Ka2 = (1-sin(Phi2*rad))/(1+sin(Phi2*rad));
Ka3 = (1-sin(Phi3*rad))/(1+sin(Phi3*rad));
Ka4 = (1-sin(Phi4*rad))/(1+sin(Phi4*rad));

%% SKIN FRICTION PARAMETERS %%
 KT  =  -kappa*alphaT*DT*(D/2)/(0.02*L);                  %  Mobilized  radial expansion coefficient
 sigma1 = gama1*L1;                                     % vertical overburden stress of soil(kN/m2)
 sigma2 = sigma1+gama2*L2;
 sigma3 = sigma2+gama3*L3;
 sigma4 = sigma3+gama4*L4;
 beta1 = chiT * Ka1 * tan(Phi1*rad);                    %side shear factor
 beta2 = chiT * Ka2 * tan(Phi2*rad);
 beta3 = chiT * Ka3 * tan(Phi3*rad);
 beta4 = chiT * Ka4 * tan(Phi4*rad);
 betaT1  =  chiT*(Ka1+(Kp1-Ka1)*KT)*tan(Phi1*rad);      %temperature-dependent side shear factor
 betaT2 = chiT*(Ka2+(Kp2-Ka2)*KT)*tan(Phi2*rad);
 betaT3 = chiT*(Ka3+(Kp3-Ka3)*KT)*tan(Phi3*rad);
 betaT4 = chiT*(Ka4+(Kp4-Ka4)*KT)*tan(Phi4*rad);
```

Ultimate Bearing Capacity

```
%% ULTIMATE END BEARING CAPACITY %%
if ~exist('Qbmax')
    if EndBearing
        qu=2000;
        Qbmax = qu * Ab;                                % Ultimate end bearing capacity (kN)
    else
        switch SoilType
            case 0                                      % Undrained soil
                sc = 1.2;                               % Shape factor
                dc = 1.5;                               % Depth factor
                Nc = 9;                                     % Bearing capacity factor
```

```
                Qbmax = Ab * (cu4 * sc*dc*Nc);         % Ultimate end bearing
capacity (kN)
            case 1                                     % Drained soil
                sigmaZD = sigma4;                        % Overburden stress
(kN/m2)
                Nq  =  exp(pi*tan(Phi4*rad))*Kp4;        % Bearing capacity
factor.
                qb=11000;                                   %  Ultimate end
bearing resistance(KPa)
                Qbmax =qb * Ab;                        % Ultimate end bearing
capacity (kN)
            case 2                                     % Rock
                Qbmax = qu * Ab;                       % Ultimate end bearing
capacity (kN)
        end;
    end;
end;
clear sc dc Nc sigmaZD Nq;

%% ULTIMATE SIDE FRICTION BEARING CAPACITY %%
if ~exist('capp')
    capp = 0;
end;
if N>0 && N<=161
   if Layer1==0                                      % Undrained soil
        FsmaxM = As * (alpha1 * cu1);                    % Undrained ultimate
side shear stress for layer 1(kN/m2)
        FsmaxMT = As * (alpha1 * cu1);                   % Undrained ultimate
side shear stress after heating(kN/m2)
   else                                              % Drained soil
        sigv1=gama1*z;                                  %Effective vertical
stress of soil(kN/m2)
        FsmaxM = As.* qs1;                              % Ultimate side shear
force for each element (kN)
        FsmaxMT = As.* qs1;                             % Ultimate side shear
force for each element after heating (kN)
   end;
elseif N>161 && N<=482
   if Layer2==0                                       % Undrained soil
        FsmaxM = As * (alpha2 * cu2);                    % Undrained ultimate
side shear stress (kN/m2)
        FsmaxMT = As * (alpha2 * cu2);                   % Undrained ultimate
side shear stress after heating(kN/m2)
   else                                               % Drained soil
        sigv2=gama2*z;                                  %Effective vertical
stress of soil(kN/m2)
        FsmaxM = As.* qs2;                              % Ultimate side shear
force for each element (kN)
        FsmaxMT = As.* qs2;                             % Ultimate side shear
force for each element after heating (kN)
   end;
elseif N>482 && N<=946
   if Layer3==0                                      % Undrained soil
        FsmaxM = As * (alpha3 * cu3);                    % Undrained ultimate
side shear stress (kN/m2)
```

```
        FsmaxMT = As * (alpha3 * cu3);                  % Undrained ultimate
side shear stress after heating(kN/m2)
   else                                              % Drained soil
        sigv3=gama3*z;                                   %Effective vertical
stress of soil(kN/m2)

        FsmaxM = As.* qs3;                             % Ultimate side shear
force for each element (kN)
        FsmaxMT = As.* qs3;                            % Ultimate side shear
force for each element after heating (kN)
   end;
 elseif N>946 && N<=1000
   if Layer4==0                                      % Undrained soil
        FsmaxM = As * (alpha4 * cu4);                   % Undrained ultimate
side shear stress (kN/m2)
        FsmaxMT = As * (alpha4 * cu4);                  % Undrained ultimate
side shear stress after heating(kN/m2)
   else                                              % Drained soil
        sigv4=gama4*z;                                   %Effective vertical
stress of soil(kN/m2)

        FsmaxM = As.* qs4;                             % Ultimate side shear
force after heating (kN)
        FsmaxMT = As.* qs4;                            % Ultimate side shear
force for each element after heating (kN)
   end;
end
clear KT alpha sigv K beta betaT;
clear rad K0 Ka Kp;
```

Calculation of Mechanical Loading

```
pbo = 0;                                           % Last assumed displacement
at toe
R = 0;                                                % Force at head obtained
from equilibrium
pb = 1;                                              % Assumed displacement at
toe
while abs(P+R)>tol
    for i = N:-1:1                                       % Steps down from N to
1
 % Initialize the force and displacement for element i
        if i == N                               % For the bottom element first
            QtM(i) = 0;                            % Set the force at the top
equal to an initially small value
            pbM(i) = pb;                        % For the bottom element, set
this equal to the initial value of pb (zero to start)
            QbM(i)=-Qbmax*pbM(i)/(ab+pbM(i)*bb);           % Force at bottom
from Q-z curve
        else
            pbM(i) = ptM(i+1);  % Set the displacement of the bottom of the
next element equal to the force on the previous element
            QbM(i) = -QtM(i+1); % Set the force of the bottom of the next
element equal to the force on the previous element
            QtM(i) = 0;           % Set the force on the top of the next
element to zero initially
```

```
        end;
        DQt = 999;                                       % Set the change in
force at top to an initially high value
        % This loop is used to find QtM(i) to make the element i converged.
        while DQt > tol
            QaveM(i) = (QtM(i)-QbM(i))/2;              % Average axial force
at ith element
            deltaM(i) = QaveM(i)/Ki(i);                % Axial elongation of
ith elemnet
            ptM(i) = pbM(i) + deltaM(i);               % Dispalcement at the
head of ith element
            psM(i) = pbM(i) + deltaM(i)/2;             % Displacement at the
middle of ith element
            FsM(i)=-FsmaxM(i)*psM(i)/(as+psM(i)*bs);  %  Side  shear  force  of
ith element
            QtnewM(i) = - (FsM(i) + QbM(i));          % Force at the head of
ith element obtained by equilibium
            DQt = QtnewM(i) - QtM(i);                  % Change of the force
at the head of ith element
            QtM(i) = QtnewM(i);                        % Update the force at
the head of ith element
        end
        % Convergence of ith element means the behavior of the part of pile
        % below element i is obtained for assumed toe displacement.
    end
    % Find next toe displacement to be assumed
    R = sum(FsM)+QbM(N);
    k = R/pb;                                 % Secant slope for find next pb to
be assumed
    pbo = pb;
    pb = pb-(P+R)/k;                         % (P+R)is unbalanced force
end
if ~exist('D2')
    sigmaM = QaveM/Ab;                          %Axial stress (kN/m2)
else
    sigmaM = QaveM/(Ab-pi*(D2/2)^2);
end;
epsM = deltaM./Li*1e3;                       %Axial Strain (microstrain)
clear pbo R pb i DQt QtnewM R k ;
```

Calculation of Thermomechanical Loading

```
deltaTfree (1:N,1) = Li*alphaT*DT;                          % Define elongation
under free expansion condition
% |---------------------------------------|
% |-------Calculate the buttom part------|
% |---------------------------------------|
DDTb=Inf;                                         % Change of sum(deltaT)
deltaT(N1+1:N,1)=Li(N1+1:N)*alphaT*DT;           % Initialize thermal elongation
at free expansion
while sum(abs(DDTb))>tol
    % Calculate the displacement based on deltaT
    for j=N1+1:N
        if j==N1+1                                 % Displacement at the top of
ith element
            ptT(j) = 0;                           % Case for element next to NP
```

```
        else
            ptT(j) = pbT(j-1);                    % General case
        end;
        ptMT(j) = ptM(j) + ptT(j);                 % M+T displacement at the top
of jth element
        psT(j) = ptT(j) - deltaT(j)/2;            % T displacement at the side of
jth element
        psMT(j) = psM(j)+psT(j);                   % M+T displacement at the side
of jth element
        pbT(j) = ptT(j) - deltaT(j);              % T displacement at the bottum
of jth element
        pbMT(j) = pbM(j) + pbT(j);                    % M+T displacement at the
bottum of jth element
    end;

    % ---- Calculate the force based on displacement -----
    for j=N:-1:N1+1
        if j==N
            QbMT(j) = - Qbmax * pbMT(j) / (ab + bb * pbMT(j));  % Case for
toe element
        else
            QbMT(j) = - QtMT(j+1);                             % General case
        end;
        FsMT(j) = -FsmaxMT(j)*psMT(j)/(as+psMT(j)*bs);        % MT side shear
force
        QtMT(j) = - (QbMT(j) + FsMT(j));                        % MT force at
top of jth element obtained from equilibium
    end;
    % ---- Update the deltaT ----
    QaveMT = (QtMT - QbMT) / 2;                 % Average axial forces for each
element
    if ~exist('D2');
        sigmaMT = QaveMT/Ab;                       % Average axial stresses for
each element
    else
        sigmaMT = QaveMT/(Ab-pi*(D2/2)^2);
    end;
    deltanewT              =               [zeros(N1,1);deltaTfree(N1+1:N)-
deltaM(N1+1:N)]+sigmaMT.*Li/(E); % New elongation according to current force
    deltaT = (deltanewT-deltaT)/m+deltaT;     % Update elongation to be 1/m
close to the new DeltaT
    DDTb = deltaT-deltanewT;                  % Different between new and old
deltaT
end;

% |-----------------------------------|
% |-------Calculate the top part-----|
% |-----------------------------------|

DDTb=Inf;                                     % Change of sum(deltaT)
deltaT(1:N1) = Li(1:N1)*alphaT*DT;            % Initialize thermal elongation
at free expansion
while sum(abs(DDTb))>tol
    % ---- Calculate the displacement based on deltaT -----
    for j=N1:-1:1
```

```
        if j==N1                                % Displacement at the bottum of
ith element
            pbT(j) = 0;                         % Case for element next to NP
        else
            pbT(j) = ptT(j+1);                  % General case
        end;
        pbMT(j) = pbM(j) + pbT(j);                  % M+T displacement at the
bottum of jth element
        psT(j) = pbT(j) + deltaT(j)/2;          % T displacement at the side of
jth element
        psMT(j) = psM(j)+psT(j);                 % M+T displacement at the side
of jth element
        ptT(j) = pbT(j) + deltaT(j);             % T displacement at the top of
jth element
        ptMT(j) = ptM(j) + ptT(j);                % M+T displacement at the top
of jth element
    end;

    % ---- Calculate the force based on displacement -----
    for j=1:N1
        if j==1
            QtMT(j) = -Kh*(ptMT(j)-ptM(j)) + P;    % Case for head element
        else
            QtMT(j) = - QbMT(j-1);                 % General case
        end;
        if chiT==0
            FsMT(j)=0;                             % Non-friction case
        else
            FsMT(j)  =  -  FsmaxMT(j)*(  psMT(j)/as  +  (-FsM(j))/FsmaxM(j)  -
(1/((FsmaxM(j)/(-FsM(j)))-bs)) ); % side friction for unloading
        end;
        QbMT(j) = -( QtMT(j) + FsMT(j) );           % MT force at bottum of
jth element obtained from equilibium
    end;
    % ---- Update the deltaT ----
    QaveMT = (QtMT(1:N1) - QbMT(1:N1))/2;          % Average axial forces for
each element
    if ~exist('D2');
        sigmaMT = QaveMT/Ab;                          % Average axial stresses
for each element
    else
        sigmaMT = QaveMT/(Ab-pi*(D2/2)^2);
    end;
    deltanewT           =           [deltaTfree(1:N1)+sigmaMT.*Li(1:N1)/(E)-
deltaM(1:N1);deltaT(N1+1:N)]; % New elongation according to current force
    deltaT = (deltanewT-deltaT)/m+deltaT;          % Update elongation to be
1/m close to the new DeltaT
    DDTb = deltaT-deltanewT;                        % Different between new
and old deltaT
end;
if ~exist('D2')
    sigmaMT = (QtMT - QbMT)/2/Ab;      % M-T axial stresses
else
    sigmaMT = (QtMT - QbMT)/2/(Ab-pi*(D2/2)^2);
end;
sigmaT=sigmaMT-sigmaM;                 % T axial stresses
```

```
epsMT = (deltaM+deltaT)./Li*1e6;        % M-T axial strains
epsT = deltaT./Li*1e6;                  % T axial straines
epsM = deltaM./Li*1e6;                  % M axial strains
QaveMT = (QtMT - QbMT)/2;               % M-T axial average force in elements
FsT=FsMT-FsM;                           % T side friction force
QtT=QtMT-QtM;                           % T force at top

clear j deltanewT deltaTfree;
```

Analysis of Thermomechanical Loading of Energy Pile

```
%%%%%%%%%%%%%%%%%%%%%%%%%%%%%%%%%%%%%%%%%%%%%%%%
%   Thermo-Mechanical Load Transfer Analysis   %
%%%%%%%%%%%%%%%%%%%%%%%%%%%%%%%%%%%%%%%%%%%%%%%%
clear;
clear all
format long e
warning off

%% CALL DEFINITION %%
DefSoil;
DefPileGeometryMaterial;
DefTzQzCurveParameter;
DefLoad;
ReDefParameter;
UltBearingCapacityParameters;

%% THERMO-MECHANICAL T-Z ANALYSIS %%
N = 100;                             % INPUT Number of pile elements
tol = 1e-10;                         % Tolerance for the thermal T-z analysis
InitializeVari;

% CALCULATE THE BEHAVIOR OF PILE BY ITERATION %
while true
    DiscretizePile;
    UltBearingCapacityCalc;
    calcM;                           % Launch Mechanical T-z Analysis
    calcMT;                          % Launch Thermo-Mechanical T-z Analysis
    if abs(NP-NPo)<=tol
```

Appendix B: Pile foundation layout (United Bank HQ Building)

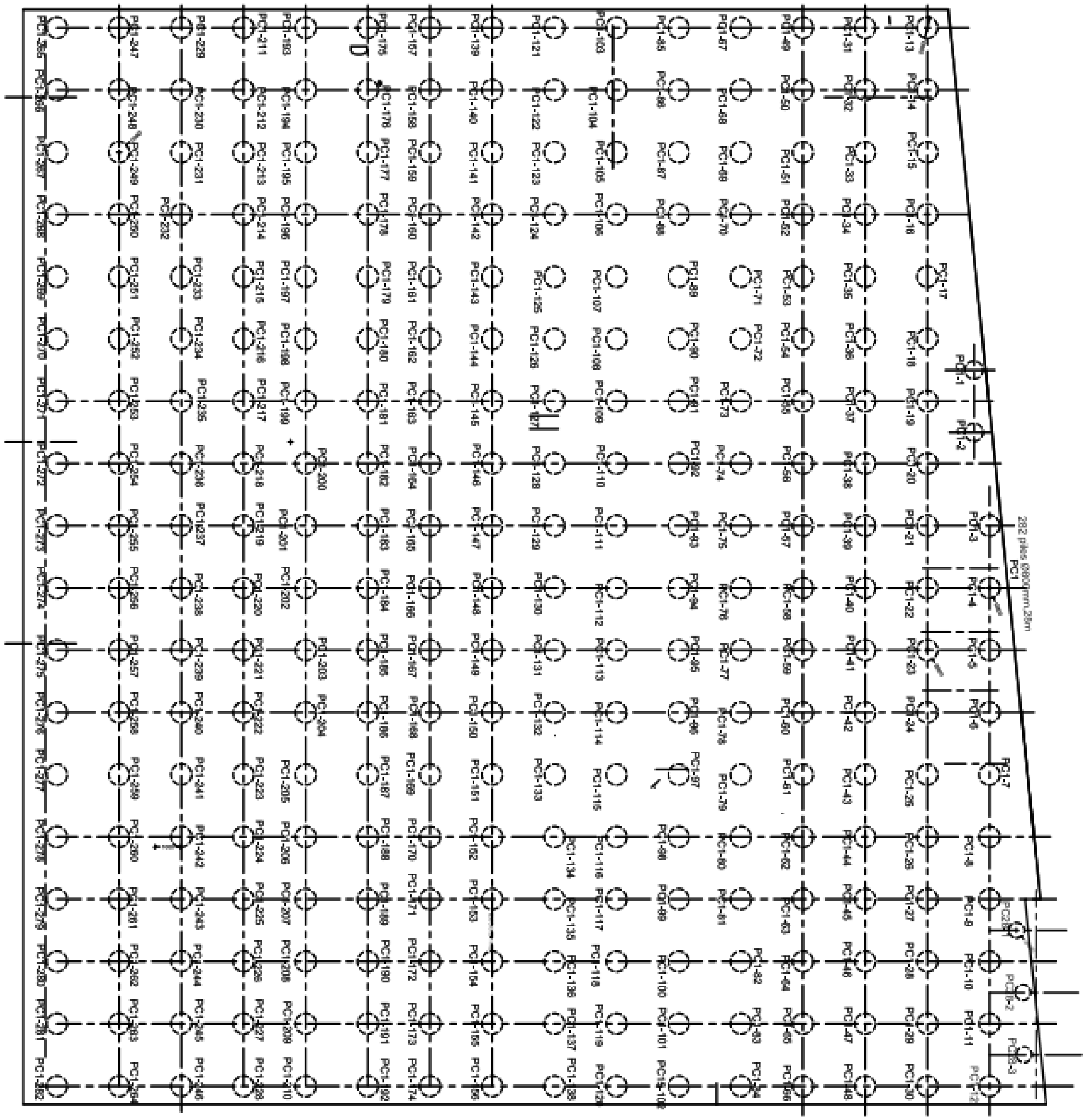

PILE FOUNDATION PLAN

Appendix C: Soil Profile

CONSTRUCTION DESIGN SCo. | OF/CDSCO/104

Title: **Borehole Log Sheet** | Issue No 1 | Page No Page 1 of 3

PROJECT HEAD OFFICE BUILDING | BORING TYPE ROTARY CORING
LOCATION ADDIS ABABA, SENGATERA | GROUND WATER LEVEL 6.60m
CLIENT UNITED BANK SHARE COMPANY | BH ELEVATION 2357m
DATE STARTED 14/10/2013 | INCLINATION VERTICAL
DATE COMPLETED 22/10/2013 | COORDINATES 472290.91E 996172.96N

BH 1

DEPTH (m)	CASING SIZE (mm)	DRILLING SIZE (mm)	SAMPLE RECORD	S.P.T. (N-VALUE)	DEPTH (m)	TCR (%)	RQD (%)	STRATA DESCRIPTION	REMARK
0–2.70	130	130			0.00, 1.70, 2.00	100, 100		Firm to stiff, brownish grey to light grey clay mixed with sand and gravel	Fill material
					2.00, 2.70	100, 100		Stiff, brownish grey, silty CLAY	
		100		26, 24	3.00, 4.40, 4.70, 6.00, 6.60	100, 100, 100, 100		Dense reddish brown, silty sandy GRAVEL, derived from highly weathered vesicular Basalt	
					7.30, 7.60, 8.00, 8.20, 8.70, 9.30, 9.70	100, 100, 100, 100, 100, 100, 100		Very dense, grey, sandy GRAVEL, derived from highly fragmented and weathered dark grey aphanetic basalt	
					10.90, 11.00, 11.70	100, 100, 100		Dense reddish brown, silty sandy GRAVEL, derived from highly weathered vesicular Basalt	
–15					12.10, 12.70, 13.10, 13.40, 14.30, 14.50, 14.70	100, 100, 100, 100, 100, 100, 100		Very dense, grey, sandy GRAVEL, derived from highly fragmented and weathered dark grey aphanetic basalt	

(Nc) CONE PENETRATION TEST
N BLOWS/30cm
RS ROCK SAMPLE
W WATER SAMPLE
TCR TOTAL CORE RECOVERY
RQD ROCK QUALITY DESIGNATION
DISTURBED SOIL SAMPLE
UNDISTURBED SOIL SAMPLE
SPT STANDARD PENETRATION
END OF DRILLING

CREW Gessese Abebe | DRAWN BY Bezunesh W/Tsadik
SUPERVISOR Lamesgin Melese | SIG
LOGGED BY Lamesgin Melese | SIG
APPROVED BY Getachew Teferi | SIG

PLEASE MAKE SURE THAT THIS IS THE CORRECT ISSUE BEFORE USE

Company Name		Form No
CONSTRUCTION DESIGN SCo. (Construction Design SCo. Architects, Engineers & Town Planners)		OF/CDSCO/104
Title: **Borehole Log Sheet**	Issue No: 1	Page No: Page 2 of 3

PROJECT HEAD OFFICE BUILDING — BORING TYPE ROTARY CORING
LOCATION ADDIS ABABA, SENGATERA — GROUND WATER LEVEL 6.60m
CLIENT UNITED BANK SHARE COMPANY — BH ELEVATION 2357m
DATE STARTED 14/10/2013 — INCLINATION VERTICAL
DATE COMPLETED 22/10/2013 — COORDINATES 472290.91E 996172.96N

BH 1

DEPTH (m)	CASING SIZE (mm)	DRILLING SIZE (mm)	SAMPLE RECORD	S.P.T. /N-VALUE/	DEPTH (m)	TCR (%)	RQD (%)	STRATA DESCRIPTION	REMARK
15		100			15.00	100		Dense reddish brown, silty sandy GRAVEL, derived from highly weathered vesicular Basalt	
					15.20	100			
16					16.20	100			
17					16.80	100			
					17.80	100			
18			18.20		18.00	100		Hard, reddish brown silty CLAY (paleo soil)	
					18.20	100			
19				31	19.00	100			
20			20.20		20.00	100			
21				65	21.00	100			
22			22.20		22.10	100			
23				73	23.00	100			
					23.90	100			
24			24.10		24.10	100			
					24.60	100			
25				50	25.10	68			
26			26.10		26.10	68			
27				40	27.00	64			
28			28.10		28.10	70			
					28.40	70		Dense, light grey, sandy GRAVEL, highly weathered Basalt	
29				>50	29.40	70			
30									

(Nc) CONE PENETRATION TEST
N BLOWS/30cm
RS ROCK SAMPLE
W WATER SAMPLE
TCR TOTAL CORE RECOVERY
RQD ROCK QUALITY DESIGNATION
DISTURBED SOIL SAMPLE
UNDISTURBED SOIL SAMPLE
SPT STANDARD PENETRATION
END OF DRILLING

CREW Gessese Abebe — DRAWN BY Bezunesh W/Tsadik
SUPERVISOR Lamesgin Melese — SIG
LOGGED BY Lamesgin Melese — SIG
APPROVED BY Getachew Teferi — SIG

Company Name		Form No
CONSTRUCTION DESIGN SCo.		OF/CDSCO/104
Title: Borehole Log Sheet	Issue No: 1	Page No: Page 3 of 3

PROJECT HEAD OFFICE BUILDING — BORING TYPE ROTARY CORING
LOCATION ADDIS ABABA, SENGATERA — GROUND WATER LEVEL 6.60m
CLIENT UNITED BANK SHARE COMPANY — BH ELEVATION 2357m
DATE STARTED 14/10/2013 — INCLINATION VERTICAL
DATE COMPLETED 22/10/2013 — COORDINATES 472290.91E 996172.96N

BH 1

DEPTH (m)	CASING SIZE (mm)	DRILLING SIZE (mm)	SAMPLE RECORD	S.P.T. /N-VALUE/	DEPTH (m)	TCR (%)	RQD (%)	STRATA DESCRIPTION	REMARK
30–34		85		41	30.00, 30.40, 31.70, 32.10, 32.80, 33.00, 34.00	100, 100, 100, 100, 100, 100, 100		Dense, light grey, sandy GRAVEL, highly weathered Rock	
34–36		85	35.10		34.00, 35.00, 35.70, 36.00	100, 100, 100, 100		Hard, reddish brown silty CLAY with some sand (paleo soil)	
36–42.70		85	37.50	40, >50, >50	36.00, 37.50, 38.00, 38.80, 40.00, 40.70, 42.00, 42.70	100, 100, 100, 100, 100, 100		Dense to very dense, light grey, sandy GRAVEL, derived from highly weathered Basalt	
42.70–45		85		55	42.70, 43.80, 45.00	100, 100		Dense, reddish brown with yellowish spots, silty sandy GRAVEL, derived from completely weathered vesicular Basalt	

(Nc) CONE PENETRATION TEST
N BLOWS/30cm
RS ROCK SAMPLE
W WATER SAMPLE
TCR TOTAL CORE RECOVERY
RQD ROCK QUALITY DESIGNATION
DISTURBED SOIL SAMPLE
UNDISTURBED SOIL SAMPLE
SPT STANDARD PENETRATION
END OF DRILLING

CREW Gessese Abebe — DRAWN BY Bezunesh W/Tsadik
SUPERVISOR Lamesgin Melese — SIG
LOGGED BY Lamesgin Melese — SIG
APPROVED BY Getachew Teferi — SIG

Construction Design Share Company

PLEASE MAKE SURE THAT THIS IS THE CORRECT ISSUE BEFORE USE